Electronic Supplementary Material (ESI) for Dalton Transactions.
This journal is © The Royal Society of Chemistry 2022

Supporting Information For:

Diamino group-functionalized Zr-based metal-organic framework for fluorescence sensing of free chlorine in aqueous phase and Knoevenagel condensation

Chiranjib Gogoi,[a] Nagarathinam Nagarjun,[b] Abhijeet Rana,[a] Amarajothi Dhakshinamoorthy[b] and Shyam Biswas*[a]*

[a]*Department of Chemistry, Indian Institute of Technology Guwahati, Guwahati, 781039 Assam, India.*

[b]*School of Chemistry, Madurai Kamaraj University, Madurai, 625021, Tamil Nadu, India*

* Corresponding author. Tel: 91-3612583309, Fax: 91-3612582349.

E-mail address: sbiswas@iitg.ac.in; admguru@gmail.com

Materials and General Methods:

All the reagents and solvents were procured from commercial sources and used without purification, except the $H_2NDC\text{-}(NH_2)_2$ ligand. The notations used for characterization of the bands are broad (br), strong (s), very strong (vs), medium (m), weak (w) and shoulder (sh). 9KW Powder X-Ray Diffraction System, Make: Rigaku Technologies, JAPAN, Model: Smartlab was employed for X-ray powder diffraction (XRPD) measurements. The Attenuated Total Reflectance Infrared (ATR-IR) spectra were recorded using PerkinElmer UATR Two at ambient condition in the region 400-4000 cm^{-1} (USA). Thermogravimetric analysis (TGA) was carried out with a TG 209 F1 Libra; Make: M/s Netzsch, Germany thermogravimetric analyzer in the temperature range of 25-700 °C in an air atmosphere at the rate of 10 °C min^{-1}. N_2 sorption isotherms were recorded by using Quantachrome AutosorbiQ-MP (USA) volumetric gas adsorption equipment at −196 °C. Before the sorption analysis, the degassing of the compound was carried out at 100°C under a high vacuum for 12 h. Fluorescence sensing studies were performed with a HORIBA JOBIN YVON Fluoromax-4 (Japan) spectrofluorometer. A BrukerAvance III 600 NMR (Germany) spectrometer was used for recording ^1H NMR spectra at 600 MHz. Mass spectra were recorded with an Agilent 6520 Q-TOF (USA) high-resolution mass spectrometer (HR-MS). Picosecond Time-resolved and Steady StateLuminescence Spectrometer, Make: Edinburg Instruments, Model: Lifespec II & FSP 920 was used for the TRPL study. Pawley refinement was carried out using Materials Studio software. The DICVOL program[1] incorporated within STOE's WinXPow software package[2] was used to determine the lattice parameters.

Synthesis of $H_2NDC\text{-}(NH_2)_2$ linker:

4,8-Dinitronapthalene-2,6-dicarboxylic acid ($H_2NDC\text{-}(NO_2)_2$ linker was prepared from naphthalene-2,6-dicarboxylic acid (H_2NDC) by following the protocol reported in the literature.[3] In a 250 mL round-bottom flask, 1 g (3.3 mmol) of $H_2NDC\text{-}(NO_2)_2$ was taken and 100 mL of methanol and 50 mL of tetrahydrofuran (THF) were added at room temperature. The reaction mixture was stirred to completely dissolve the reactant. Then, 280 mg of Pd/C was added very slowly in stirring conditions at room temperature. The flask was fitted with a condenser and a nitrogen filled balloon. Then, the solution was heated at 60 °C. After 10 min, 4 mL of hydrazine hydrate was added very slowly and after complete addition, the mixture was heated at 80 °C for overnight. A dark greenish precipitate was obtained and the precipitate was filtered through a filter paper. The precipitate was dissolved in 1M NaOH (100 mL). Then, the precipitate was again filtered off and conc. HCl was slowly added to the filtrate to acidify the solution, resulting in dark yellowish precipitation. The obtained solid product, i.e. 4,8-diaminenapthalene-2,6-dicarboxylic acid ($H_2NDC\text{-}(NH_2)_2$) linker was filtered off, washed with large amount of water and dried in an oven at 60 °C. The reaction scheme for the preparation of $H_2NDC\text{-}(NH_2)_2$ linker is shown in Scheme S1.

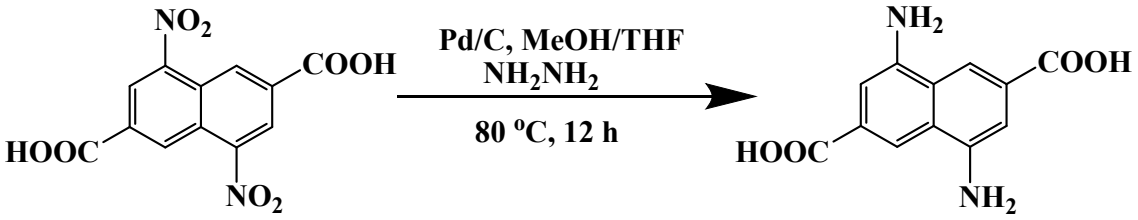

4,8-dinitronaphthalene-2,6-dicarboxylic acid [H_2NDC-$(NO_2)_2$]

4,8-diaminenaphthalene-2,6-dicarboxylic acid [H_2NDC-$(NH_2)_2$]

Scheme S1. Syntheis of H_2NDC-$(NH_2)_2$ linker.

The characterization of the linker was carried out by mass spectrometry, ^{1}H and ^{13}C NMR spectroscopy. The ^{1}H NMR spectrum (Figure S1) confirmed the presence of four types of protons in the H_2NDC-$(NH_2)_2$ linker. The naphthalene moiety contains two types of protons and one type of proton is present at the amine group and one type of proton is present in the carboxylic acid group. The different types of protons are marked by (a), (b), (c) and (d). The chemical shift values are observed at 12.67 (s, 2H, -COOH), 7.94 (s, 2H, Ar-H), 7.18 (s, 2H, Ar-H) and 5.92 (s, 4H, -NH_2) ppm, respectively. Since there are no additional protons in the ^{1}H NMR spectrum, the formation of by-products is ruled out. The ^{13}C NMR spectrum (Figure S2) revealed that there are six types of carbon atoms present in the ligand. The observed chemical shift values are 107.70, 112.83, 125.34, 128.90, 146.79 and 168.71 ppm. In the mass spectrum of the linker (Figure S3), the most intense peak was found at m/z = 247.072 (measured in positive ion mode), which corresponds to $(M-H)^+$ ion (M is the mass of H_2NDC-$(NH_2)_2$ ligand). The theoretically calculated mass of the linker is 246.06 g mol^{-1}. Therefore, it can be concluded that the desired H_2NDC-$(NH_2)_2$ linker has been synthesized in pure form.

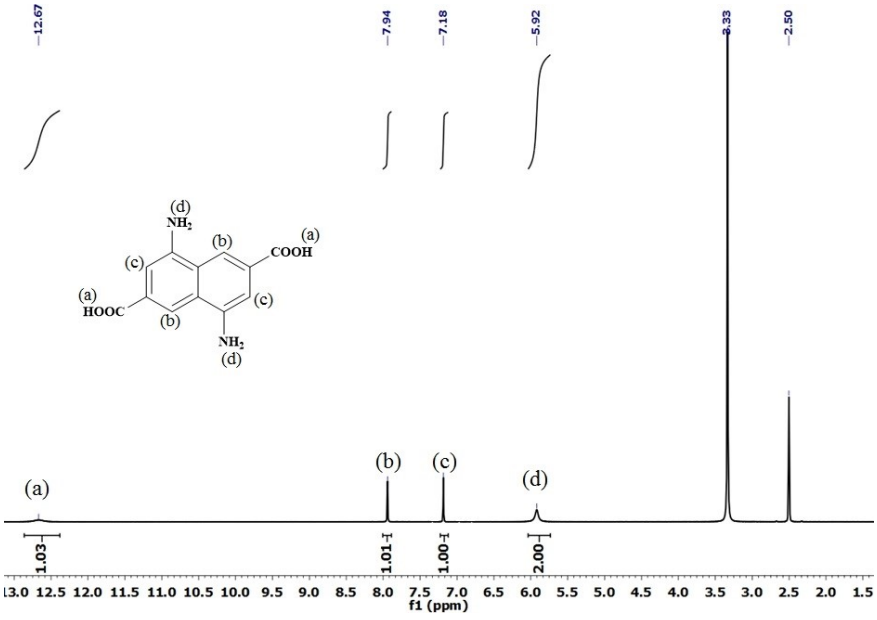

Figure S1. ^{1}H NMR spectrum of H_2NDC-$(NH_2)_2$ linker measured in DMSO-d_6.

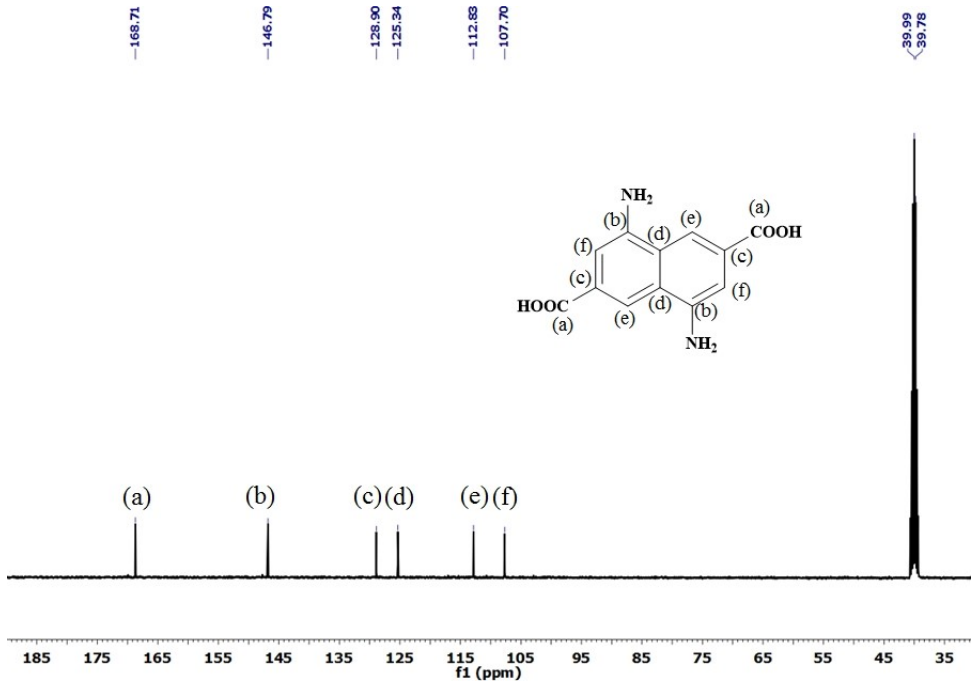

Figure S2. ^{13}C NMR spectrum of $H_2NDC\text{-}(NH_2)_2$ linker measured in DMSO-d_6.

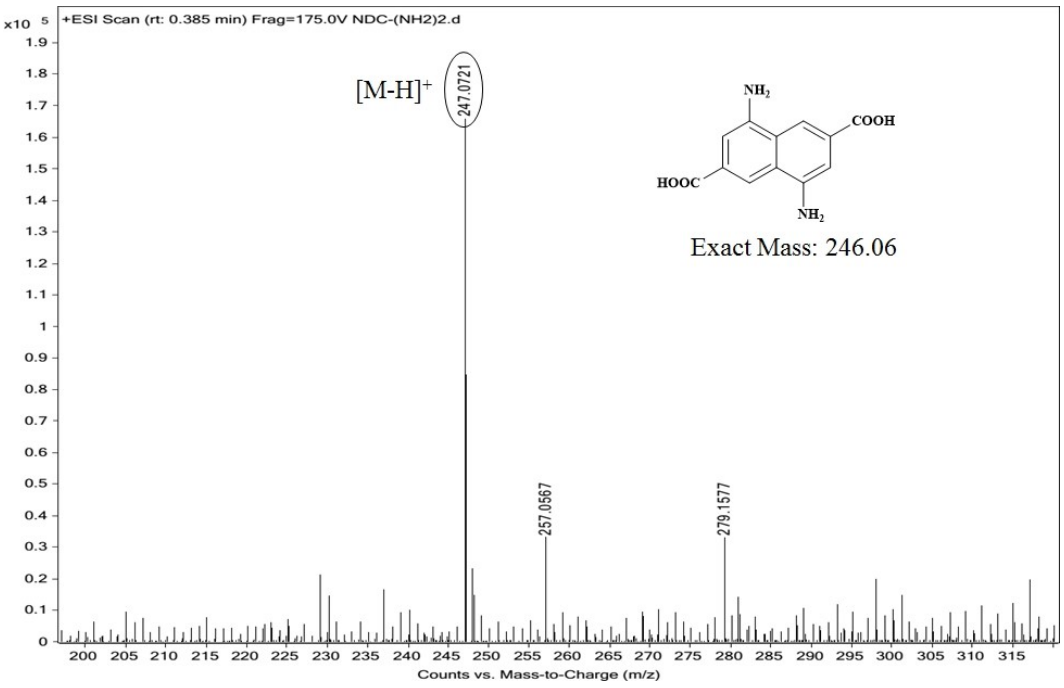

Figure S3. Mass spectrum of $H_2NDC\text{-}(NH_2)_2$ linker.

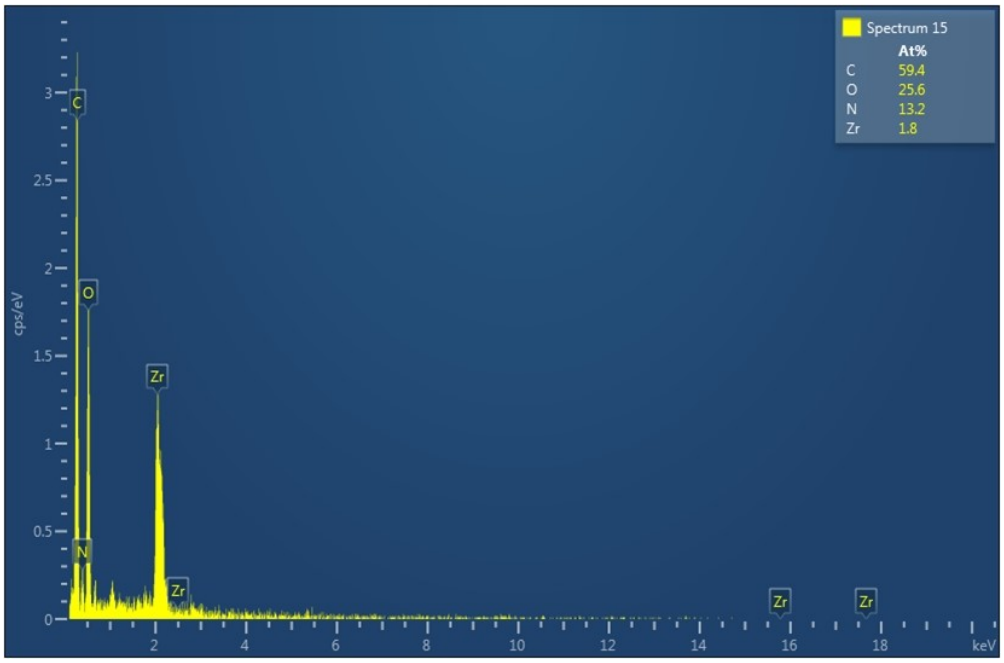

Figure S4. EDX spectrum of **DUT-52-$(NH_2)_2$-1**.

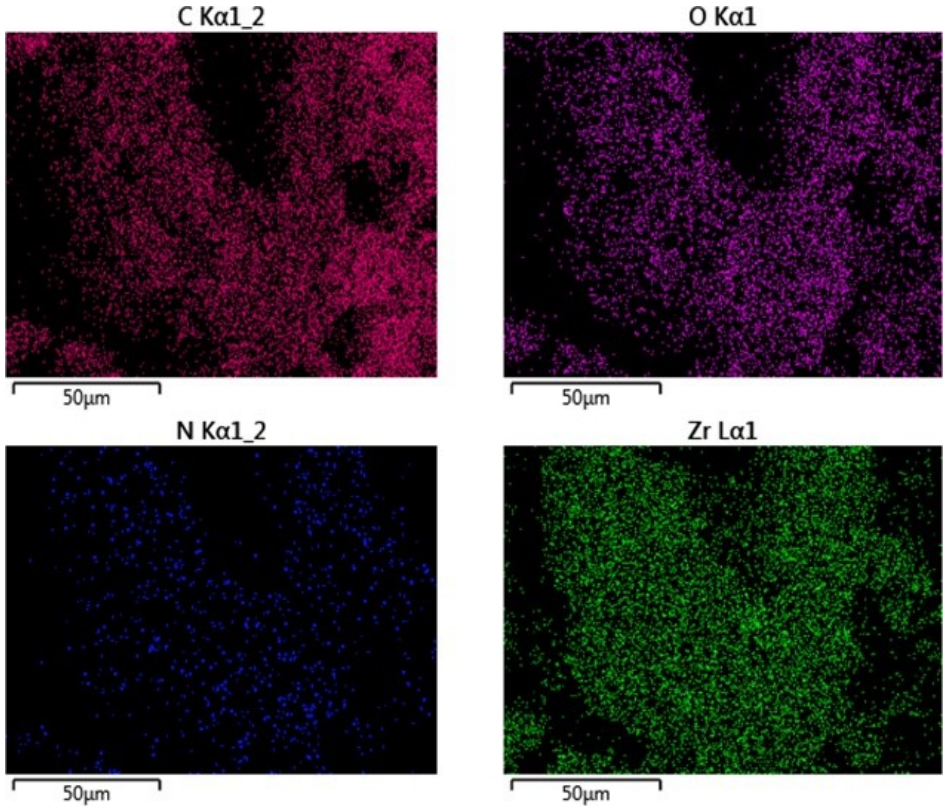

Figure S5. EDX elemental mapping of **DUT-52-$(NH_2)_2$-1**.

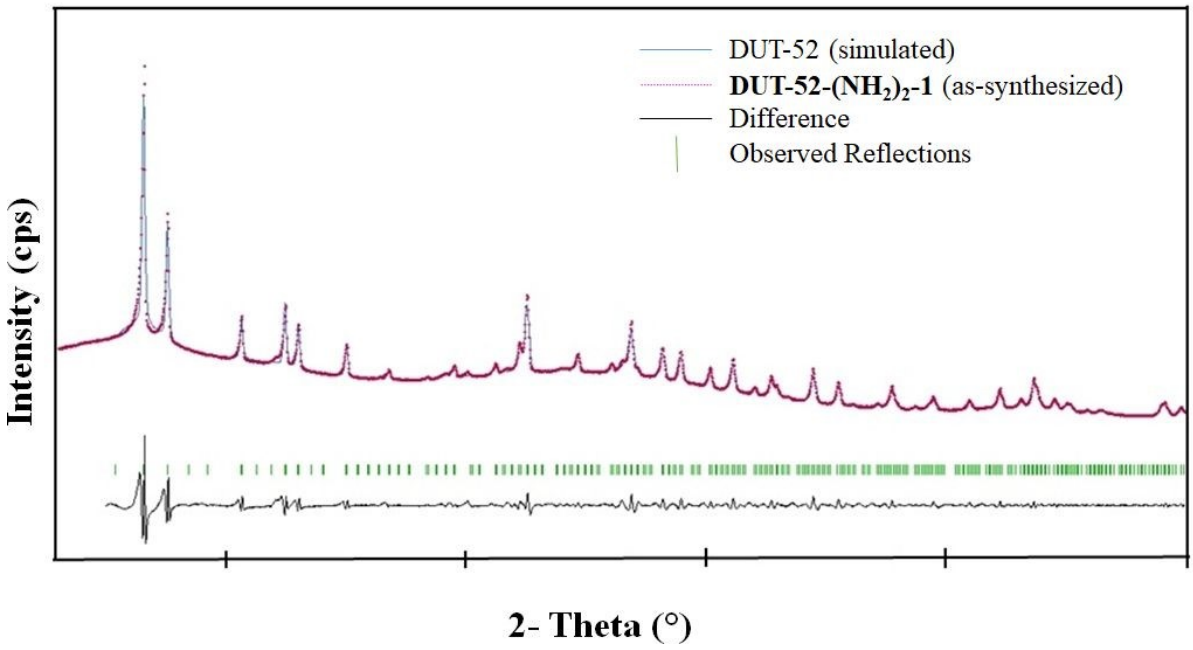

Figure S6. Pawley fit for the XRPD pattern of as-synthesized **DUT-52-$(NH_2)_2$-1**. Blue lines and red dots denote simulated and observed patterns, respectively. The peak positions and difference plot are displayed at the bottom (R_p = 2.13, R_{wp} = 3.54).

Table S1. Unit cell parameters of **DUT-52-$(NH_2)_2$-1** and parent Zr-DUT-52 MOF.

Compound name	**DUT-52-$(NH_2)_2$-1** (This work)	Zr-DUT-52 (Reported)
Space Group	$Fm\bar{3}m$	$Fm\bar{3}m$
Crystal System	Cubic	Cubic
a = b = c (Å)	23.723 (4)	23.910 (3)
α = β= γ (°)	90	90
V (Å^3)	13350 (38)	13669 (3)
Figure of Merit (FOM)	30.6	-

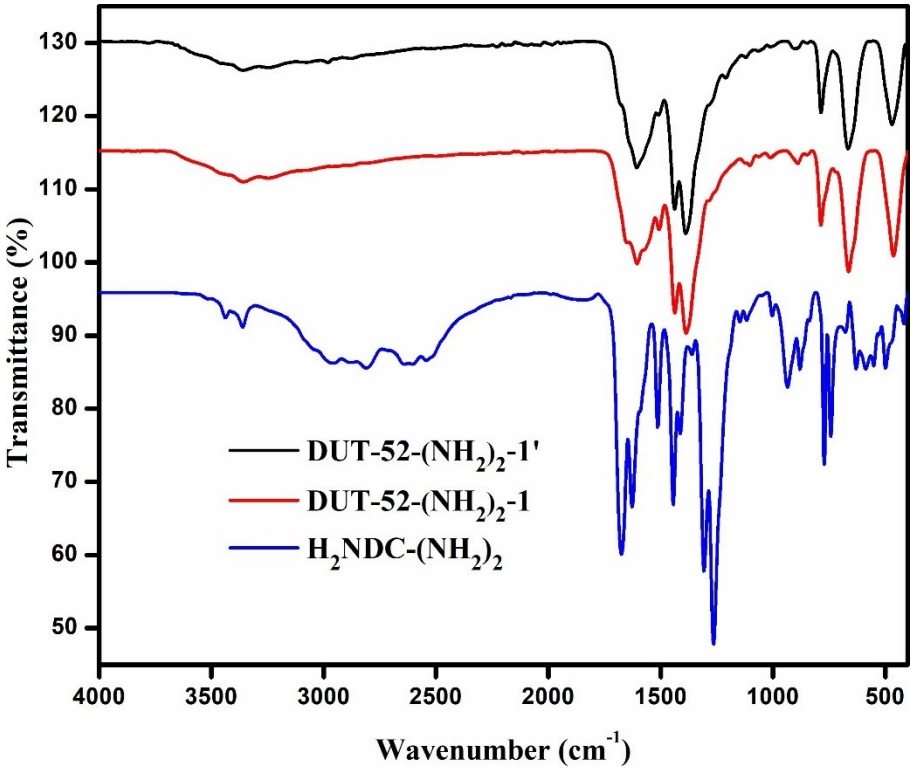

Figure S7. FT-IR spectra of $H_2NDC\text{-}(NH_2)_2$ linker, as-synthesized **DUT-52-$(NH_2)_2$-1** (red) and activated **DUT-52-$(NH_2)_2$-1'** (black).

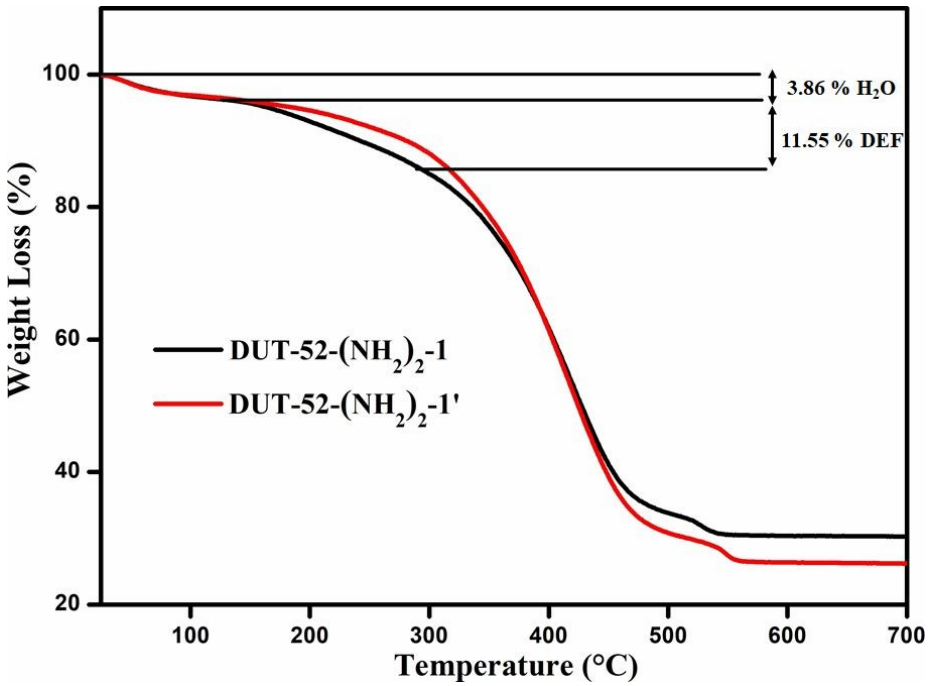

Figure S8. TG curves of as-synthesized **DUT-52-$(NH_2)_2$-1** (black) and activated **DUT-52-$(NH_2)_2$-1'** (red) recorded in an air atmosphere in the temperature range of 25-700 °C at a heating rate of 5 °C min^{-1}.

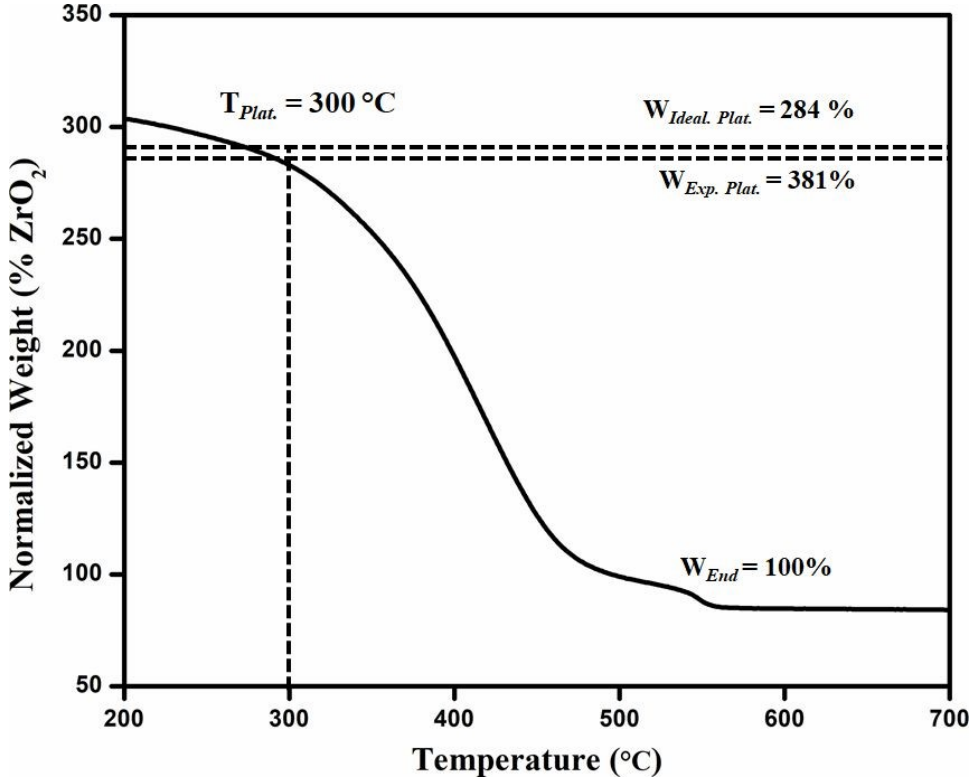

Figure S9. Calculation of missing linker defects from the TG curve of **DUT-52-$(NH_2)_2$-1'**.

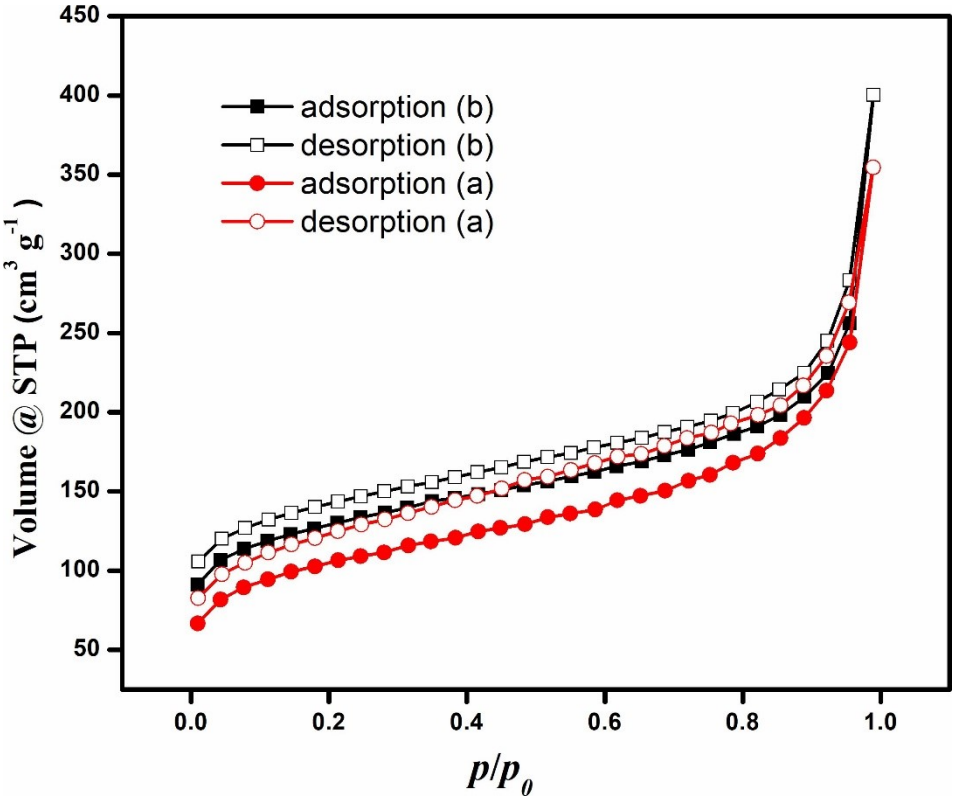

Figure S10. N_2 adsorption and desorption isotherms of (a) **DUT-52-$(NH_2)_2$-1** (b) **DUT-52-$(NH_2)_2$-1'** recorded at –196 °C.

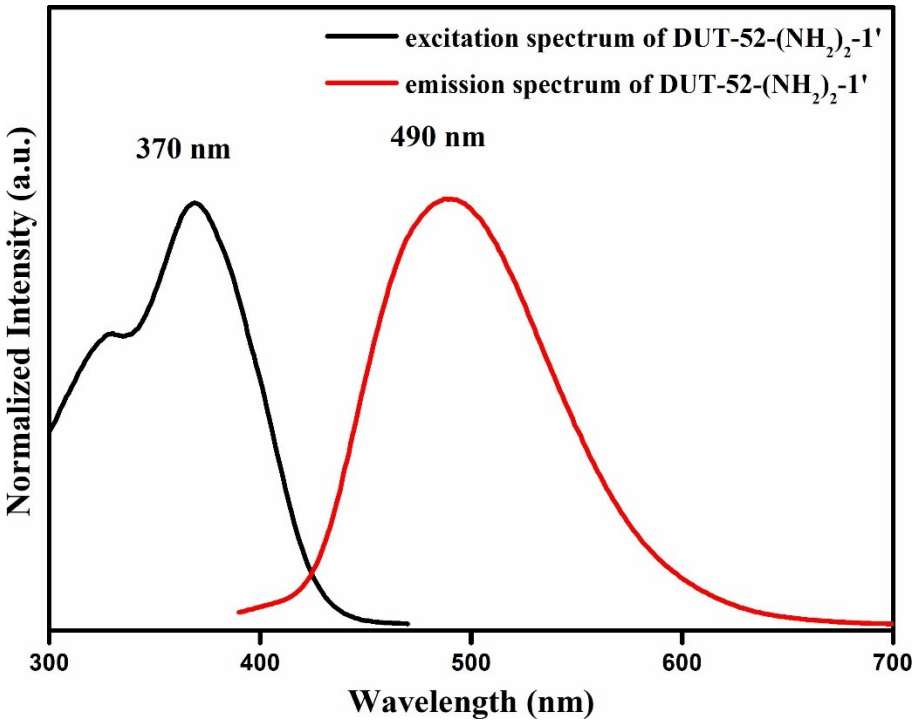

Figure S11. Fluorescence emission spectra and excitation **DUT-52-(NH$_2$)$_2$-1'**.

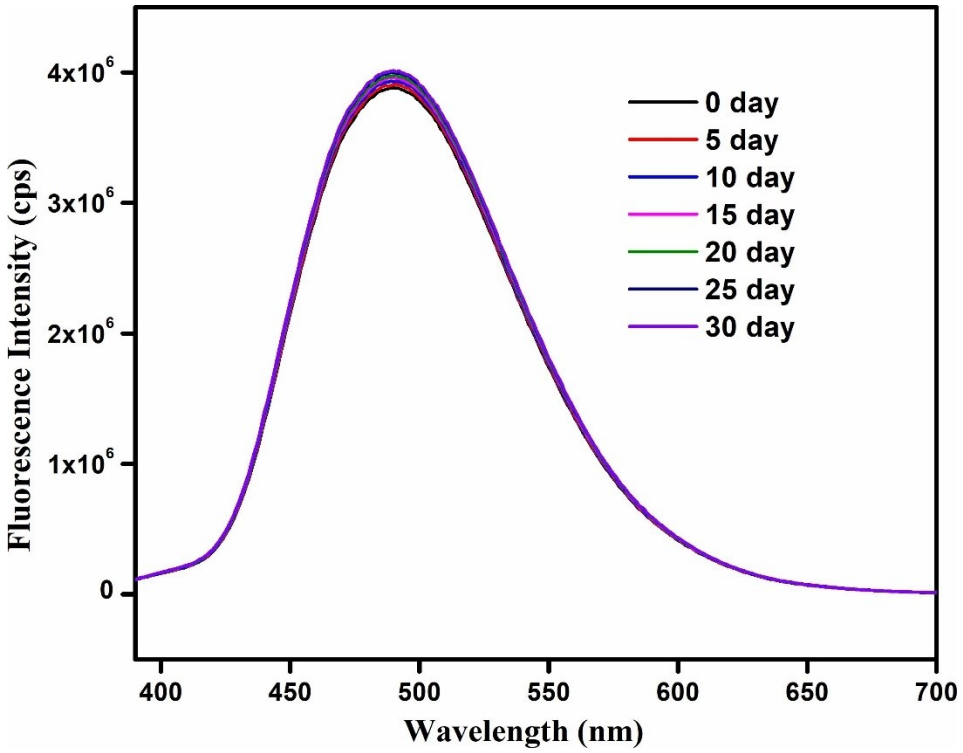

Figure S12. Day-to-day fluorescence stability of **DUT-52-(NH$_2$)$_2$-1'** in PBS (pH = 7.4).

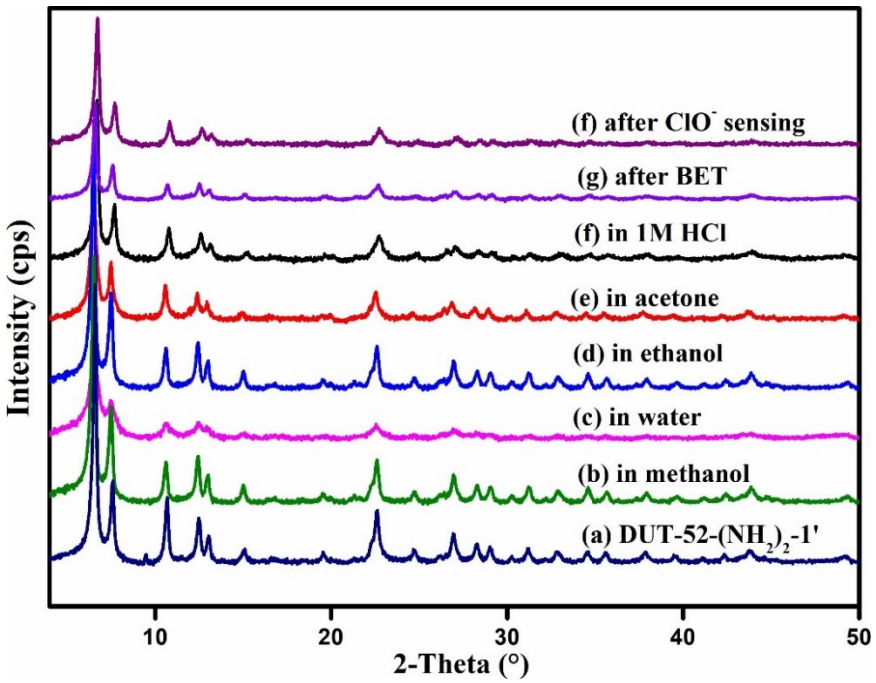

Figure S13. XRPD patterns of (a) **DUT-52-$(NH_2)_2$-1'** showing its chemical stability in (b) methanol, (c) water, (d) ethanol, (e) acetone and (f) 1M HCl. The XRPD pattern of **DUT-52-$(NH_2)_2$-1'** after (g) BET and (f) ClO^- sensing experiments.

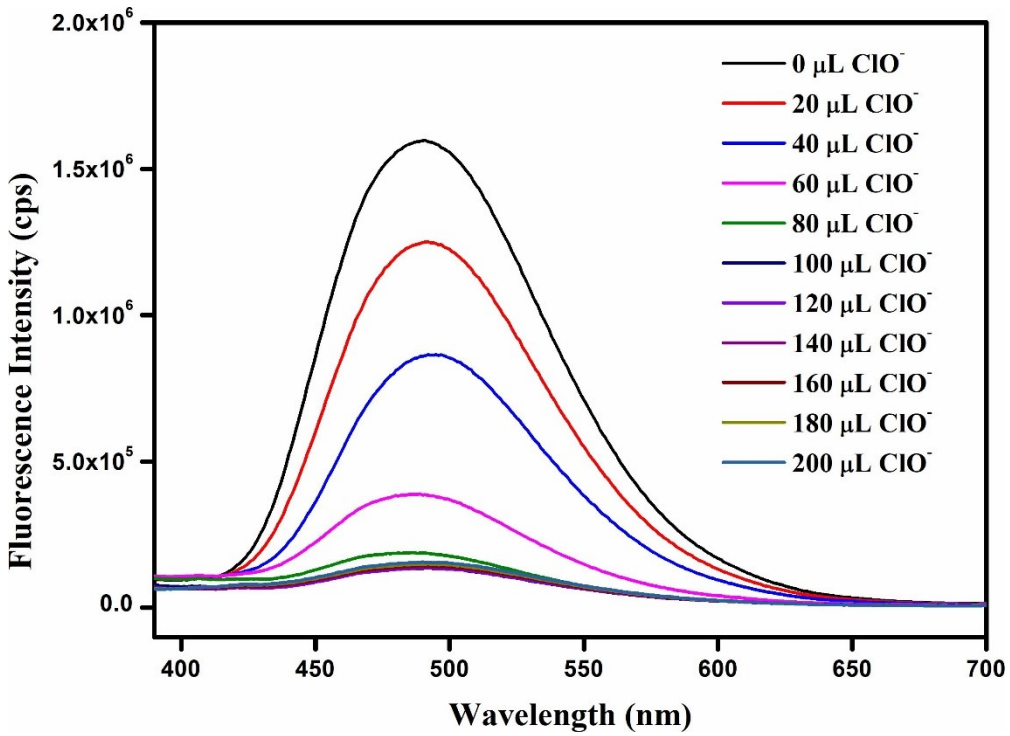

Figure S14. Change in fluorescence emission intensity of **DUT-52-$(NH_2)_2$-1'** after incremental addition of 5 mM ClO^- in water.

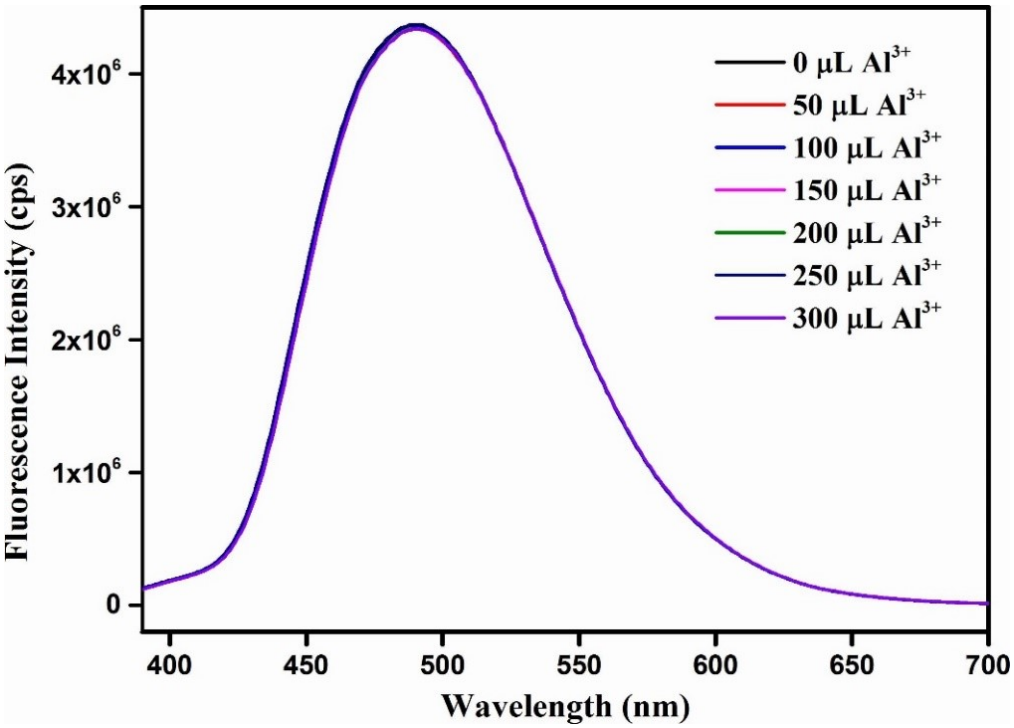

Figure S15. Change of fluorescence intensity of **DUT-52-$(NH_2)_2$-1'** dispersed in PBS after addition of 5 mM solution of Al^{3+} (300 μL).

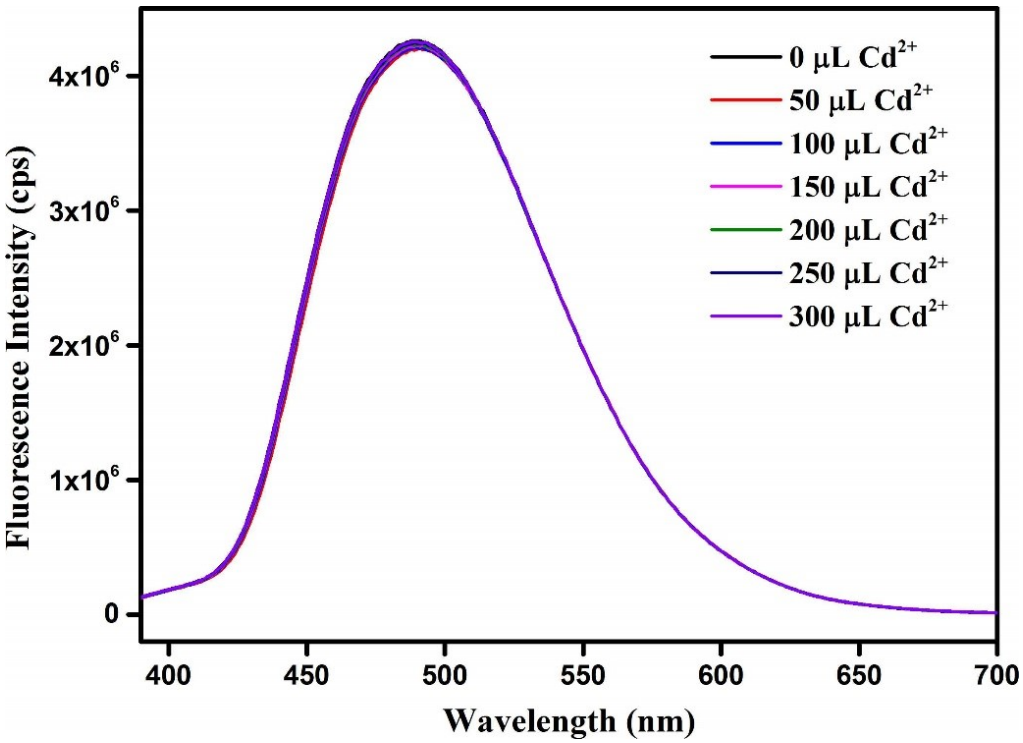

Figure S16. Change of fluorescence intensity of **DUT-52-$(NH_2)_2$-1'** dispersed in PBS after addition of 5 mM solution of Cd^{2+} (300 μL).

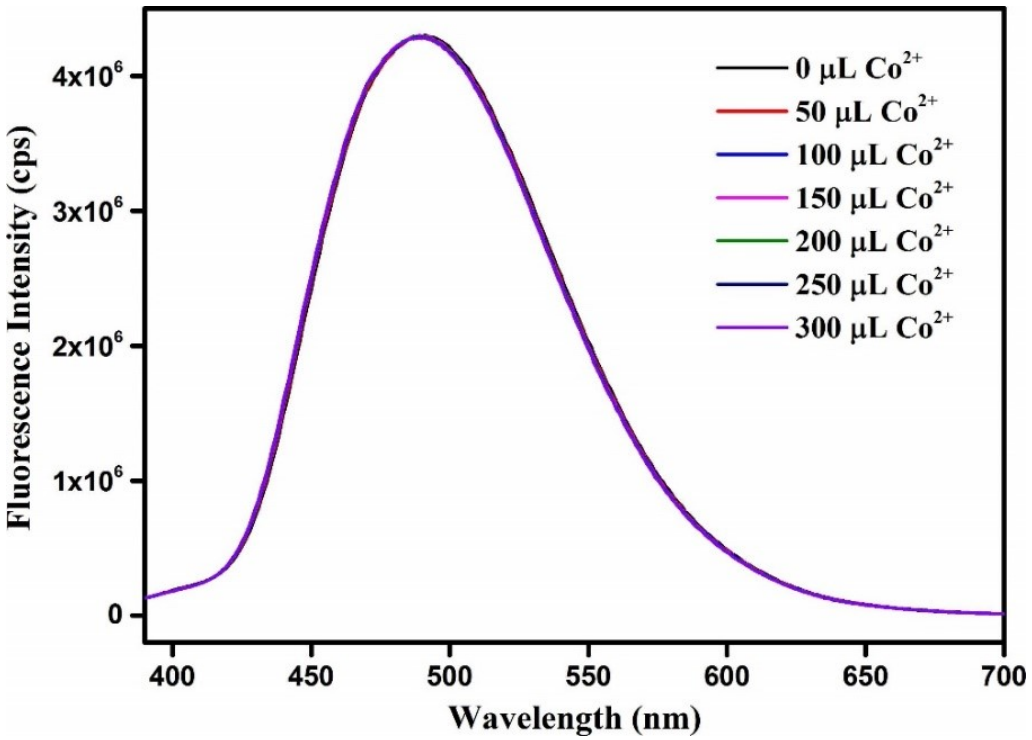

Figure S17. Change of fluorescence intensity of **DUT-52-$(NH_2)_2$-1'** dispersed in PBS after addition of 5 mM solution of Co^{2+} (300 μL).

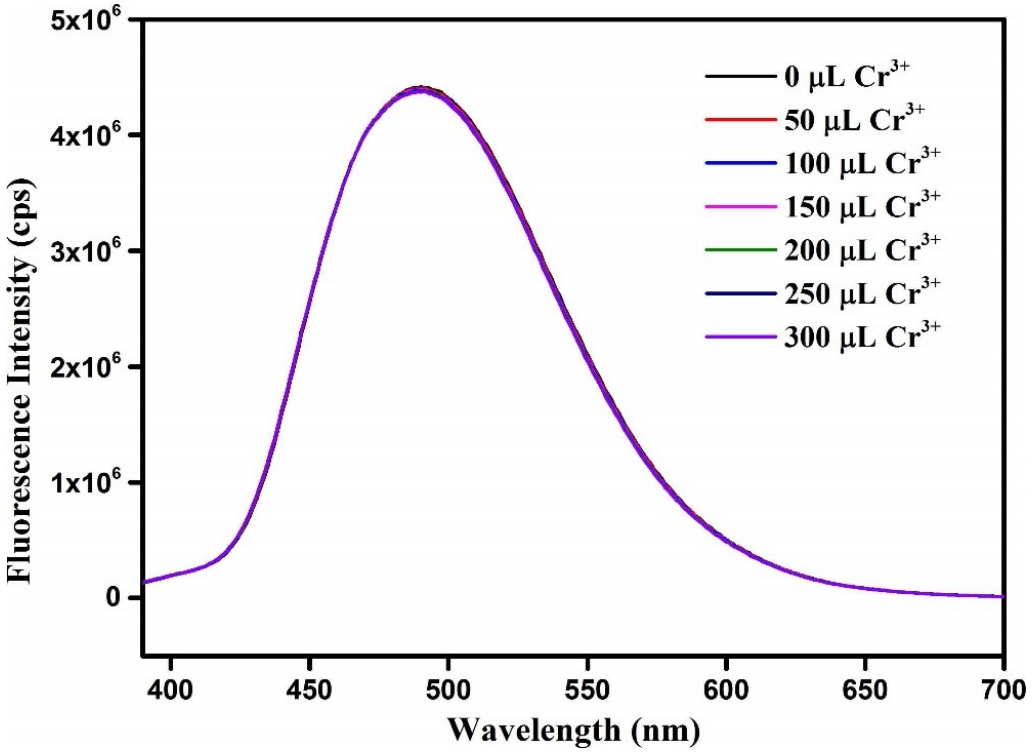

Figure S18. Change of fluorescence intensity of **DUT-52-$(NH_2)_2$-1'** dispersed in PBS after addition of 5 mM solution of Cr^{3+} (300 μL).

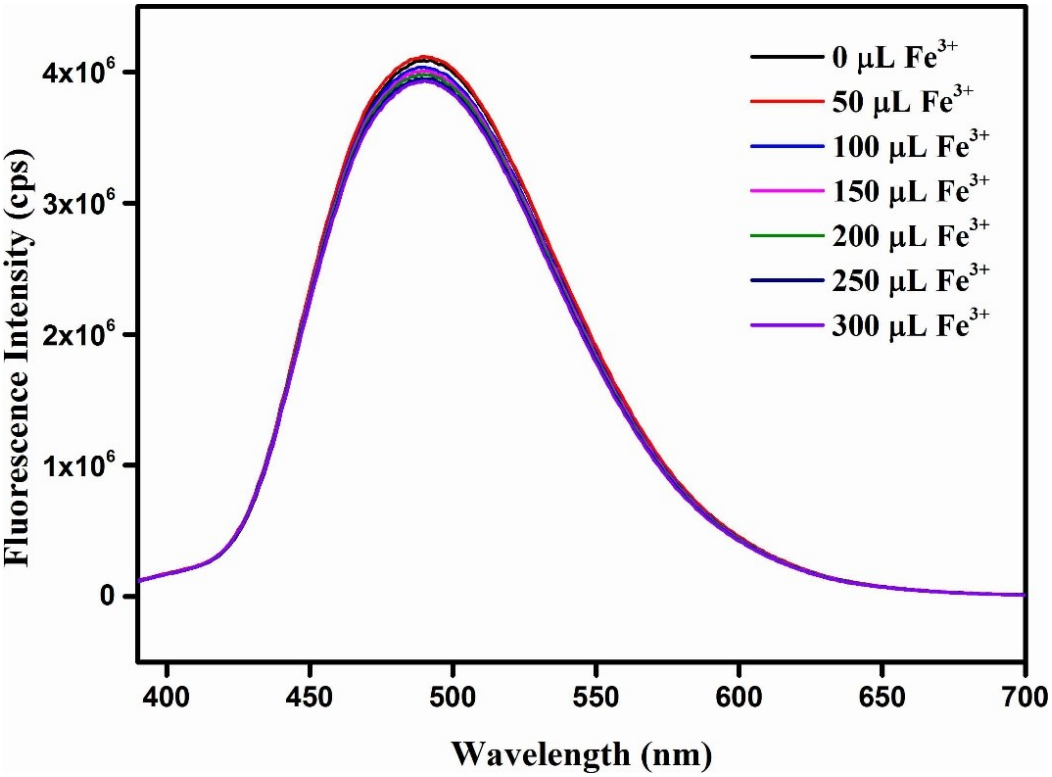

Figure S19. Change of fluorescence intensity of **DUT-52-$(NH_2)_2$-1'** dispersed in PBS after addition of 5 mM solution of Fe^{3+} (300 µL).

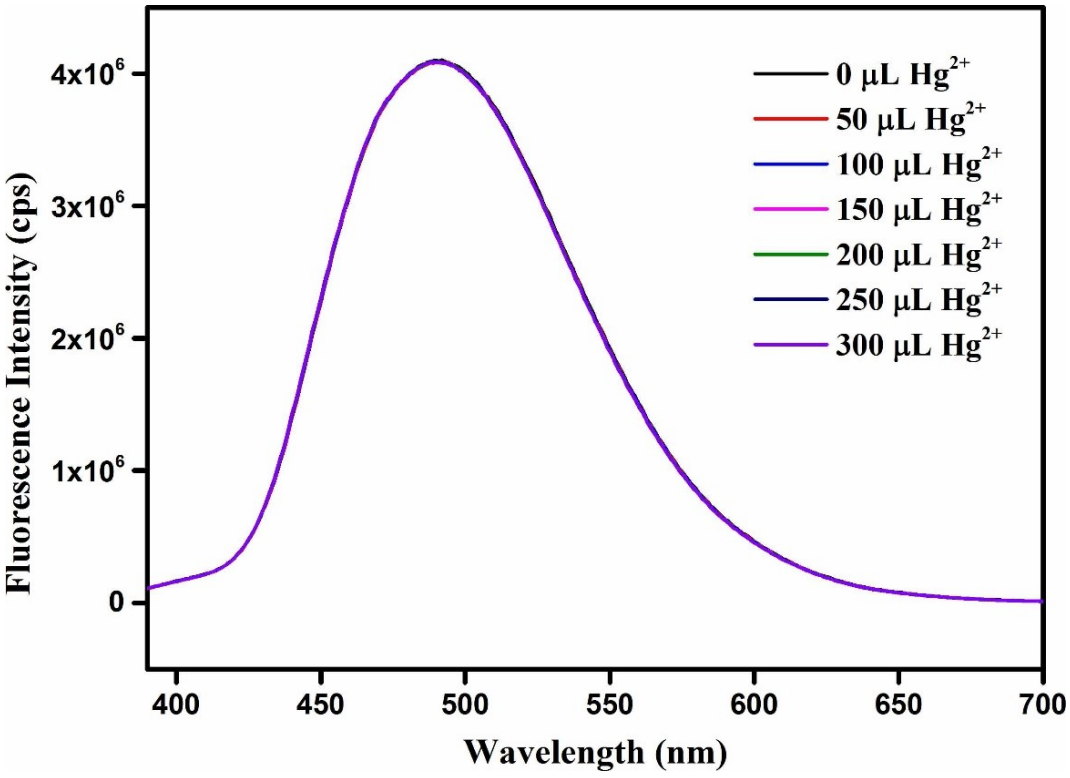

Figure S20. Change of fluorescence intensity of **DUT-52-$(NH_2)_2$-1'** dispersed in PBS after addition of 5 mM solution of Hg^{2+} (300 µL).

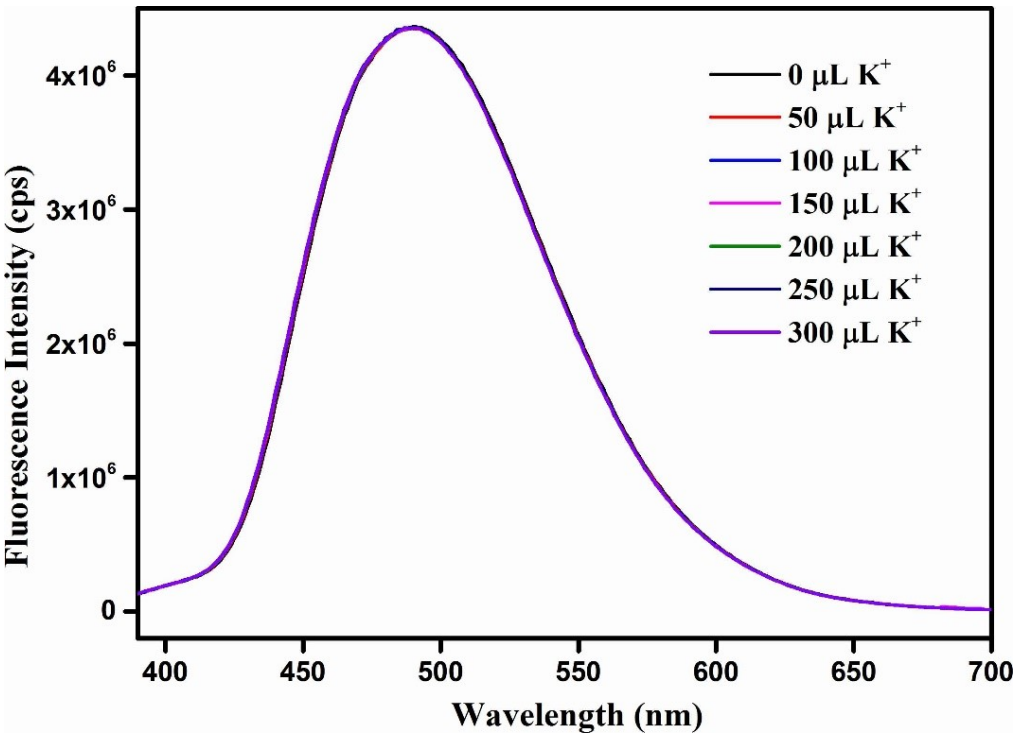

Figure S21. Change of fluorescence intensity of **DUT-52-$(NH_2)_2$-1'** dispersed in PBS after addition of 5 mM solution of K^+ (300 μL).

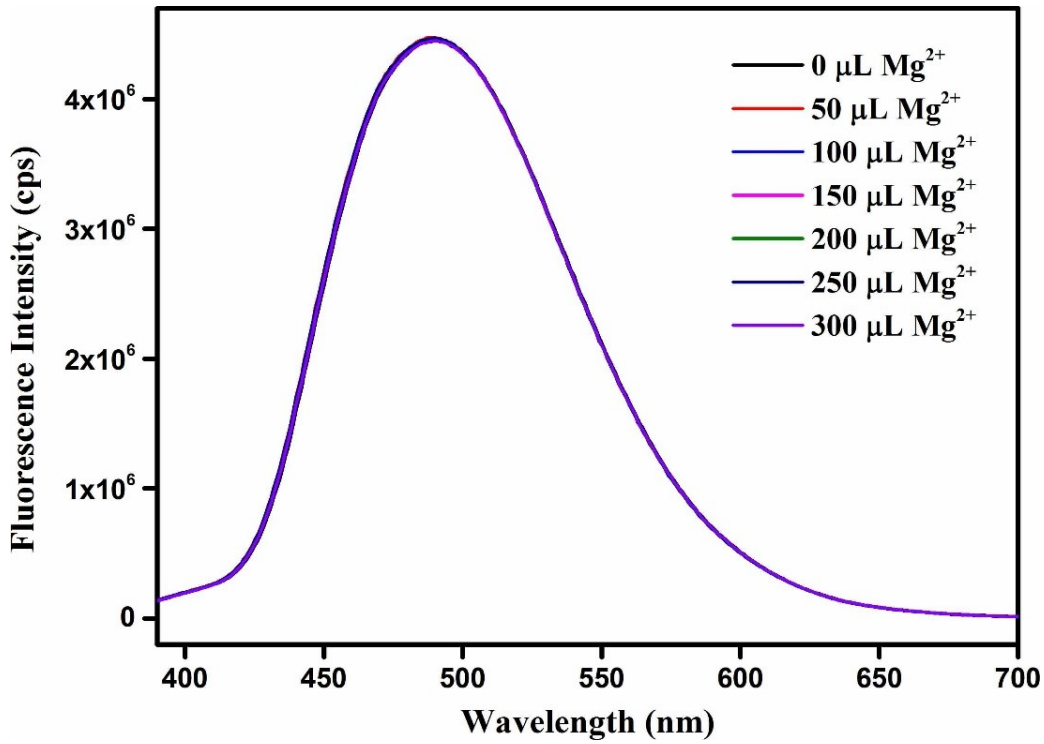

Figure S22. Change of fluorescence intensity of **DUT-52-$(NH_2)_2$-1'** dispersed in PBS after addition of 5 mM solution of Mg^{2+} (300 μL).

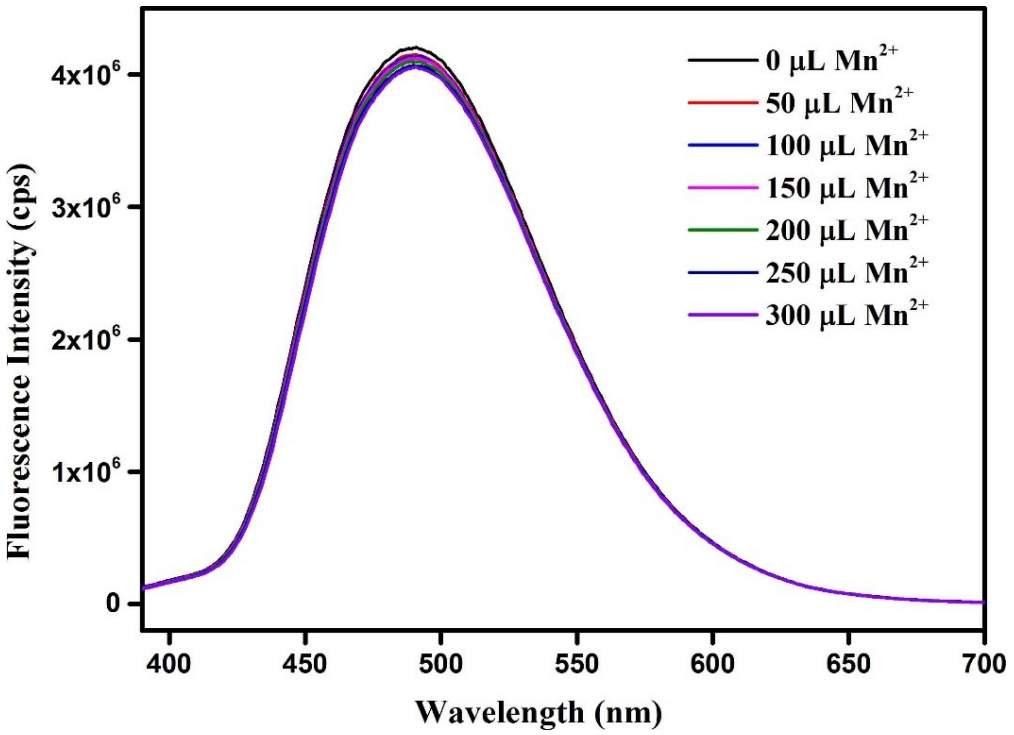

Figure S23. Change of fluorescence intensity of **DUT-52-$(NH_2)_2$-1'** dispersed in PBS after addition of 5 mM solution of Mn^{2+} (300 μL).

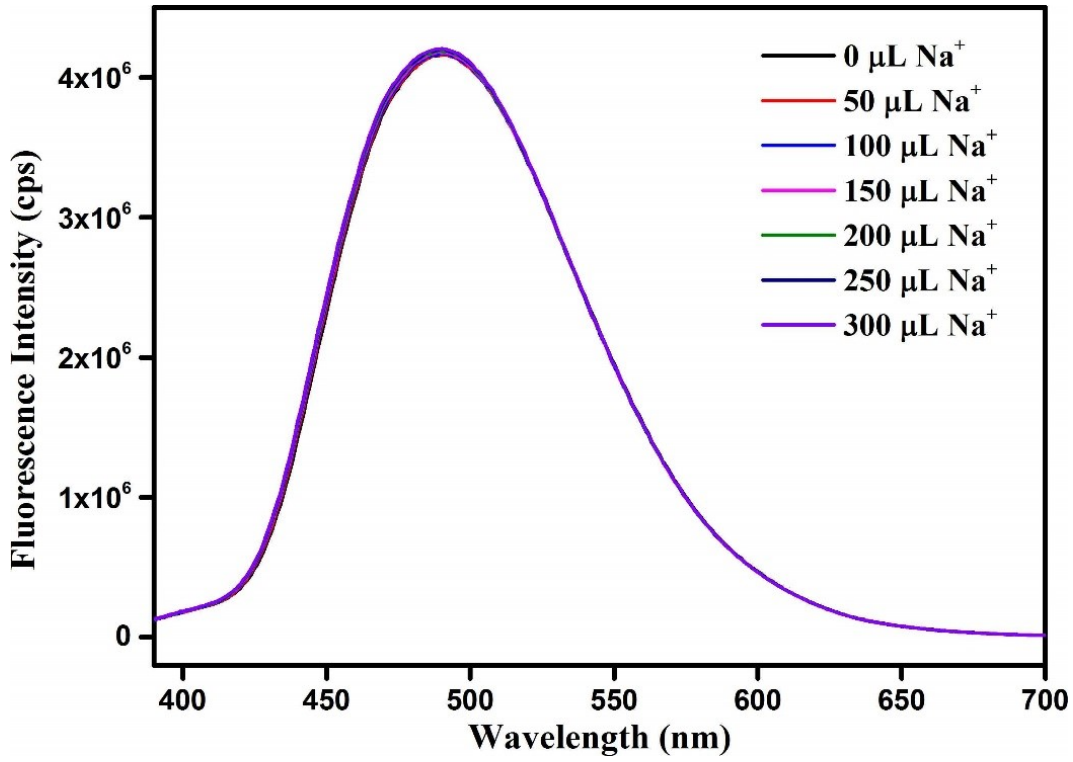

Figure S24. Change of fluorescence intensity of **DUT-52-$(NH_2)_2$-1'** dispersed in PBS after addition of 5 mM solution of Na^{+} (300 μL).

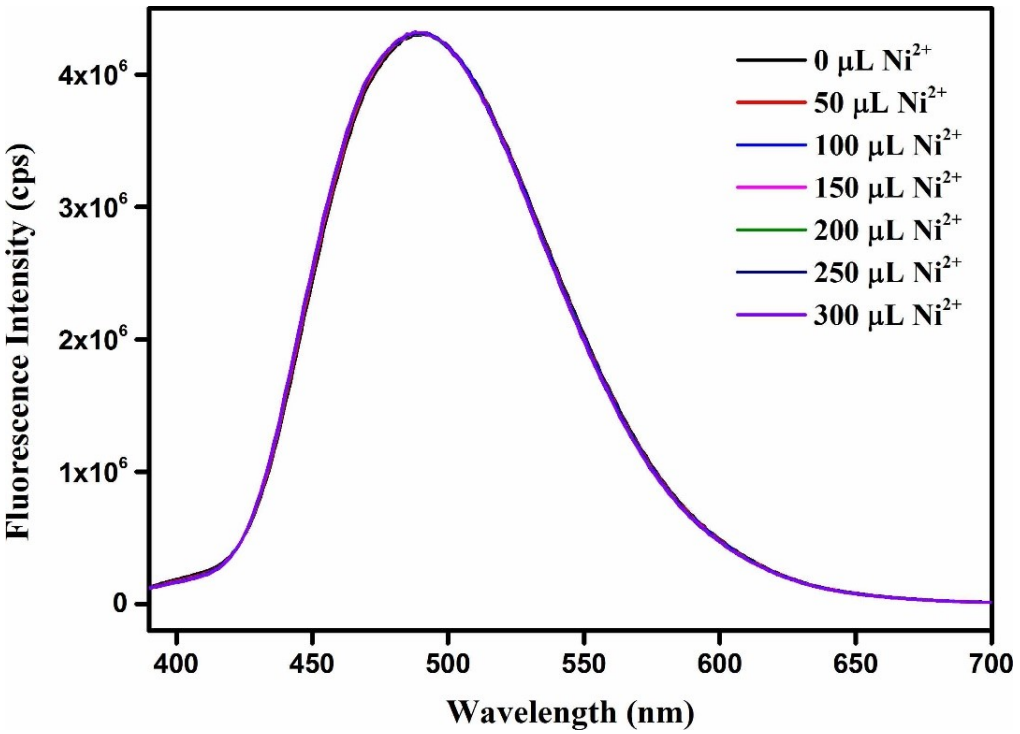

Figure S25. Change of fluorescence intensity of **DUT-52-$(NH_2)_2$-1'** dispersed in PBS after addition of 5 mM solution of Ni^{+} (300 μL).

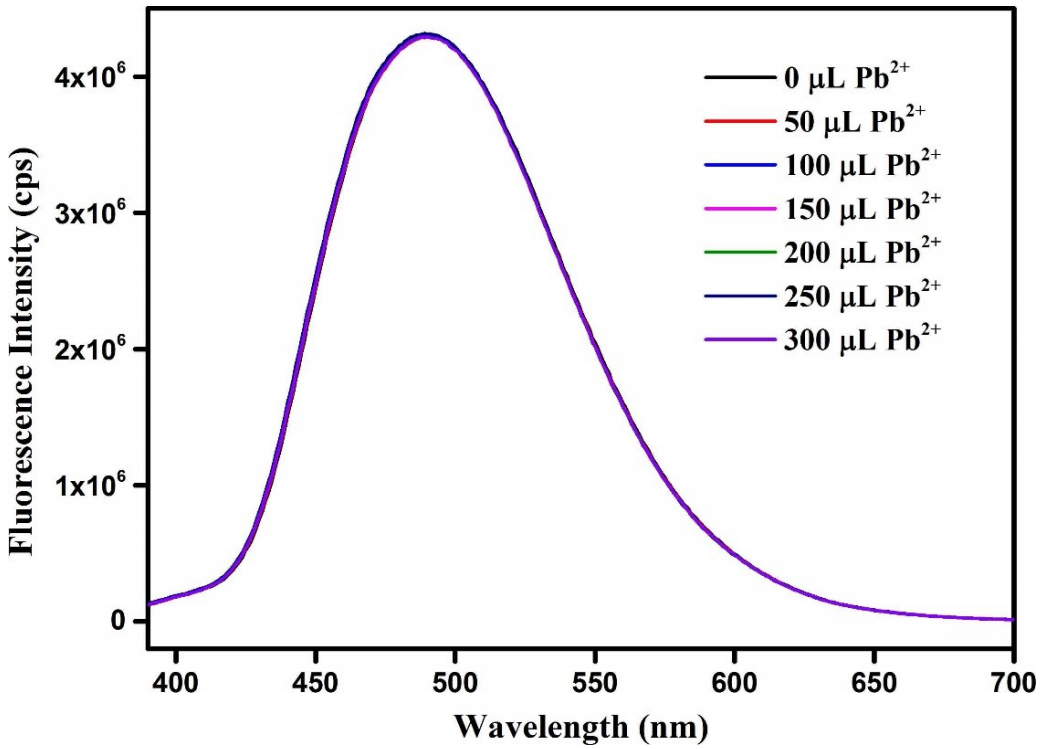

Figure S26. Change of fluorescence intensity of **DUT-52-$(NH_2)_2$-1'** dispersed in PBS after addition of 5 mM solution of Pb^{2+} (300 μL).

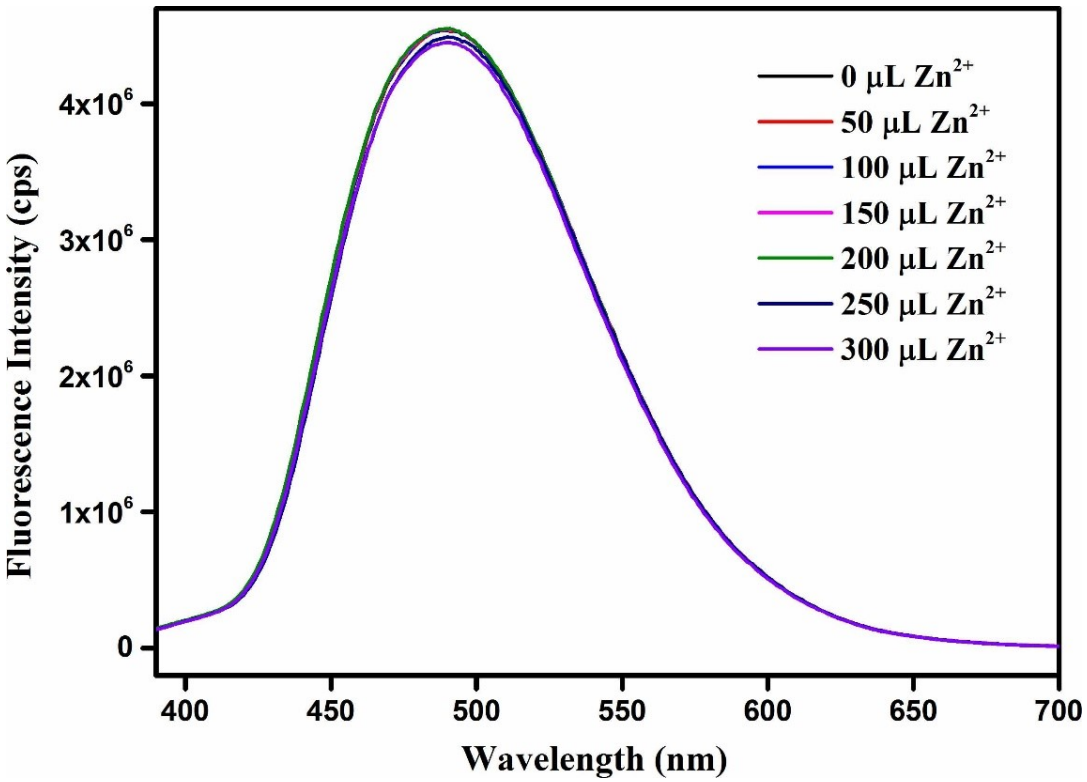

Figure S27. Change of fluorescence intensity of **DUT-52-$(NH_2)_2$-1'** dispersed in PBS after addition of 5 mM solution of Zn^{2+} (300 μL).

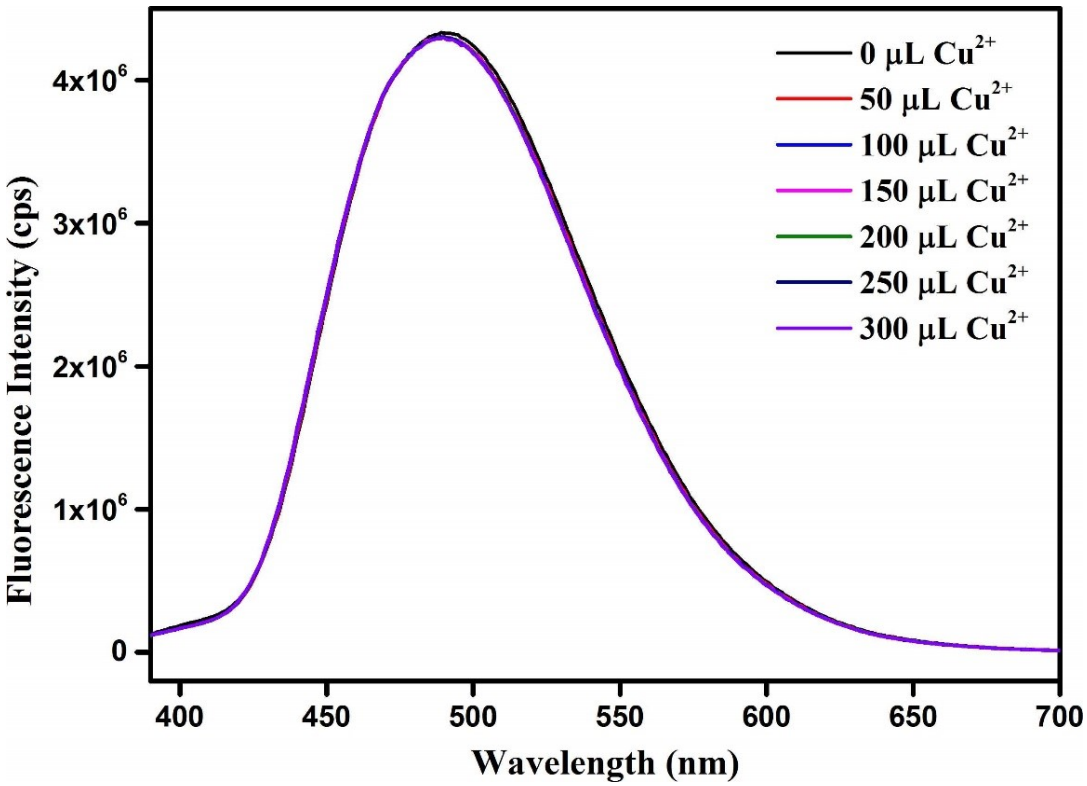

Figure S28. Change of fluorescence intensity of **DUT-52-$(NH_2)_2$-1'** dispersed in PBS after addition of 5 mM solution of Cu^{2+} (300 μL).

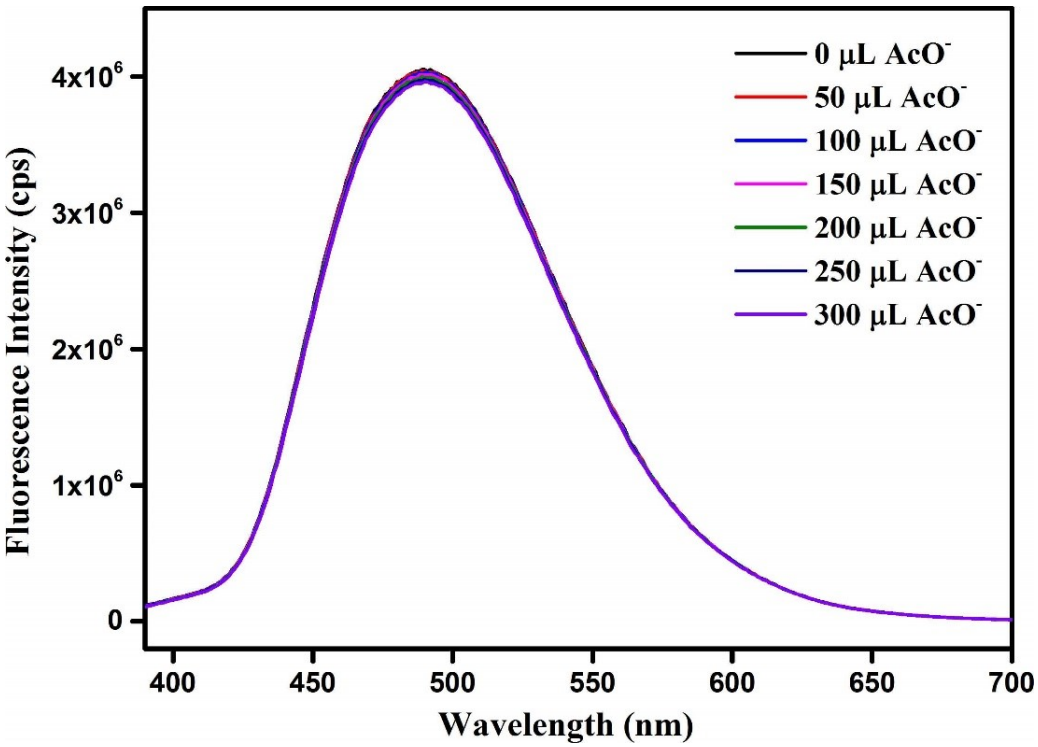

Figure S29. Change of fluorescence intensity of **DUT-52-$(NH_2)_2$-1'** dispersed in PBS after addition of 5 mM solution of AcO^- (300 μL).

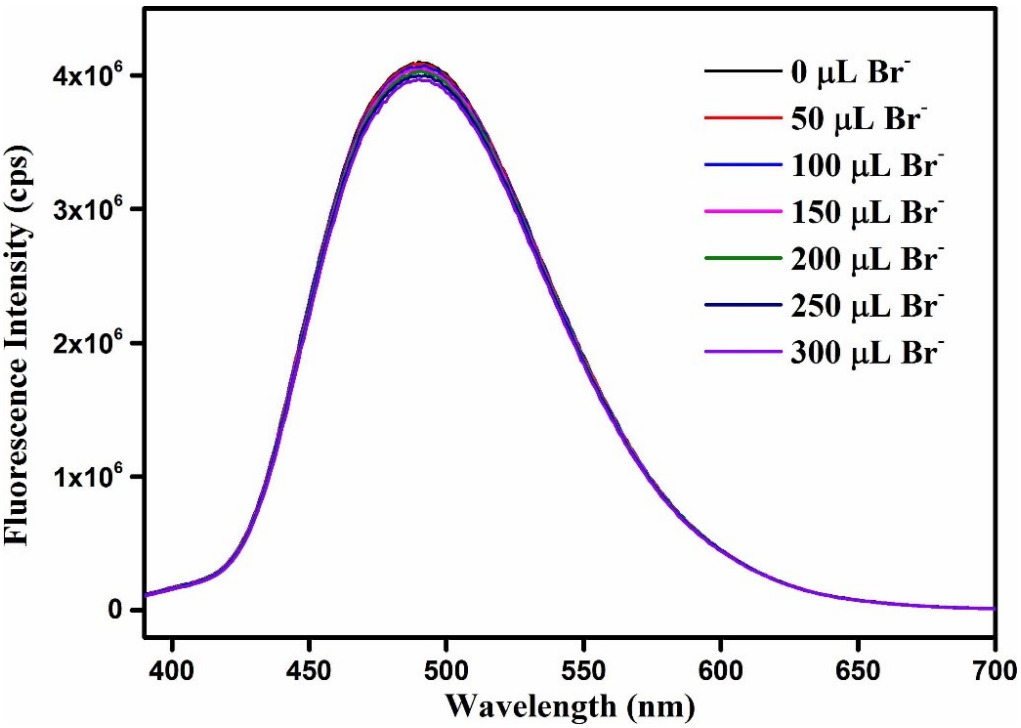

Figure S30. Change of fluorescence intensity of **DUT-52-$(NH_2)_2$-1'** dispersed in PBS after addition of 5 mM solution of Br^- (300 μL).

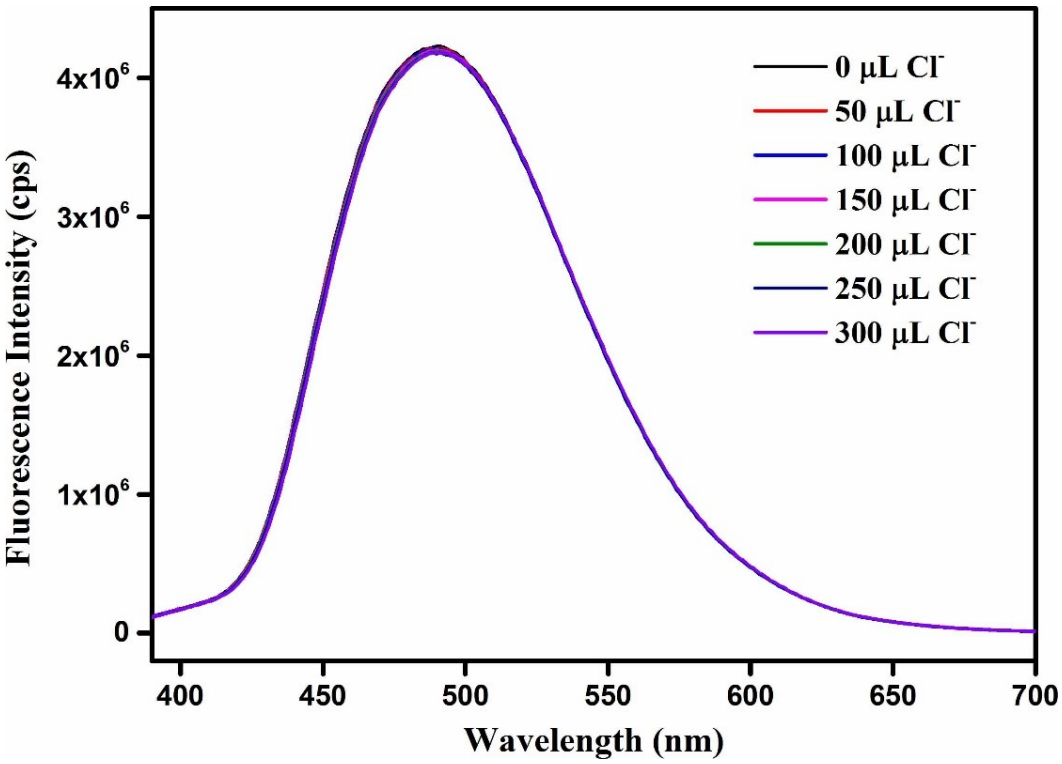

Figure S31. Change of fluorescence intensity of **DUT-52-$(NH_2)_2$-1'** dispersed in PBS after addition of 5 mM solution of Cl^- (300 µL).

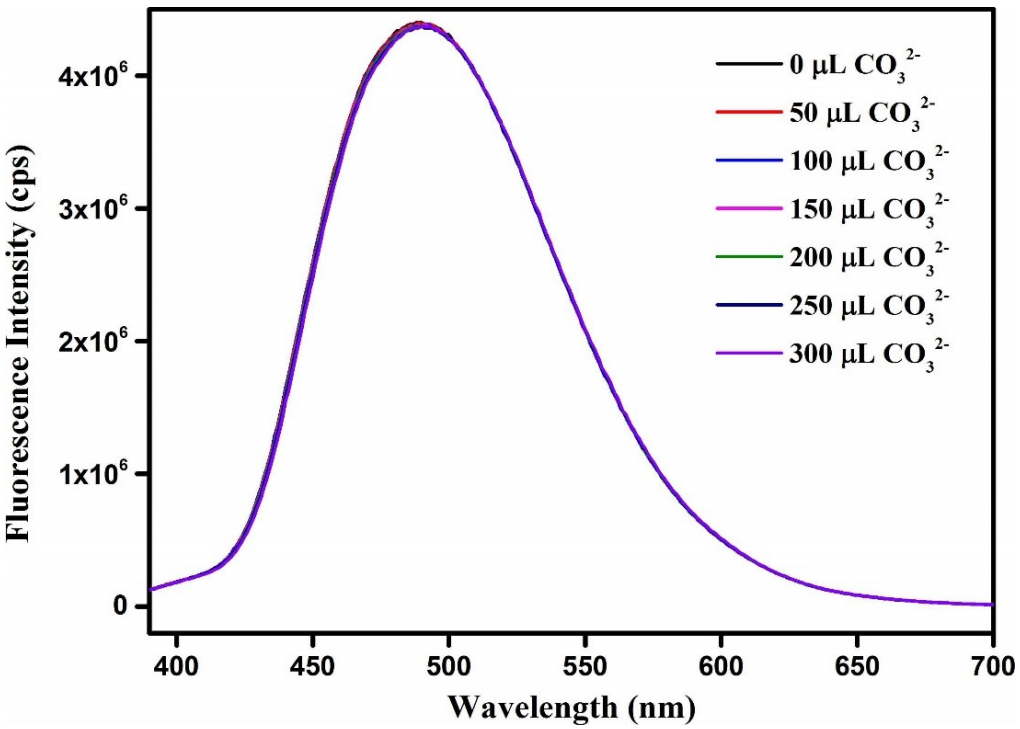

Figure S32. Change of fluorescence intensity of **DUT-52-$(NH_2)_2$-1'** dispersed in PBS after addition of 5 mM solution of CO_3^- (300 µL).

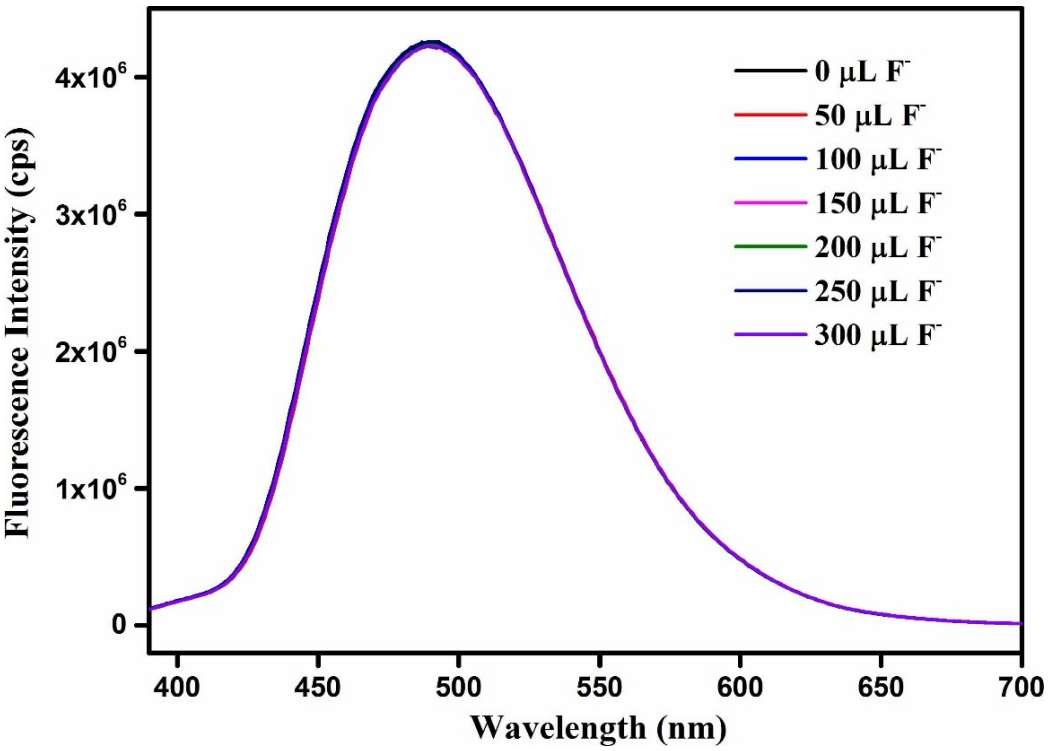

Figure S33. Change of fluorescence intensity of **DUT-52-$(NH_2)_2$-1'** dispersed in PBS after addition of 5 mM solution of F^- (300 μL).

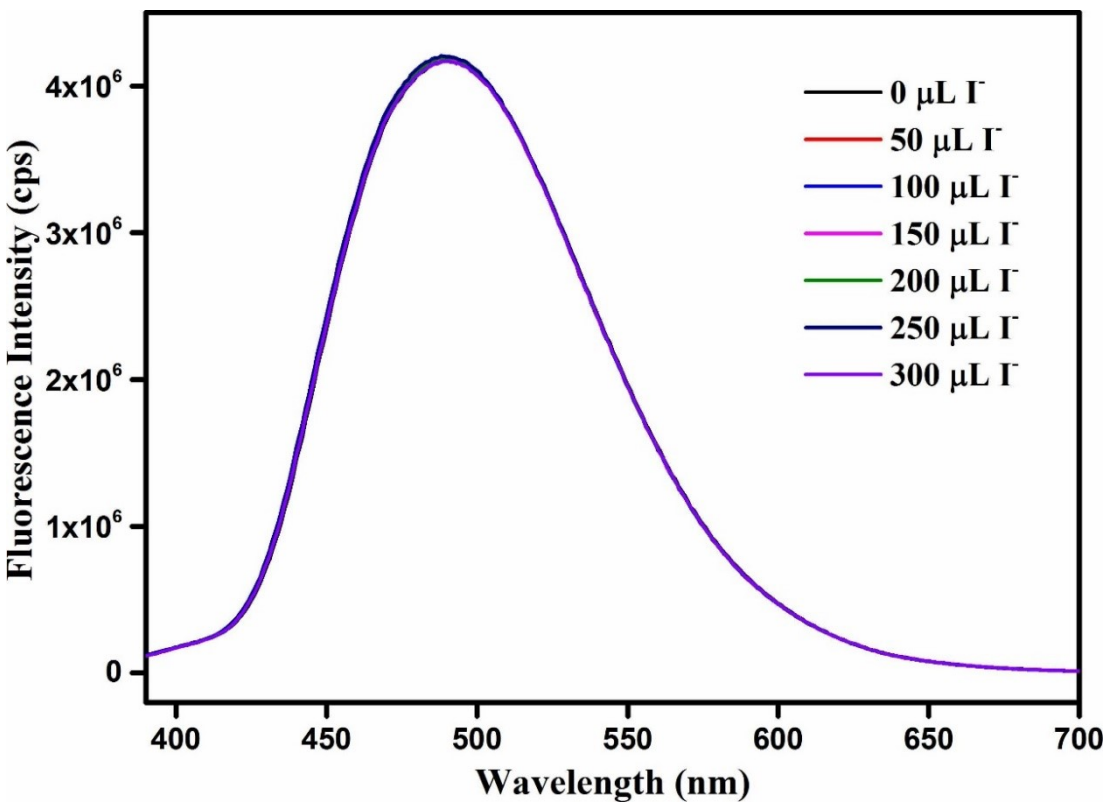

Figure S34. Change of fluorescence intensity of **DUT-52-$(NH_2)_2$-1'** dispersed in PBS after addition of 5 mM solution of I^- (300 μL).

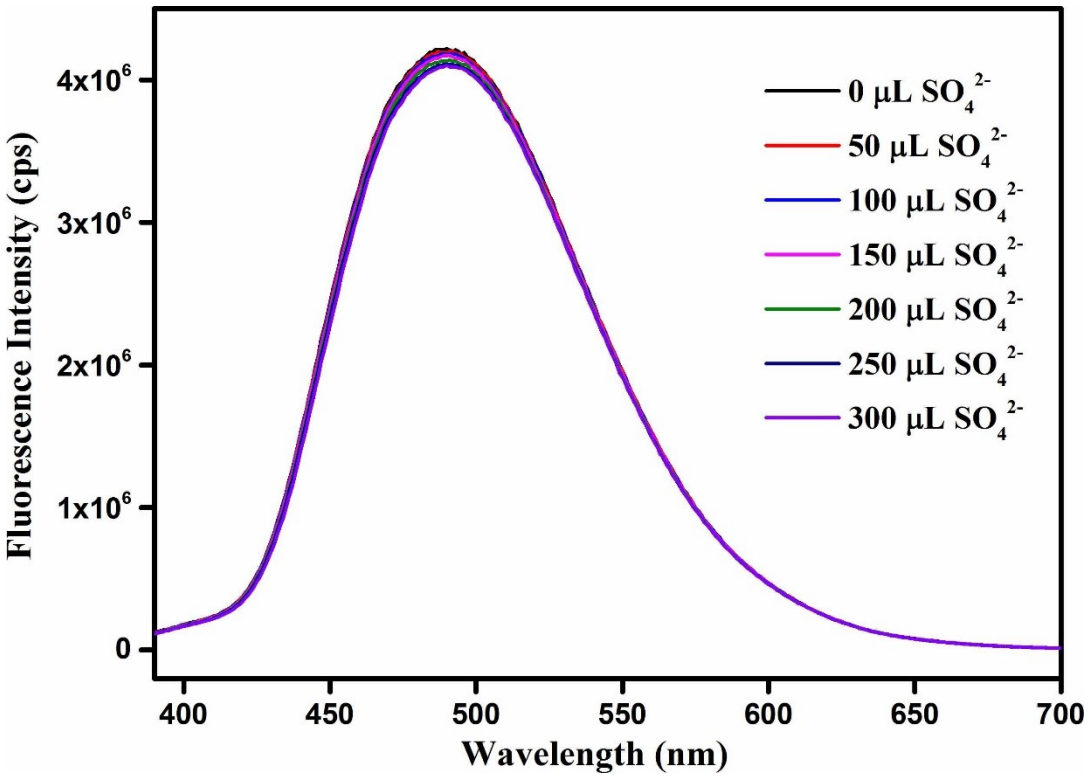

Figure S35. Change of fluorescence intensity of **DUT-52-$(NH_2)_2$-1'** dispersed in PBS after addition of 5 mM solution of SO_4^{2-} (300 μL).

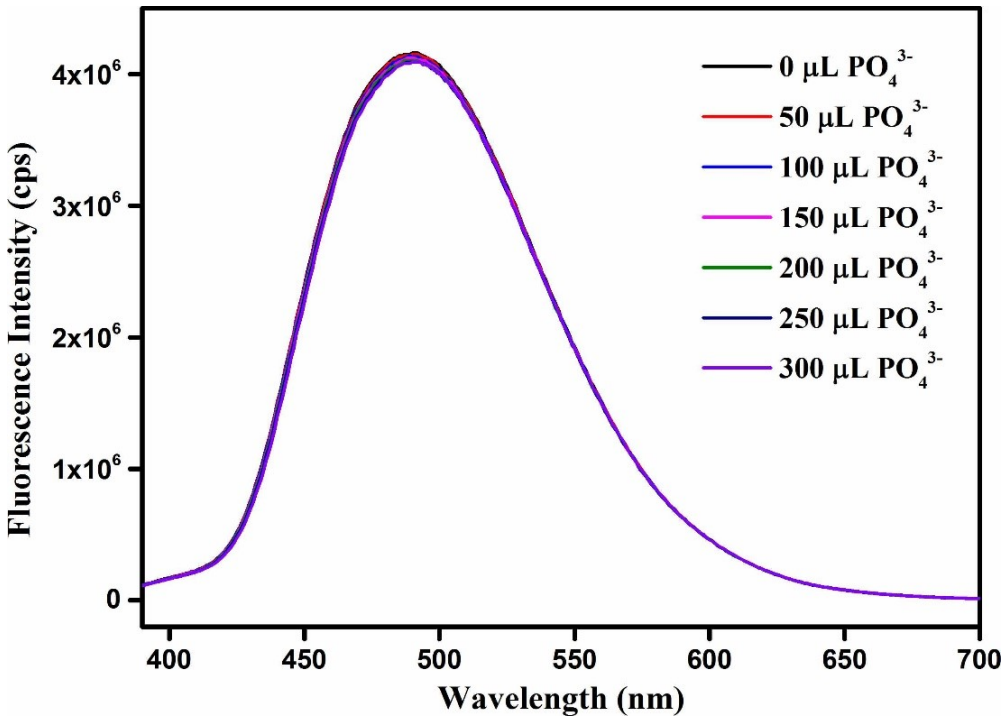

Figure S36. Change of fluorescence intensity of **DUT-52-$(NH_2)_2$-1'** dispersed in PBS after addition of 5 mM solution of PO_4^{3-} (300 μL).

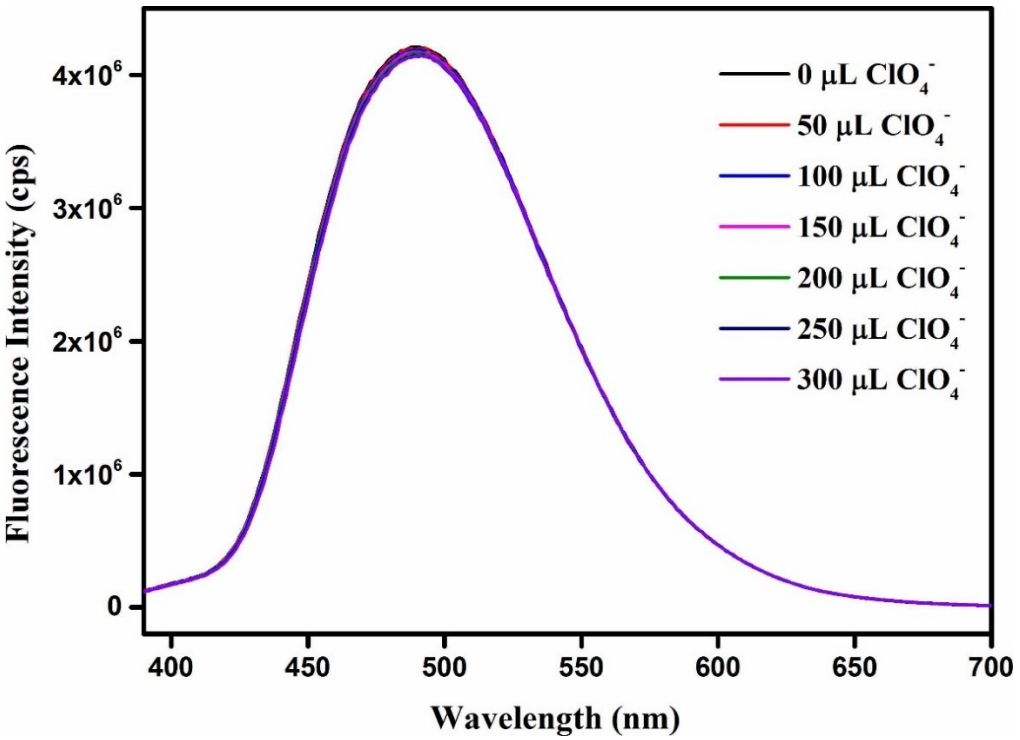

Figure S37. Change of fluorescence intensity of **DUT-52-$(NH_2)_2$-1'** dispersed in PBS after addition of 5 mM solution of ClO_4^- (300 μL).

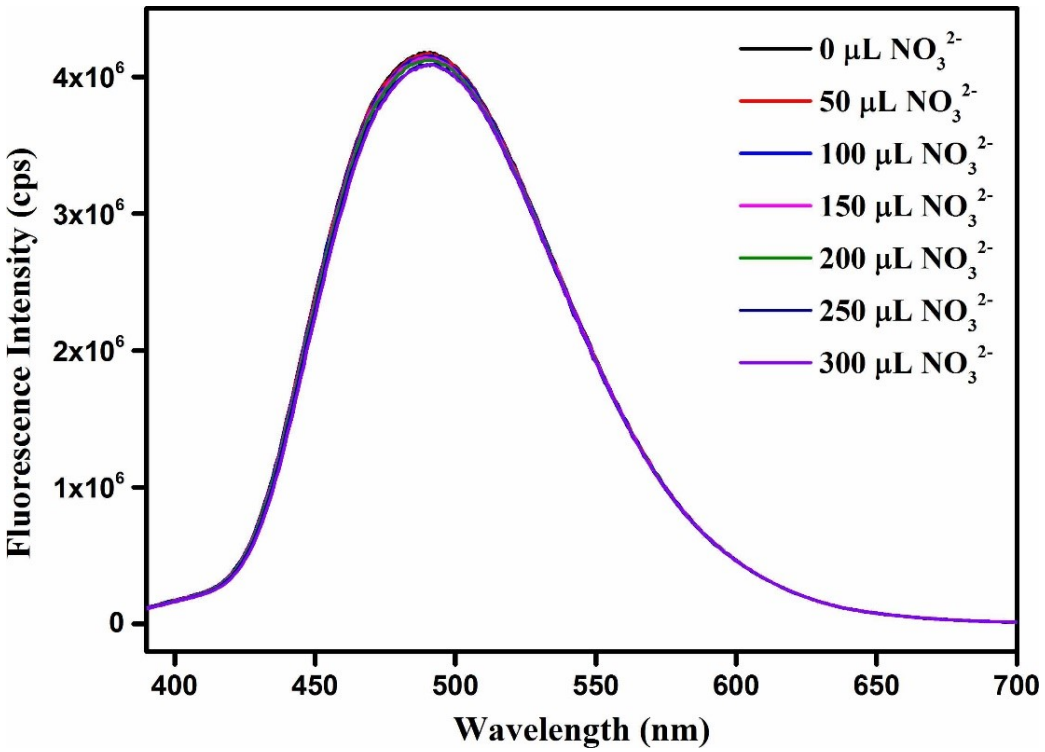

Figure S38. Change of fluorescence intensity of **DUT-52-$(NH_2)_2$-1'** dispersed in PBS after addition of 5 mM solution of NO_3^{2-} (300 μL).

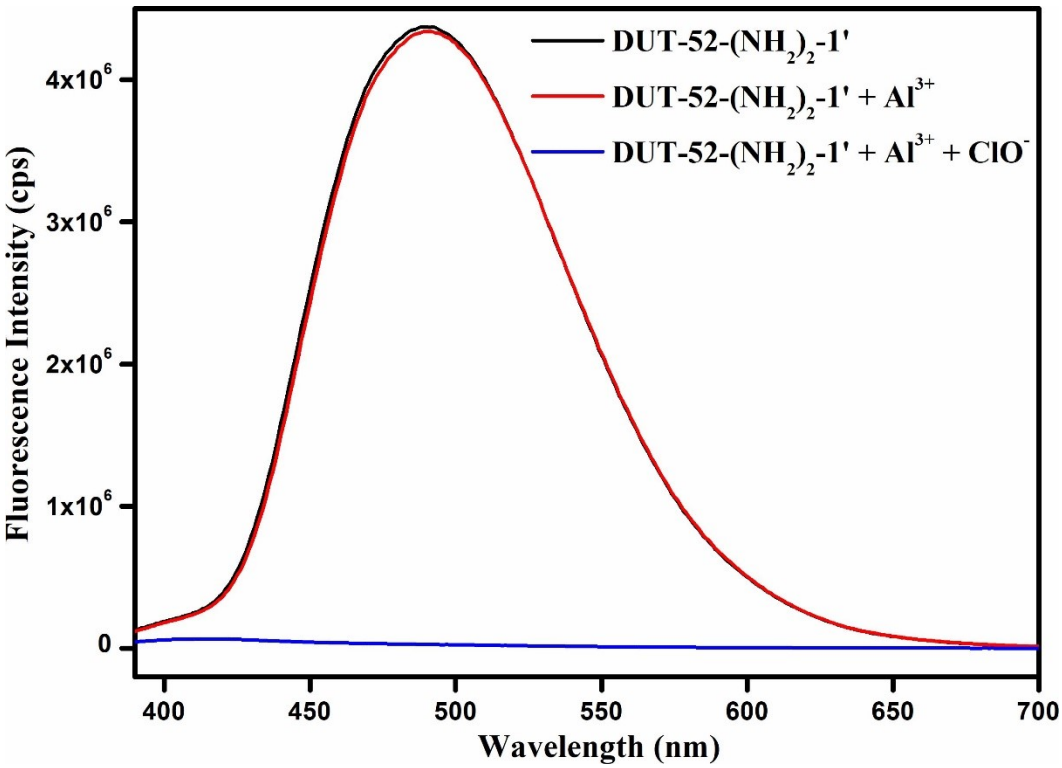

Figure S39. Change in the fluorescence emission intensity of **DUT-52-(NH$_2$)$_2$-1'** upon addition of 5 mM ClO^- solution (300 µL) in presence of 5 mM Al^{3+} (300 µL) solution.

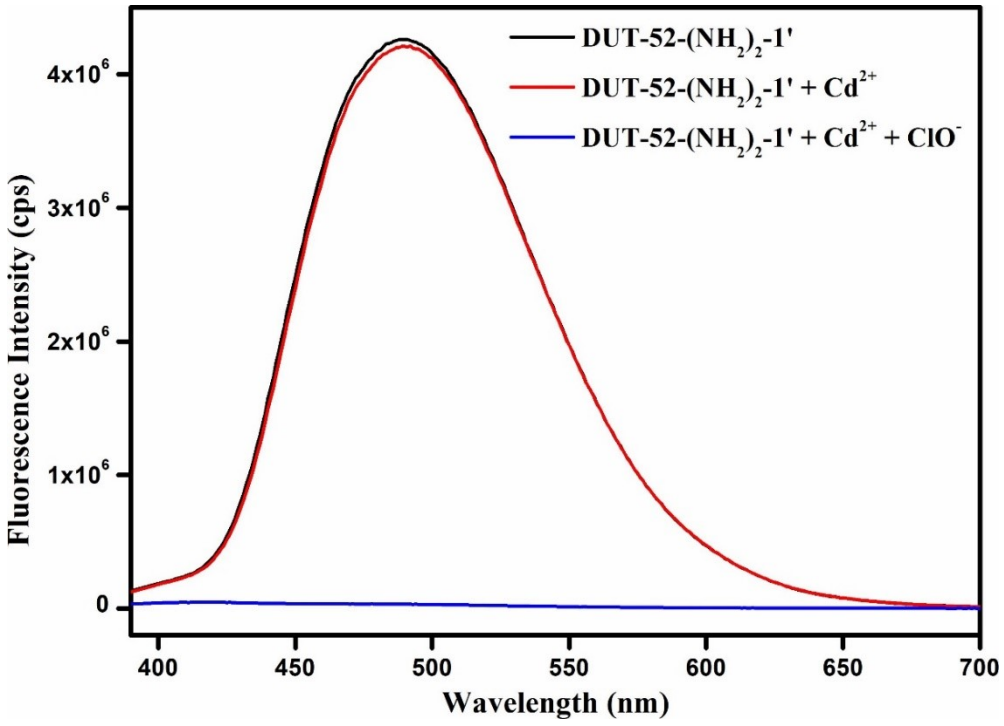

Figure S40. Change in the fluorescence emission intensity of **DUT-52-(NH$_2$)$_2$-1'** upon addition of 5 mM ClO^- solution (300 µL) in presence of 5 mM Cd^{2+} (300 µL) solution.

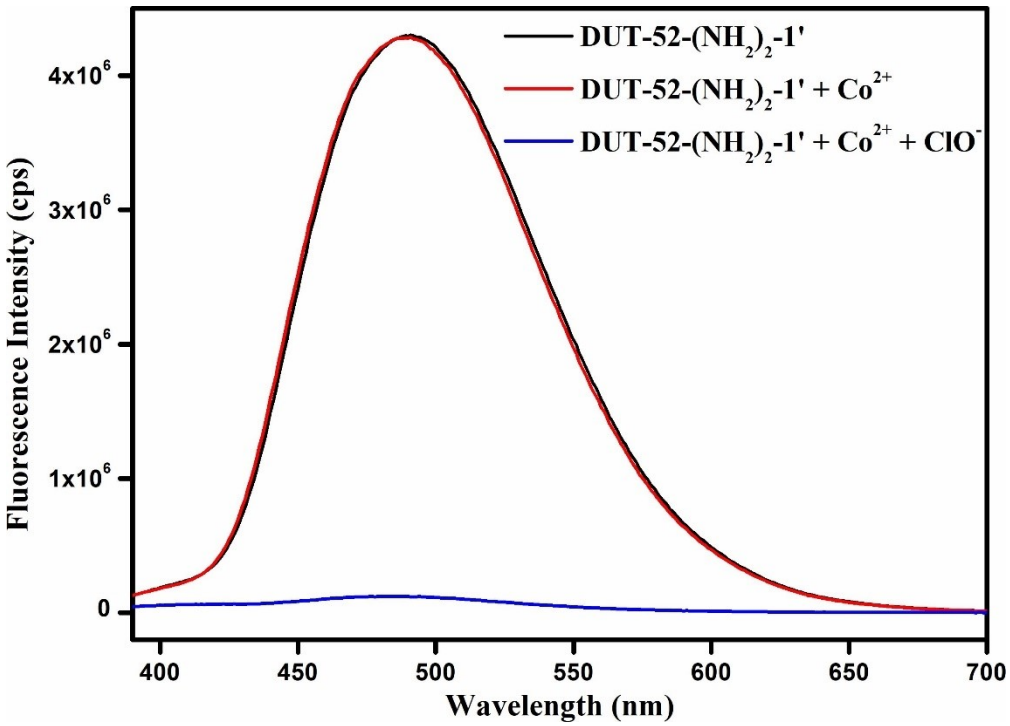

Figure S41. Change in the fluorescence emission intensity of **DUT-52-$(NH_2)_2$-1'** upon addition of 5 mM ClO^- solution (300 µL) in presence of 5 mM Co^{2+} (300 µL) solution.

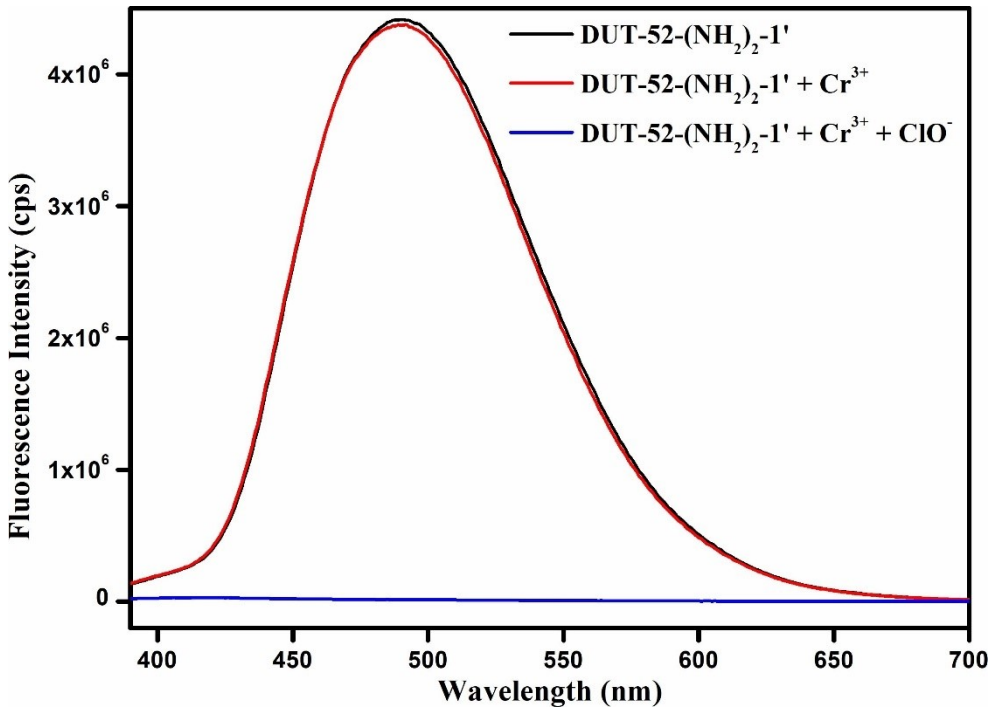

Figure S42. Change in the fluorescence emission intensity of **DUT-52-$(NH_2)_2$-1'** upon addition of 5 mM ClO^- solution (300 µL) in presence of 5 mM Cr^{3+} (300 µL) solution.

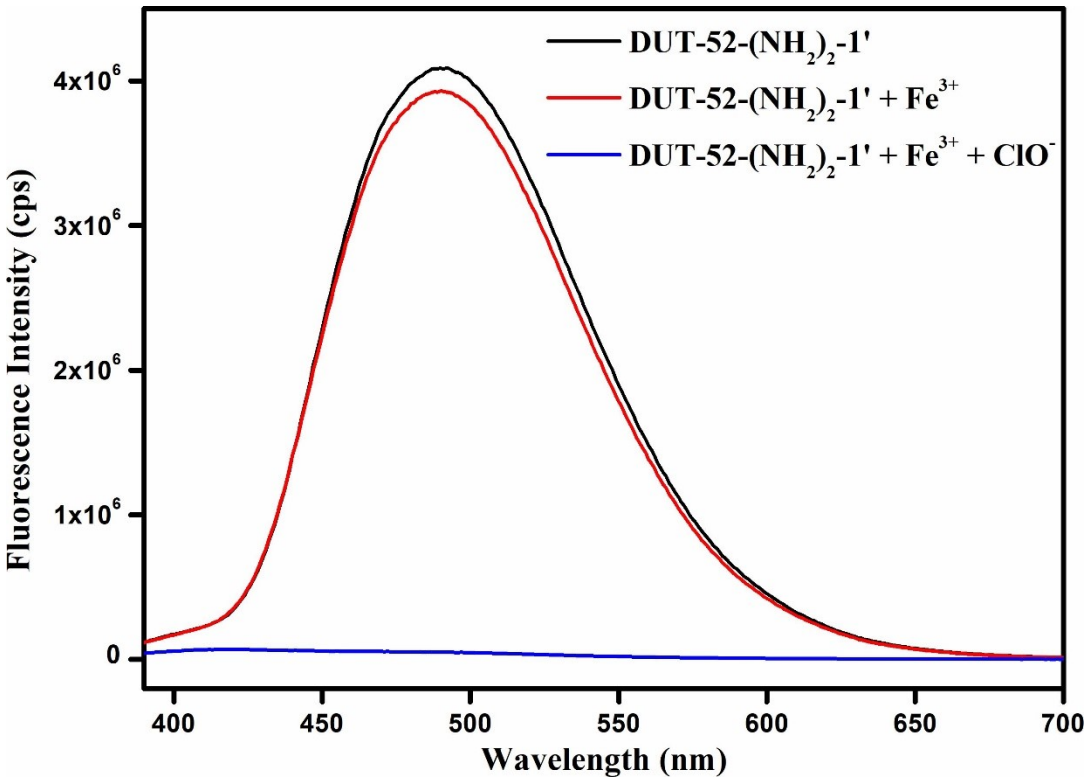

Figure S43. Change in the fluorescence emission intensity of **DUT-52-$(NH_2)_2$-1'** upon addition of 5 mM ClO^- solution (300 µL) in presence of 5 mM Fe^{3+} (300 µL) solution.

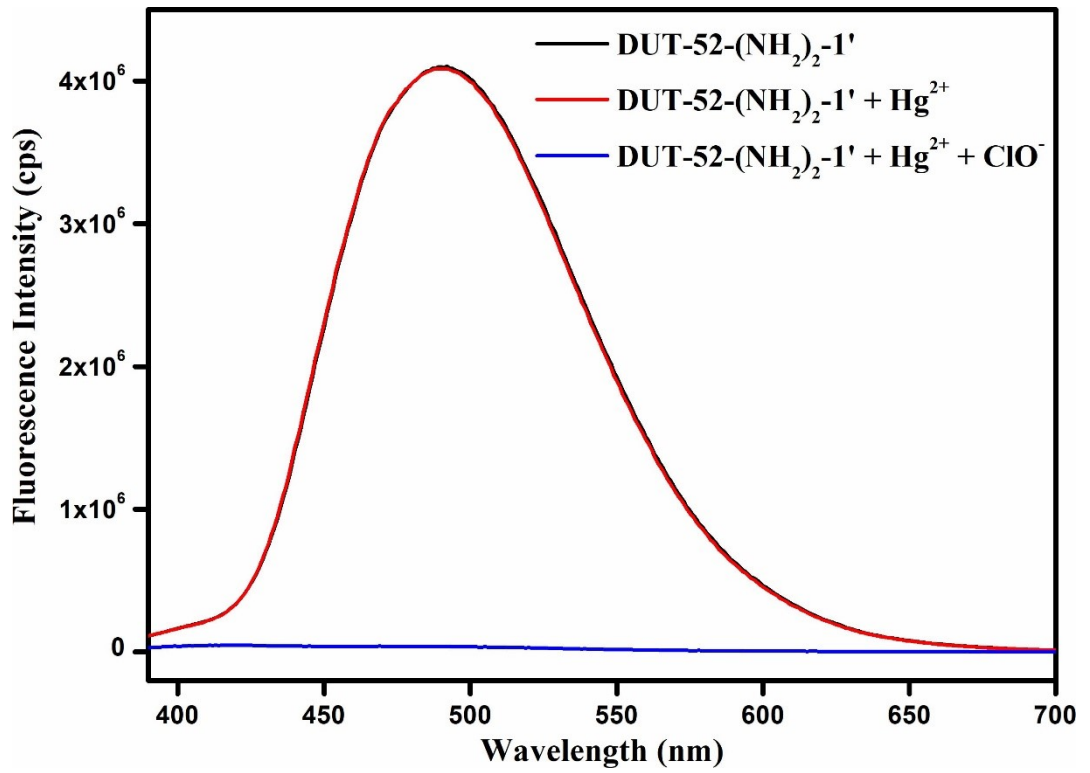

Figure S44. Change in the fluorescence emission intensity of **DUT-52-$(NH_2)_2$-1'** upon addition of 5 mM ClO^- solution (300 µL) in presence of 5 mM Hg^{2+} (300 µL) solution.

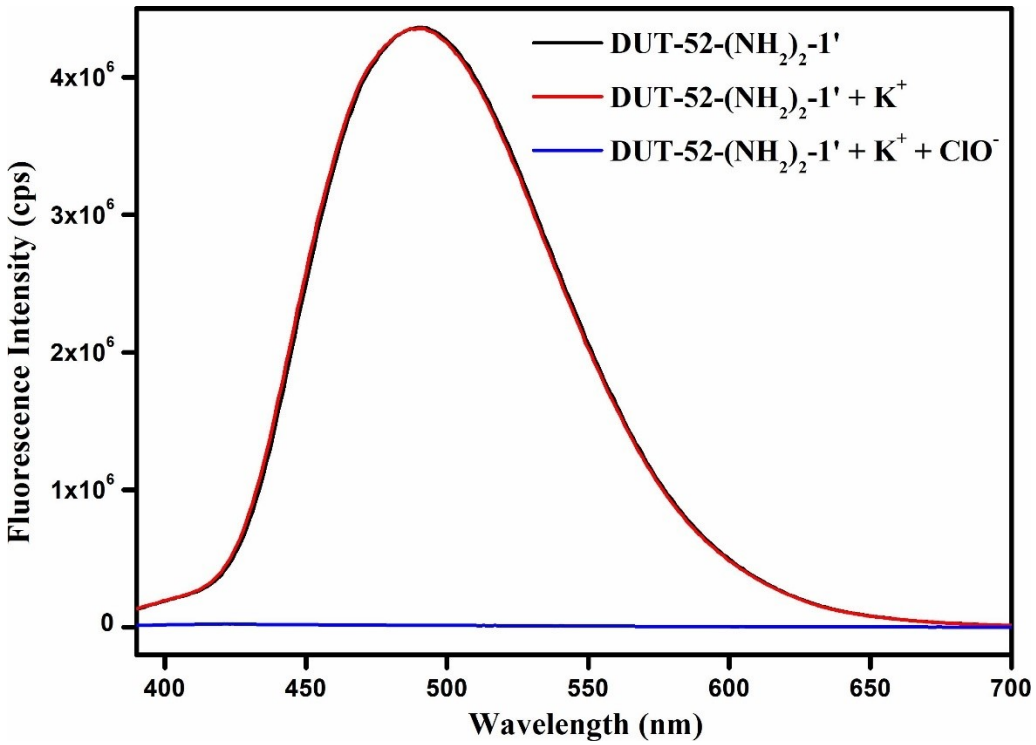

Figure S45. Change in the fluorescence emission intensity of **DUT-52-$(NH_2)_2$-1'** upon addition of 5 mM ClO^- solution (300 µL) in presence of 5 mM K^+ (300 µL) solution.

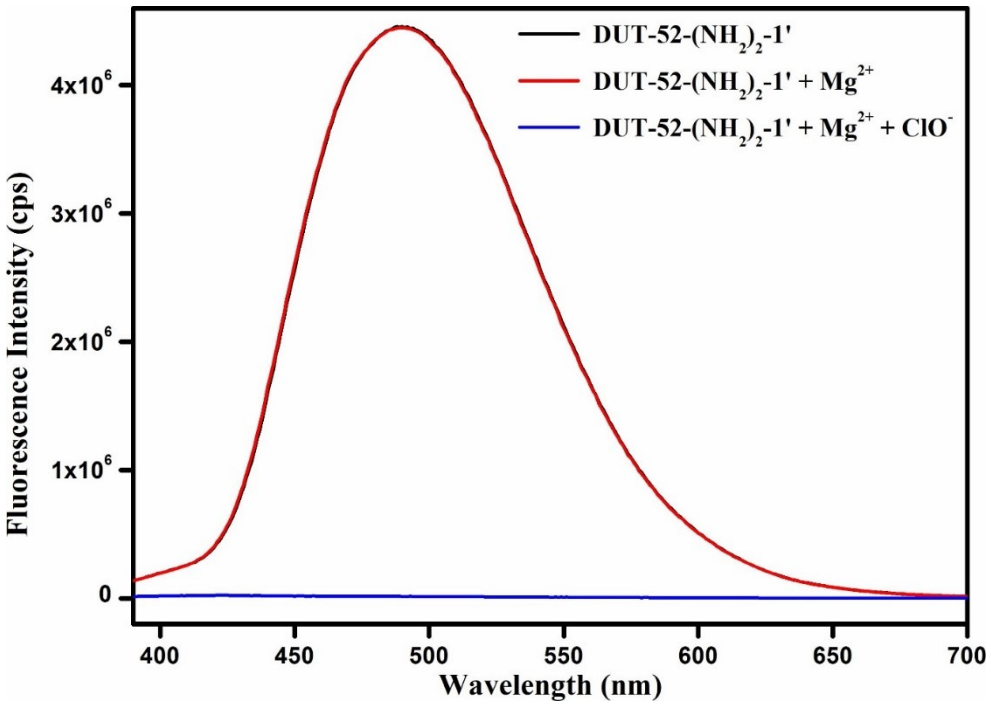

Figure S46. Change in the fluorescence emission intensity of **DUT-52-$(NH_2)_2$-1'** upon addition of 5 mM ClO^- solution (300 µL) in presence of 5 mM Mg^{2+} (300 µL) solution.

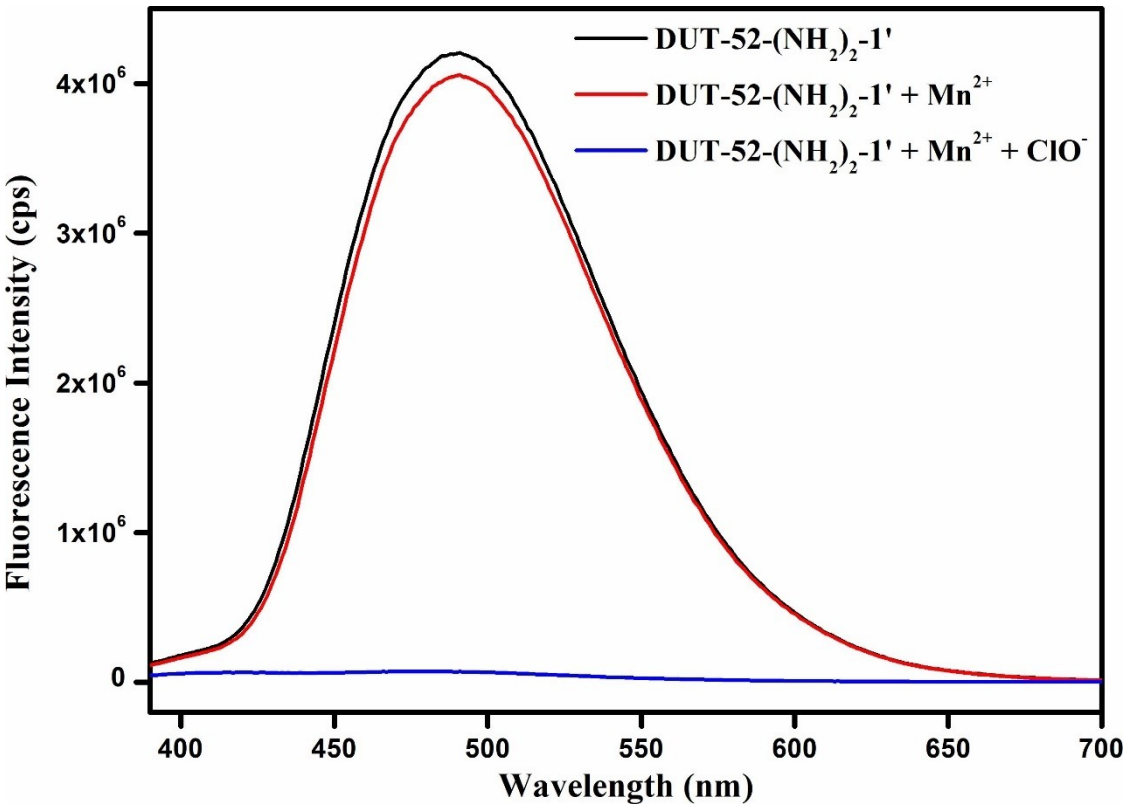

Figure S47. Change in the fluorescence emission intensity of **DUT-52-$(NH_2)_2$-1'** upon addition of 5 mM ClO^- solution (300 µL) in presence of 5 mM Mn^{2+} (300 µL) solution.

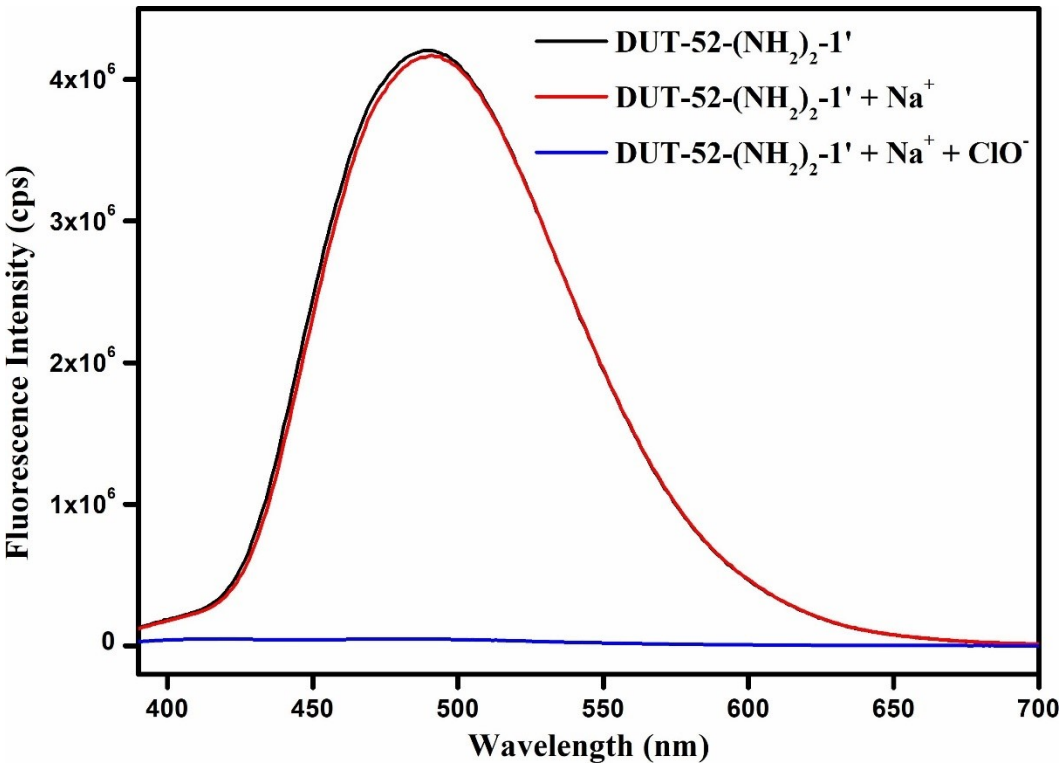

Figure S48. Change in the fluorescence emission intensity of **DUT-52-$(NH_2)_2$-1'** upon addition of 5 mM ClO^- solution (300 µL) in presence of 5 mM Na^+ (300 µL) solution.

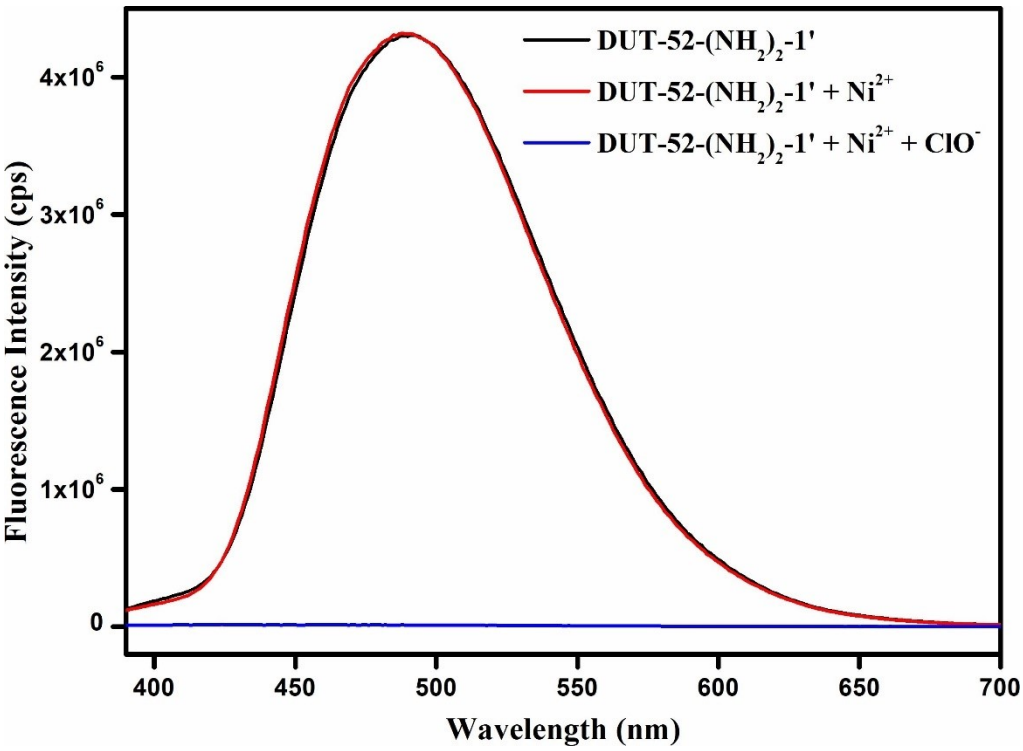

Figure S49. Change in the fluorescence emission intensity of **DUT-52-$(NH_2)_2$-1'** upon addition of 5 mM ClO^- solution (300 µL) in presence of 5 mM Ni^{2+} (300 µL) solution.

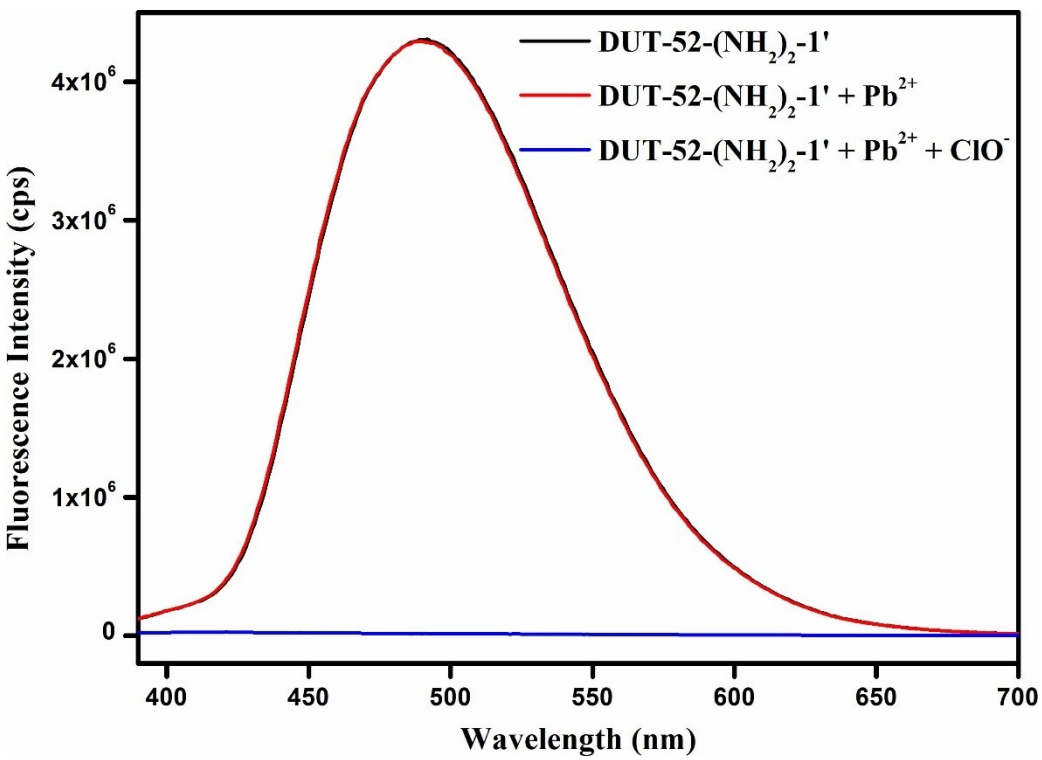

Figure S50. Change in the fluorescence emission intensity of **DUT-52-$(NH_2)_2$-1'** upon addition of 5 mM ClO^- solution (300 µL) in presence of 5 mM Pb^{2+} (300 µL) solution.

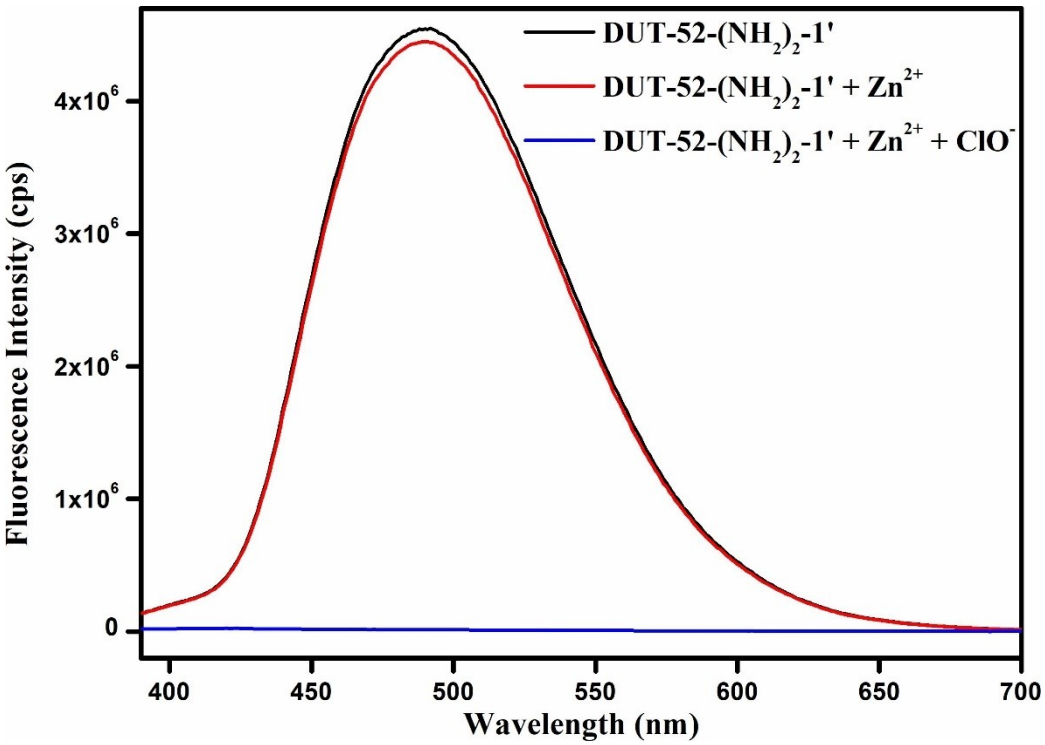

Figure S51. Change in the fluorescence emission intensity of **DUT-52-$(NH_2)_2$-1'** upon addition of 5 mM ClO^- solution (300 µL) in presence of 5 mM Zn^{2+} (300 µL) solution.

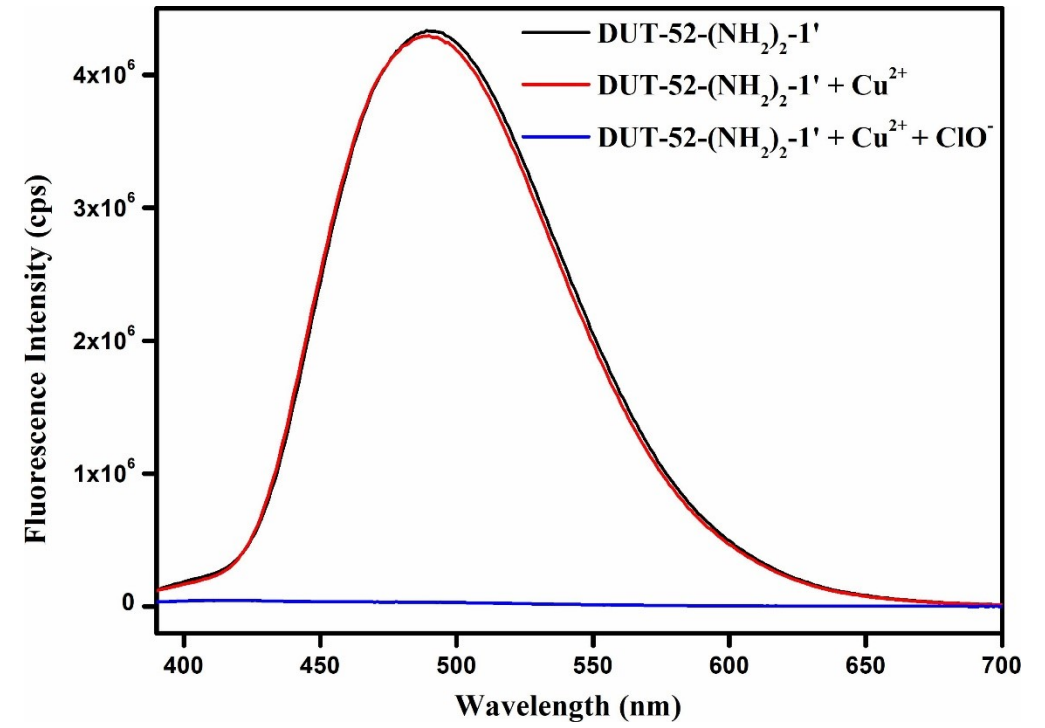

Figure S52. Change in the fluorescence emission intensity of **DUT-52-$(NH_2)_2$-1'** upon addition of 5 mM ClO^- solution (300 µL) in presence of 5 mM Cu^{2+} (300 µL) solution.

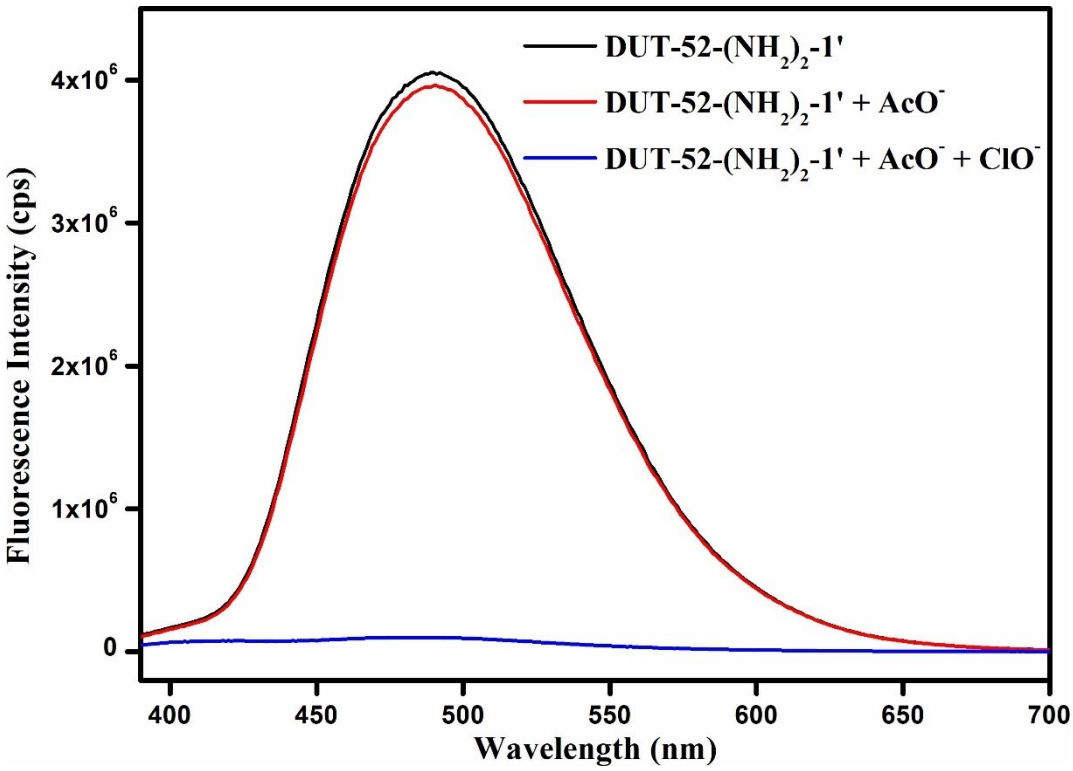

Figure S53. Change in the fluorescence emission intensity of **DUT-52-$(NH_2)_2$-1'** upon addition of 5 mM ClO^- solution (300 µL) in presence of 5 mM AcO^- (300 µL) solution.

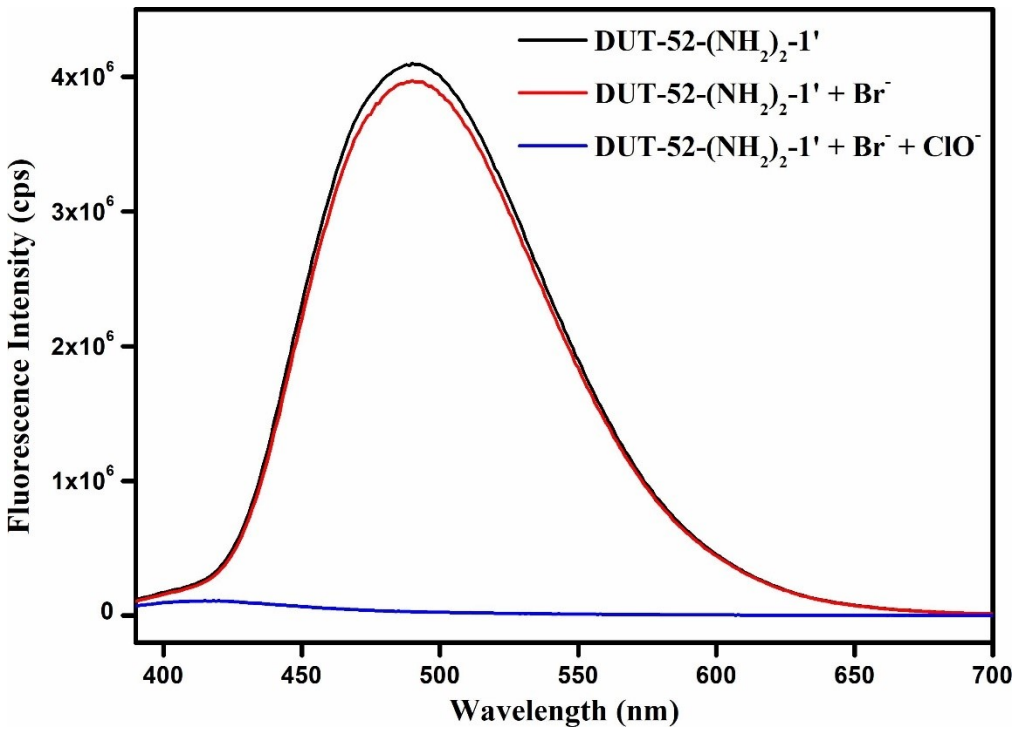

Figure S54. Change in the fluorescence emission intensity of **DUT-52-$(NH_2)_2$-1'** upon addition of 5 mM ClO^- solution (300 µL) in presence of 5 mM Br^- (300 µL) solution.

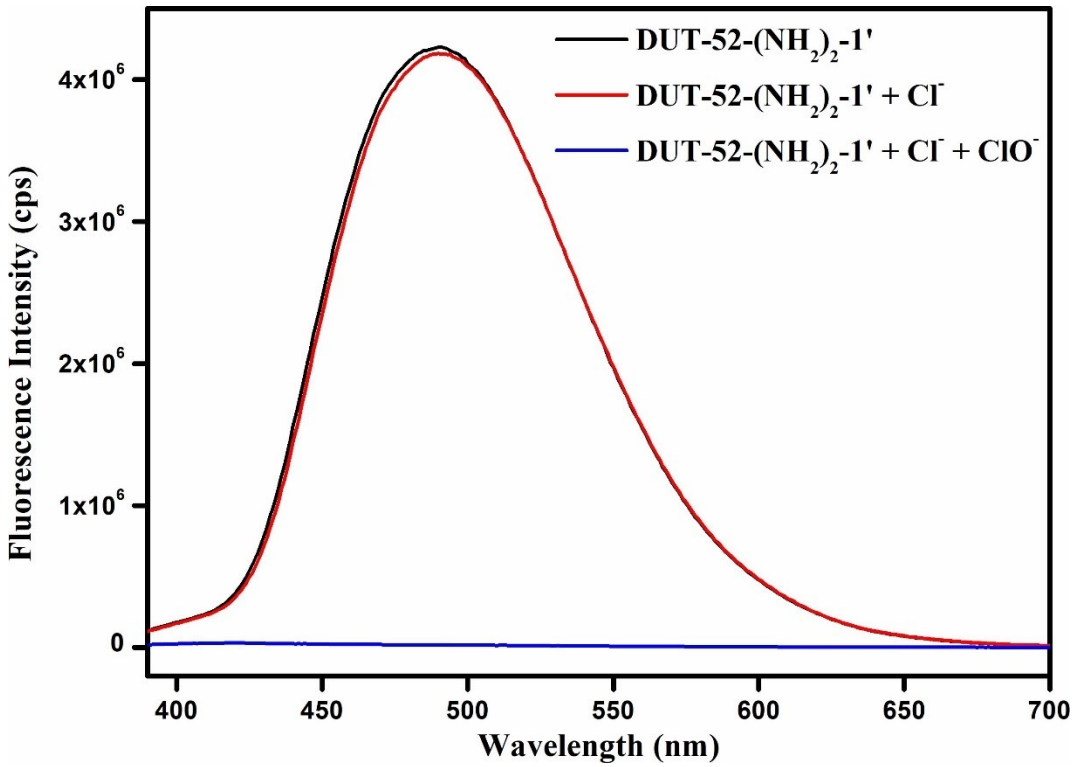

Figure S55. Change in the fluorescence emission intensity of **DUT-52-$(NH_2)_2$-1'** upon addition of 5 mM ClO^- solution (300 µL) in presence of 5 mM Cl^- (300 µL) solution.

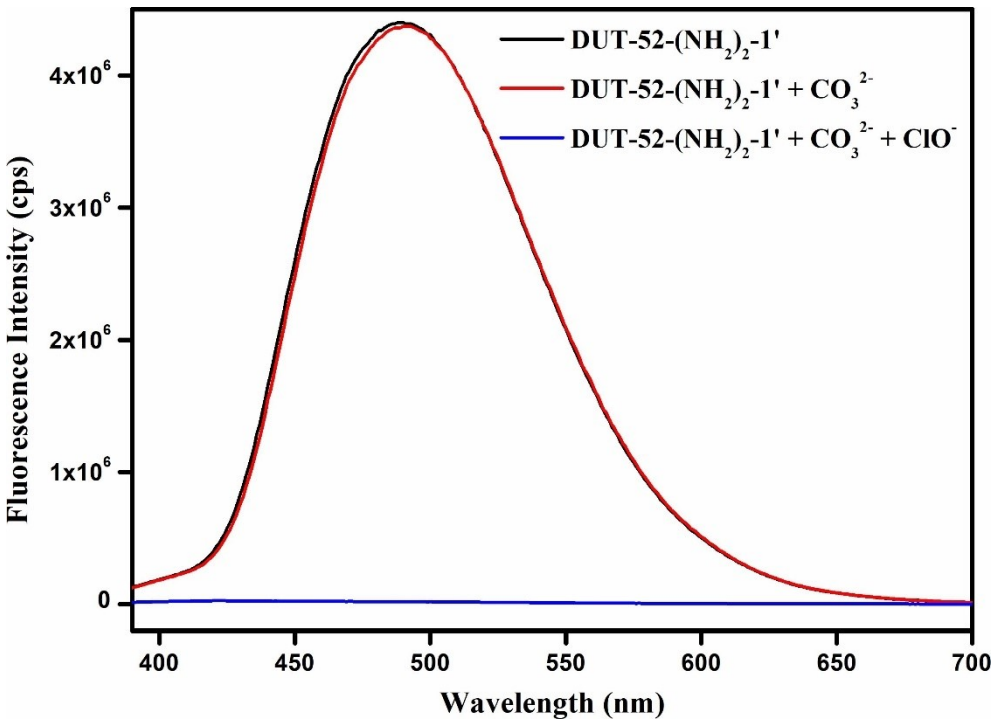

Figure S56. Change in the fluorescence emission intensity of **DUT-52-$(NH_2)_2$-1'** upon addition of 5 mM ClO^- solution (300 µL) in presence of 5 mM CO_3^{2-} (300 µL) solution.

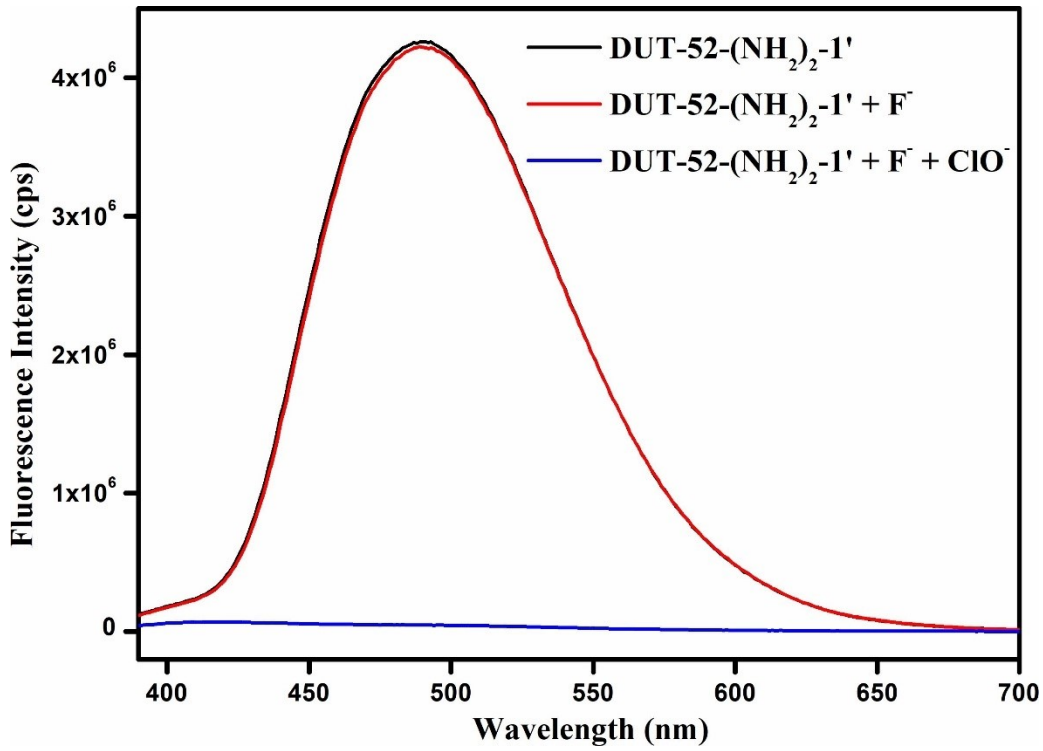

Figure S57. Change in the fluorescence emission intensity of **DUT-52-(NH$_2$)$_2$-1'** upon addition of 5 mM ClO^- solution (300 µL) in presence of 5 mM F^- (300 µL) solution.

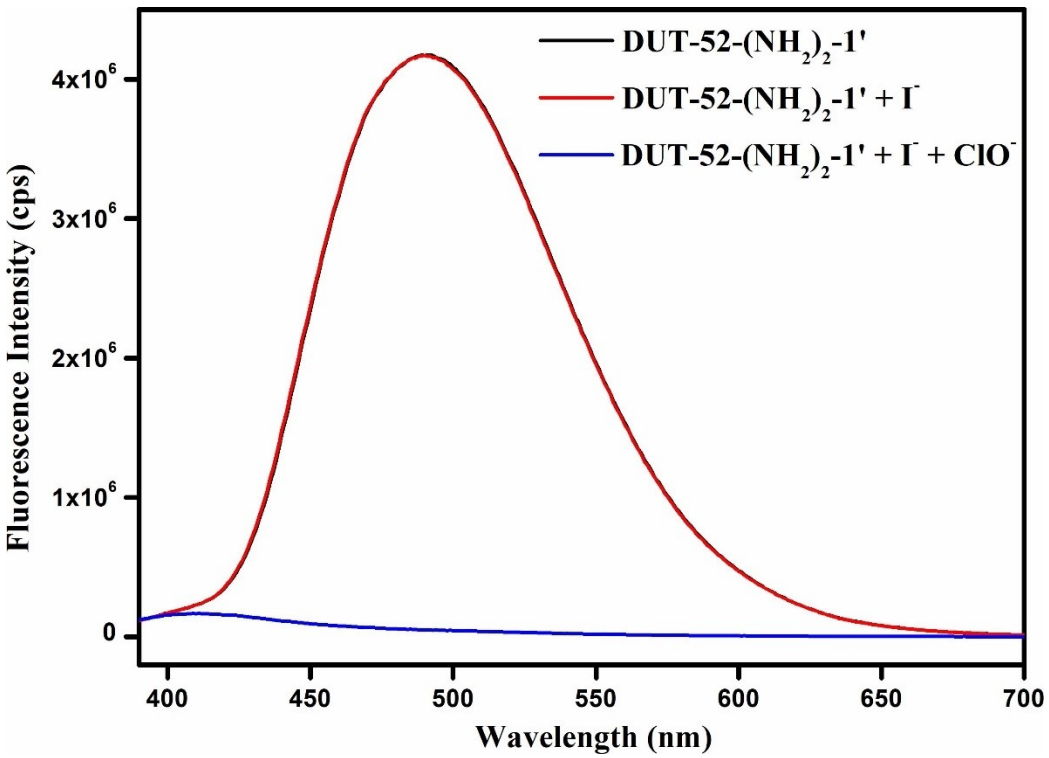

Figure S58. Change in the fluorescence emission intensity of **DUT-52-(NH$_2$)$_2$-1'** upon addition of 5 mM ClO^- solution (300 µL) in presence of 5 mM I^- (300 µL) solution.

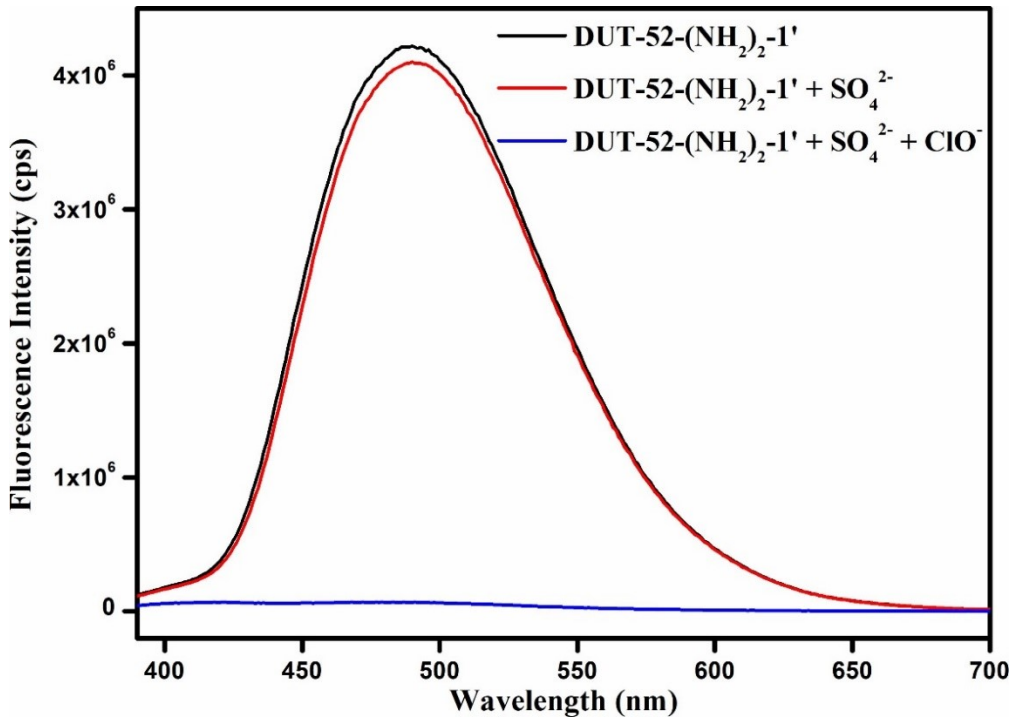

Figure S59. Change in the fluorescence emission intensity of **DUT-52-$(NH_2)_2$-1'** upon addition of 5 mM ClO^- solution (300 µL) in presence of 5 mM SO_4^{2-} (300 µL) solution.

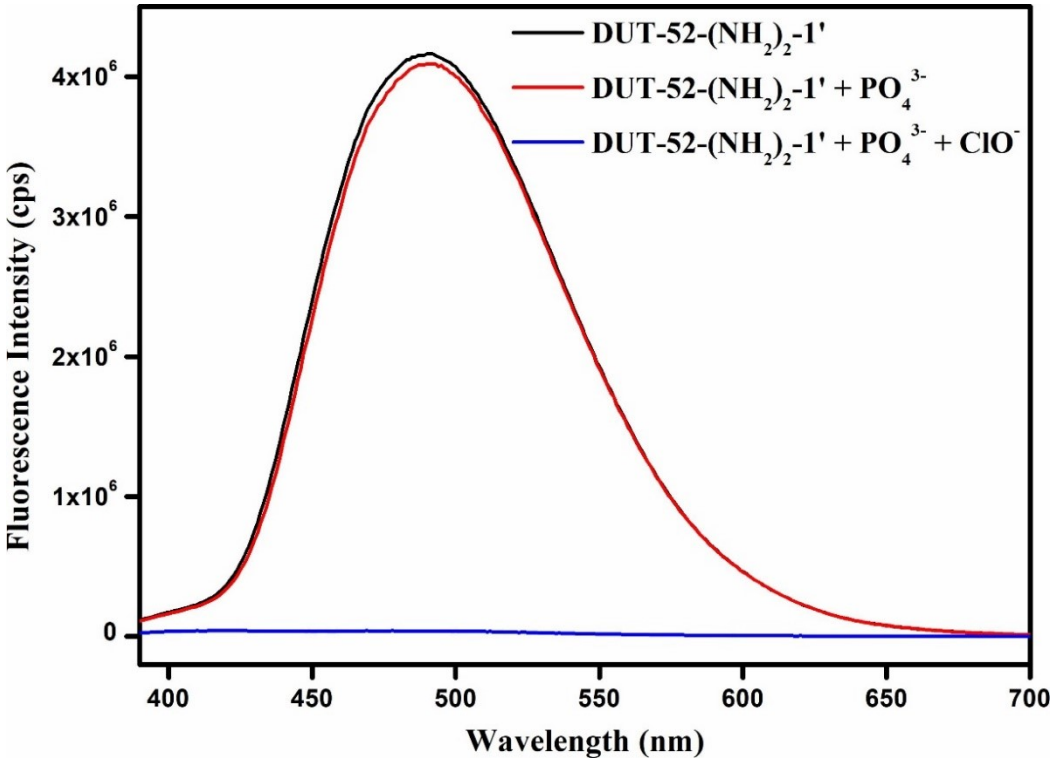

Figure S60. Change in the fluorescence emission intensity of **DUT-52-$(NH_2)_2$-1'** upon addition of 5 mM ClO^- solution (300 µL) in presence of 5 mM PO_4^{3-} (300 µL) solution.

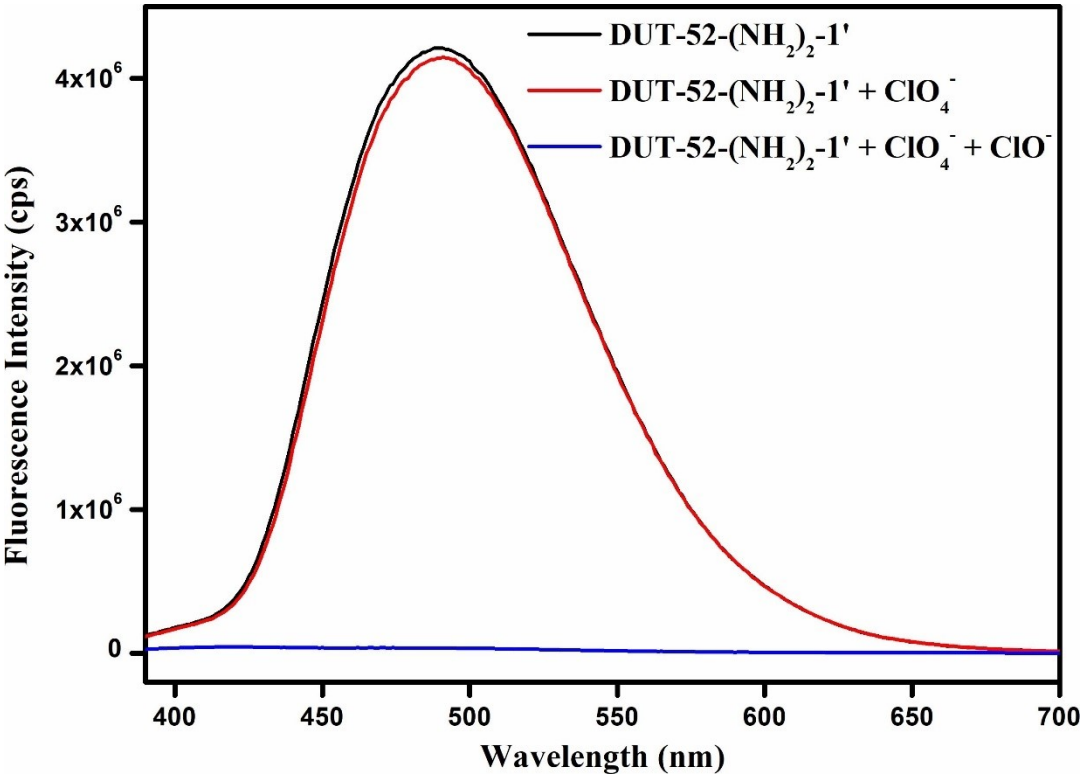

Figure S61. Change in the fluorescence emission intensity of **DUT-52-(NH$_2$)$_2$-1'** upon addition of 5 mM ClO^- solution (300 µL) in presence of 5 mM ClO_4^- (300 µL) solution.

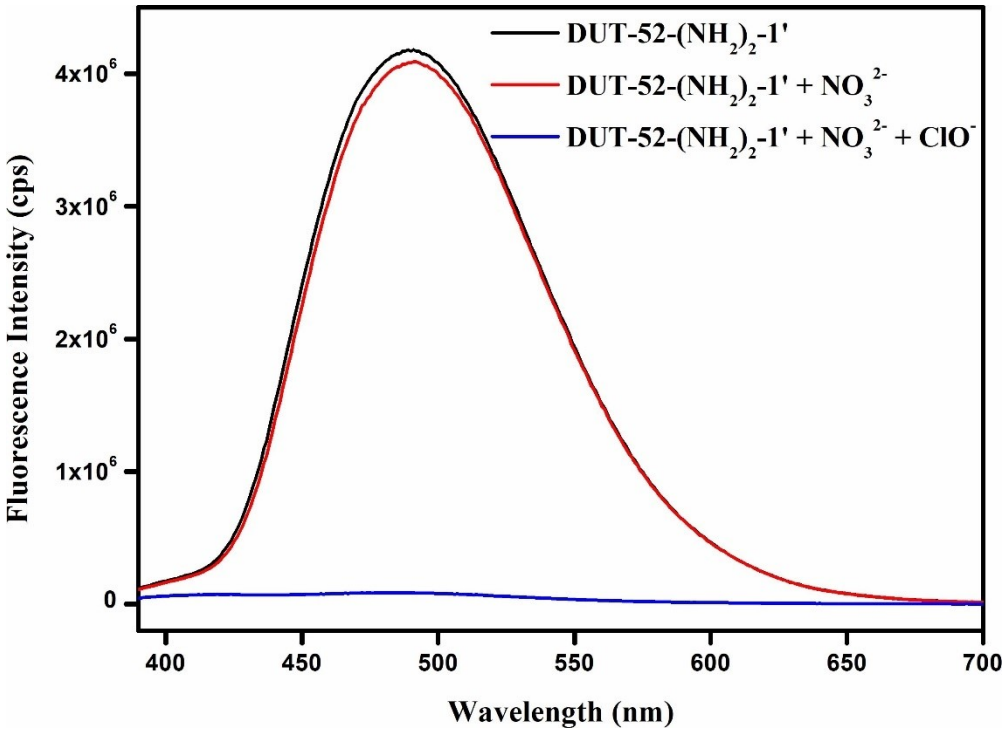

Figure S62. Change in the fluorescence emission intensity of **DUT-52-(NH$_2$)$_2$-1'** upon addition of 5 mM ClO^- solution (300 µL) in presence of 5 mM NO_3^{2-} (300 µL) solution.

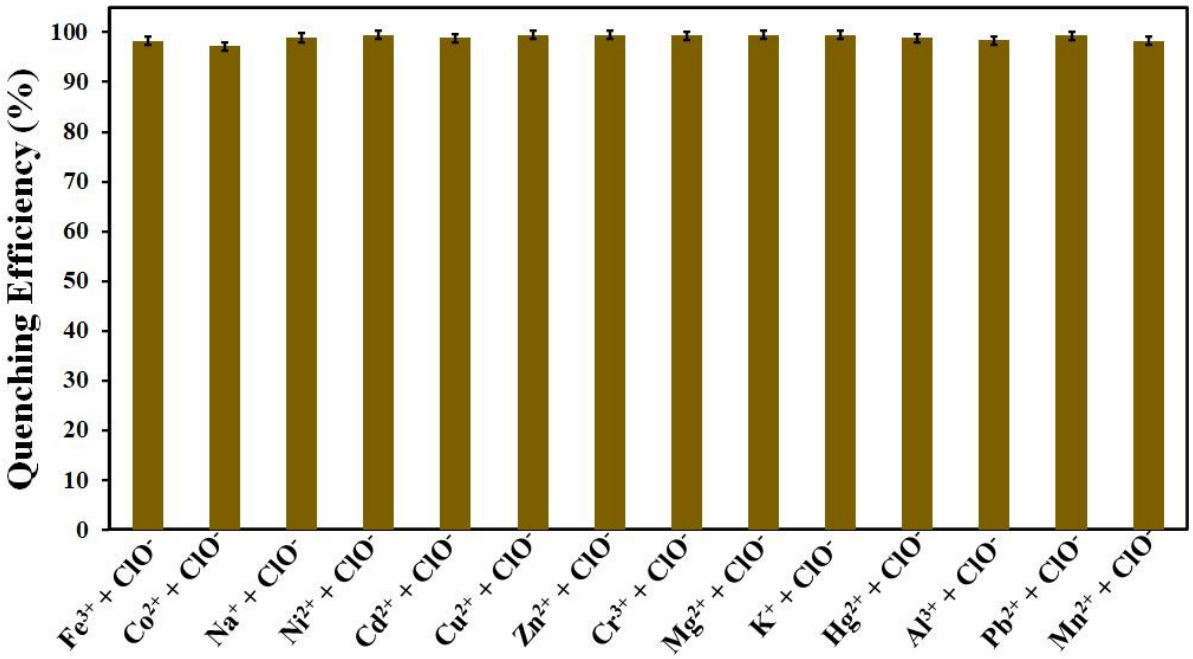

Figure S63. The effect of other metal anions on the quenching efficiency of ClO^-. The error bars indicate the standard errors of three measurements.

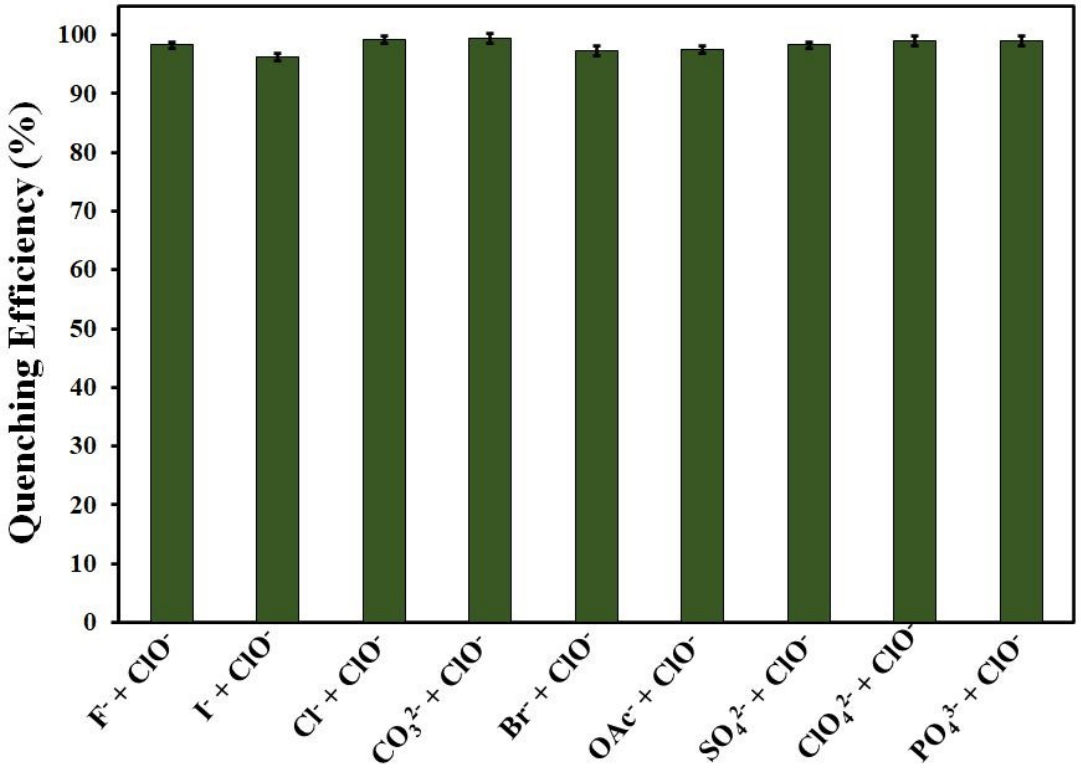

Figure S64. The effect of other metal anions on the quenching efficiency of ClO^-. The error bars indicate the standard errors of three measurements.

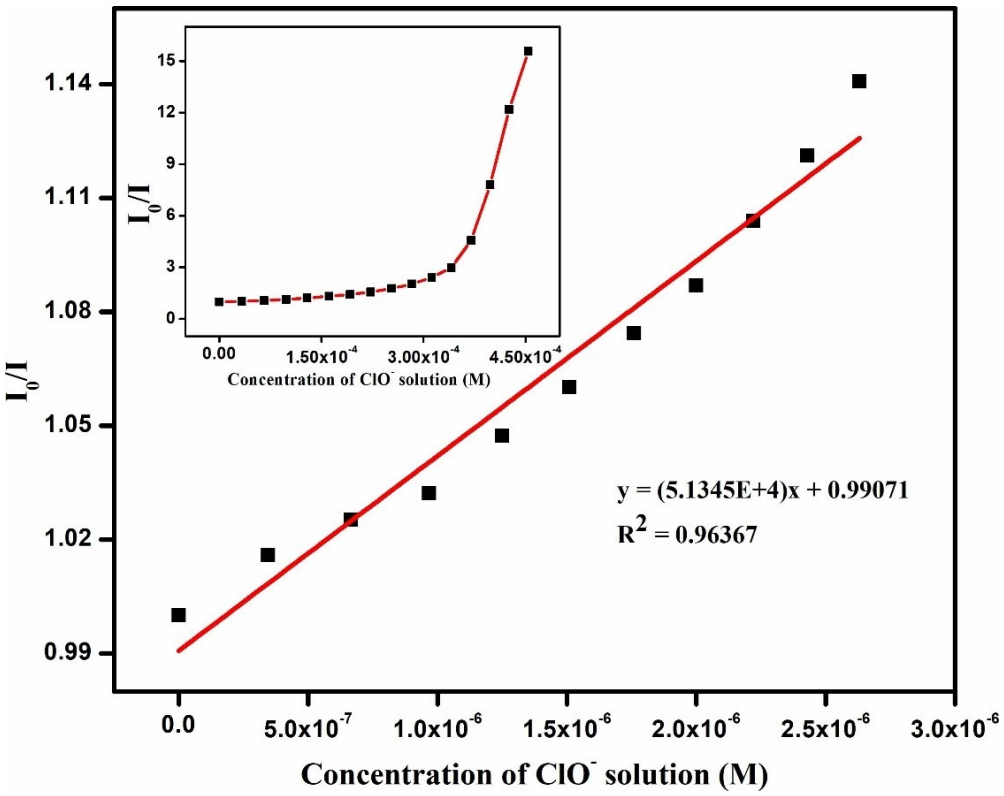

Figure S65. Stern-Volmer plot for the fluorescence emission quenching of **DUT-52-$(NH_2)_2$-1'** in presence of ClO^- solution.

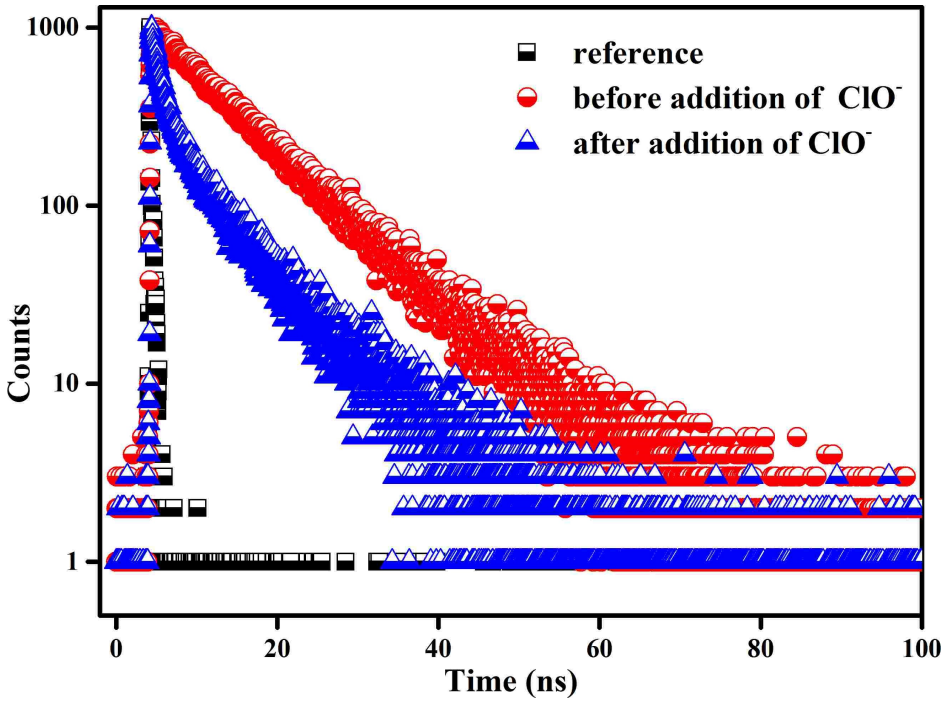

Figure S66. Lifetime decay profiles of PBS buffer suspension of **DUT-52-$(NH_2)_2$-1'** in absence and presence of ClO^- solution.

Table S2. Average excited state lifetime (<τ>) values of **DUT-52-$(NH_2)_2$-1'** before and after addition of 300 μL of 5 mM ClO^- solution (λ_{ex} = 375 nm).

Volume Added (μL)	B_1	B_2	a_1	a_1	τ_1 (ns)	τ_2 (ns)	<τ>* (ns)	X^2
0	0.005	0.121	0.007	0.993	1.80	10.07	10.01	1.05
300	0.271	0.023	0.633	0.367	0.79	5.32	2.45	1.05

* $<\tau> = a_1\tau_1 + a_2\tau_2$

Where, a_1= amplitude of the first component of the bi-exponential curve.

a_2 = amplitude of the second component of the bi-exponential curve.

τ_1 = life time of the first component of the bi-exponential curve.

τ_2 = life time of the second component of the bi-exponential curve.

Table S3. Comparison of performance of **DUT-52-$(NH_2)_2$-1'** with other reported MOF based probes.

Sl. No.	Name of the Compound	Response Time	Medium Used	Detection Limit (μM)	Ref.
1	**DUT-52-$(NH_2)_2$-1′**	< 30 s	PBS buffer	0.08	this work
2	NH_3-MIL-53(Al) MOF	180 s	PBS buffer	0.04	4
3	UiO-68-PT	< 10 s	water	0.28	5
4	Hf-UiO-66-$(NH_2)_2$ MOF	seconds	HEPES buffer	0.02	6
5	Hf-UiO-66-$(NH_2)_2$ MOF	seconds	PBS buffer	0.009	6
6	Al-MIL-53-NH_2 MOF	seconds	HEPES buffer	0.54	6
7	NH_2-HPU-17	-	water	0.026	7
8	Eu-BDC-NH_2/DPA	20 s	water	0.037	8
9	PDA/Eu/PDA-UiO-66-NH_2	< 15 s	Tris-HCl	0.10	9
10	AF@MOF-801	30 s	HEPES buffer	0.075	10
11	UiO-68-ol	5 s	PBS	0.10	11

12	UiO-Eu-L1	5 s	water	0.016	12
13	CD/CCM@ZIF-8	-	ethanol	0.067	13
14	NH_2-Cu-MOFs	10 s	water	0.036	14
15	UiO-66-NH_2	180 s	water	0.3	15

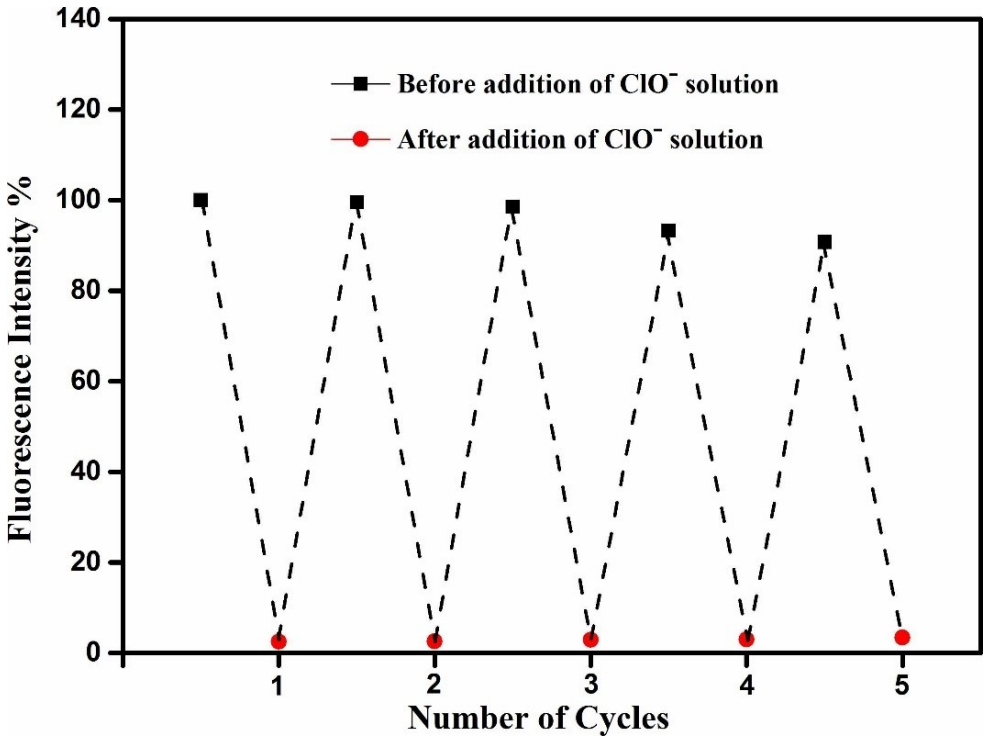

Figure S67. Recyclability of compound **DUT-52-$(NH_2)_2$-1'** up to five cycles of sensing experiments.

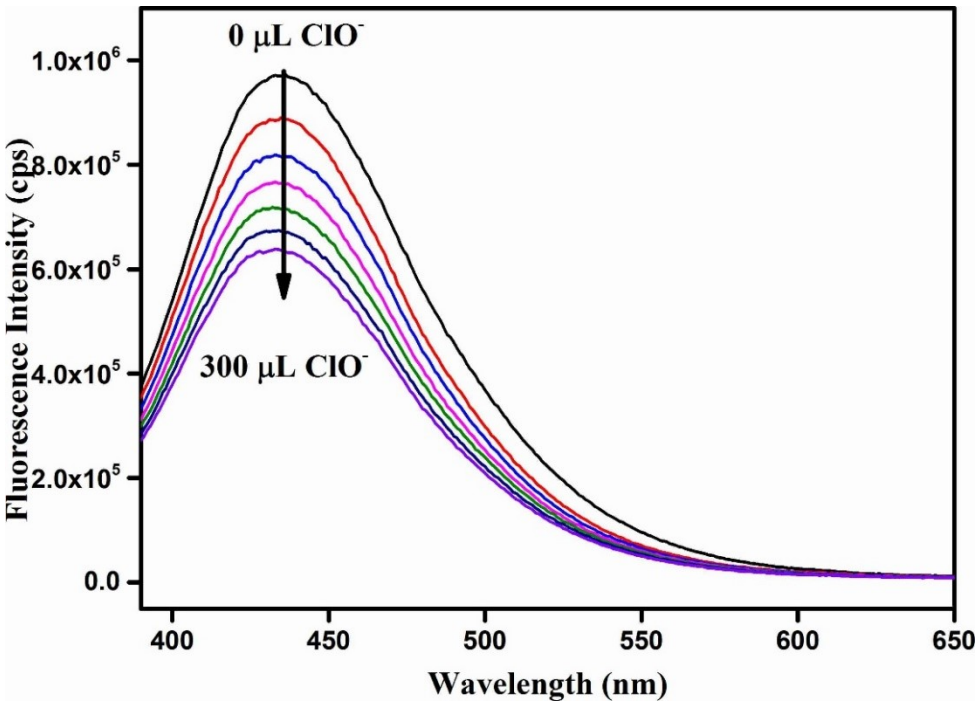

Figure S68. Change in the fluorescence intensity of DUT-52 MOF dispersed in PBS after the addition of 5 mM ClO^- solution.

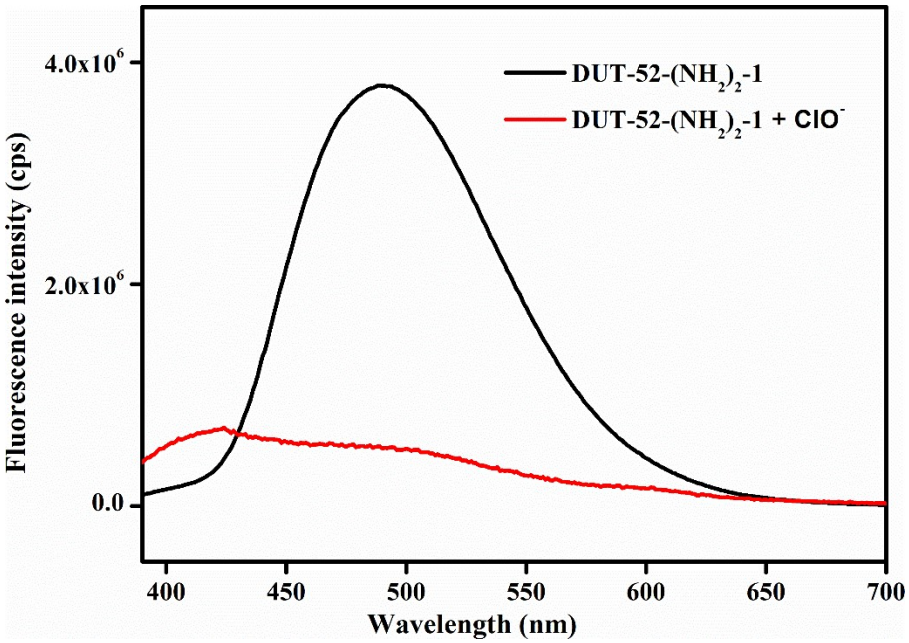

Figure S69. Change in the fluorescence intensity of **DUT-52-$(NH_2)_2$-1** MOF dispersed in PBS after the addition of 5 mM ClO^- solution.

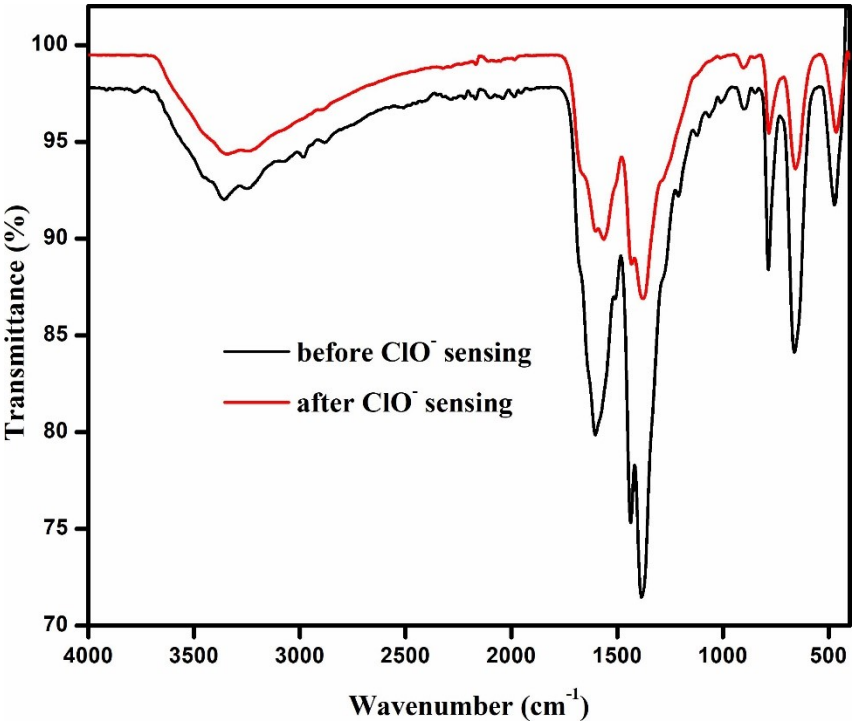

Figure S70. FT-IR spectra of **DUT-52-$(NH_2)_2$-1'** before and after ClO^- sensing.

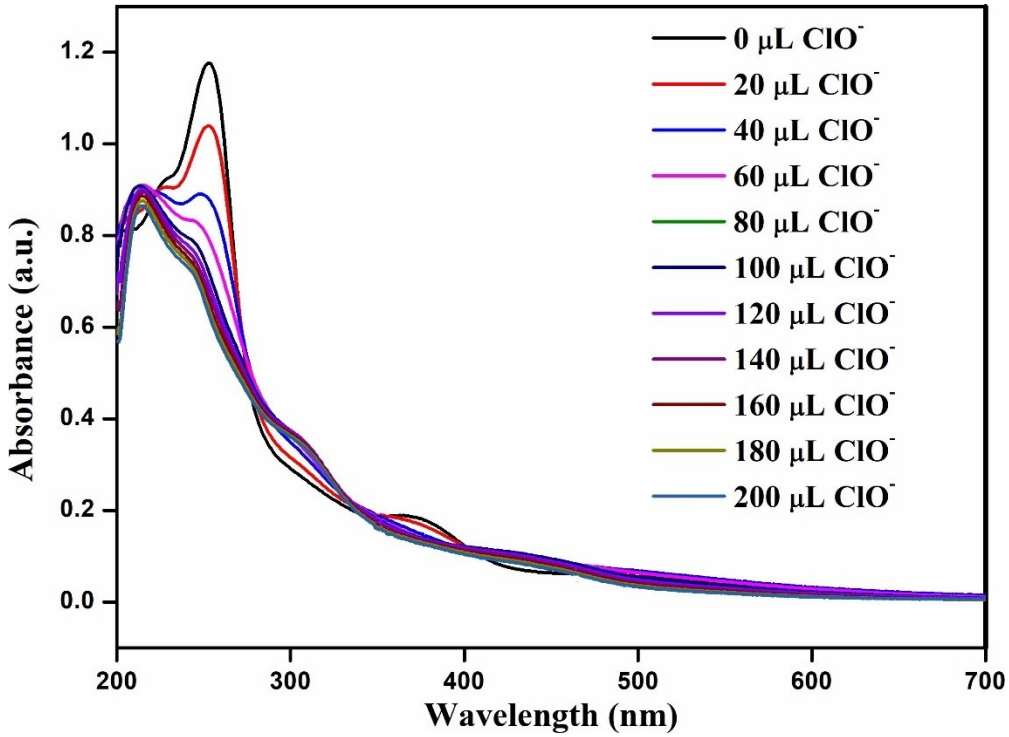

Figure S71. UV-vis spectra of **DUT-52-$(NH_2)_2$-1'** in presence of ClO^- solutions (5 mM).

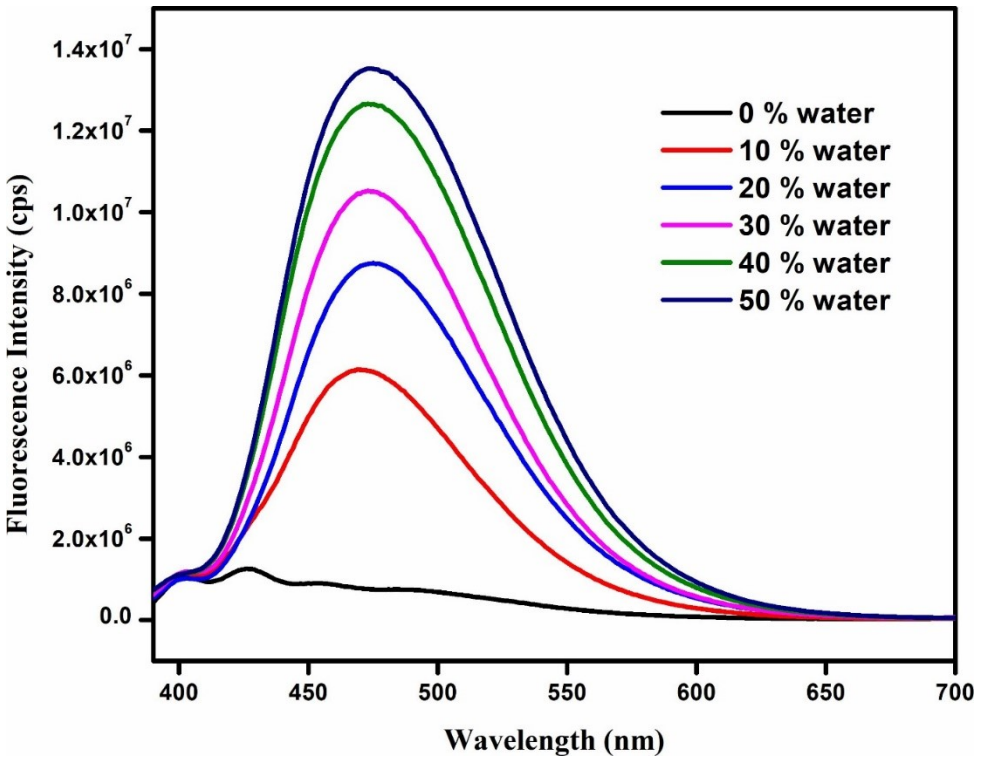

Figure S72. Fluorescence emission spectra of **DUT-52-$(NH_2)_2$-1'** response to different water content in ethanol under excitation of 370 nm.

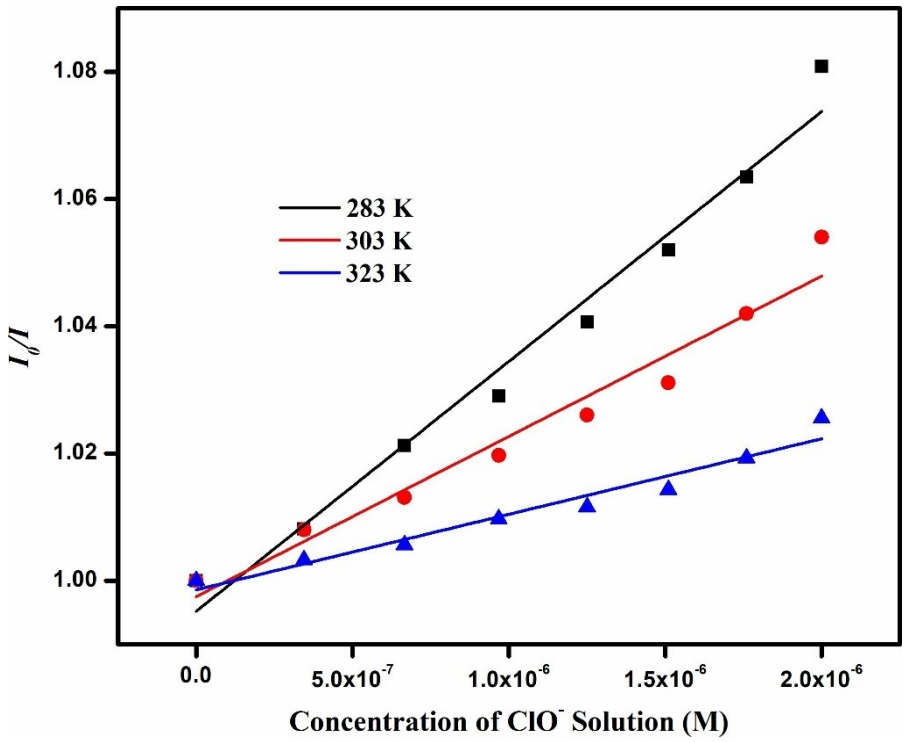

Figure S73. Stern-Volmer plots at different temperatures for quenching of **DUT-52-$(NH_2)_2$-1'** by ClO^- solution.

Table S3. Liner regression analysis of the Stern-Volmer plots (Figure S73) at different temperatures for the quenching of **DUT-52-(NH_2)$_2$-1'** by ClO^- solution.

T (*K*)	K_{sv} (M^{-1}) x 10^4	R^2
283	3.9270	0.97590
303	2.5197	0.95755
323	1.1876	0.95850

Table S4. Evaluation of intra-day, inter-day accuracy and precision study of change in fluorescence intensity of **DUT-52-(NH_2)$_2$-1'** after incremental addition of 5 mM ClO^-.

Parameter	Amount of ClO^- added (μL)	Fluorescence Intensity (cps) at λ_{max} = 490 nm			X (cps)	SD	RE%
Reproducibility Inter-day precision	0	4108760	4113620	4110620	4111000	2452	0.419
	50	2663950	2681820	2717140	2687637	27067	1.736
	100	1607700	1618730	1581910	1602780	18896	0.087
	150	8608421	869331	865643	865272	4256	0.773
	200	416166	420735	420143	419014	2484	1.014
	250	149736	148069	149952	149252	1030	1.947
	300	17790	18883	18475	18382	552	0.311
Repeatability Intra-day precision	0	4109640	4107200	4103300	4106713	3197	0.314
	50	2727430	2709920	2710650	2716000	9905	0.700
	100	1587070	1603810	1595640	1595507	8370	0.541
	150	863062	874866	876324	871417	7272	1.445
	200	421506	423536	421613	422218	1142	1.513
	250	150020	148770	153707	150832	2566	0.908
	300	18067	19073	19006	18715	562	1.493

Where: X, mean values; SD, standard deviation; %RE, percentage of relative error.

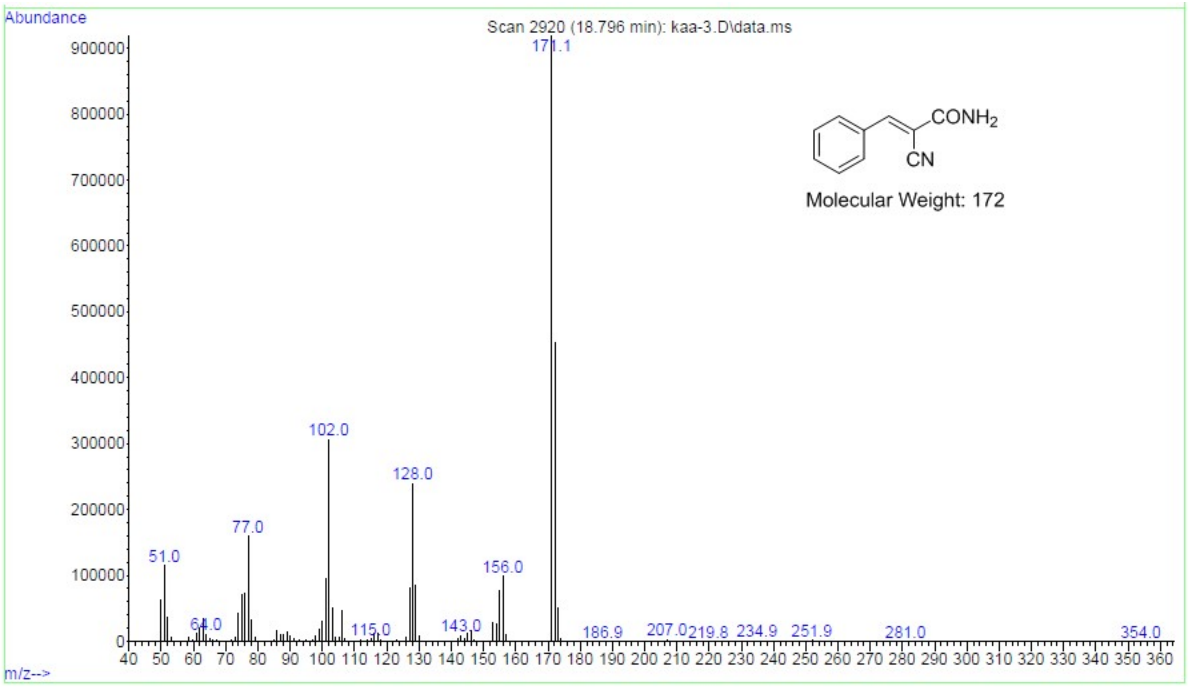

Figure S74. GC-MS trace of 2-cyano-3-phenylacrylamide.

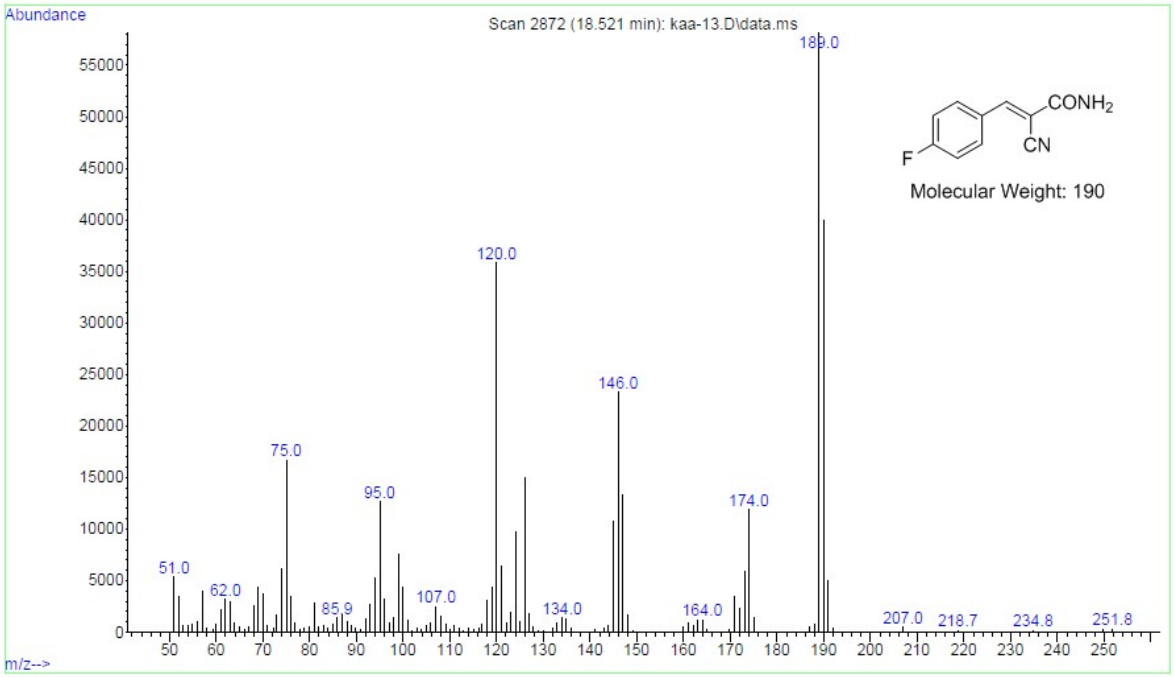

Figure S75. GC-MS trace of 2-cyano-3-(4-fluorophenyl)acrylamide.

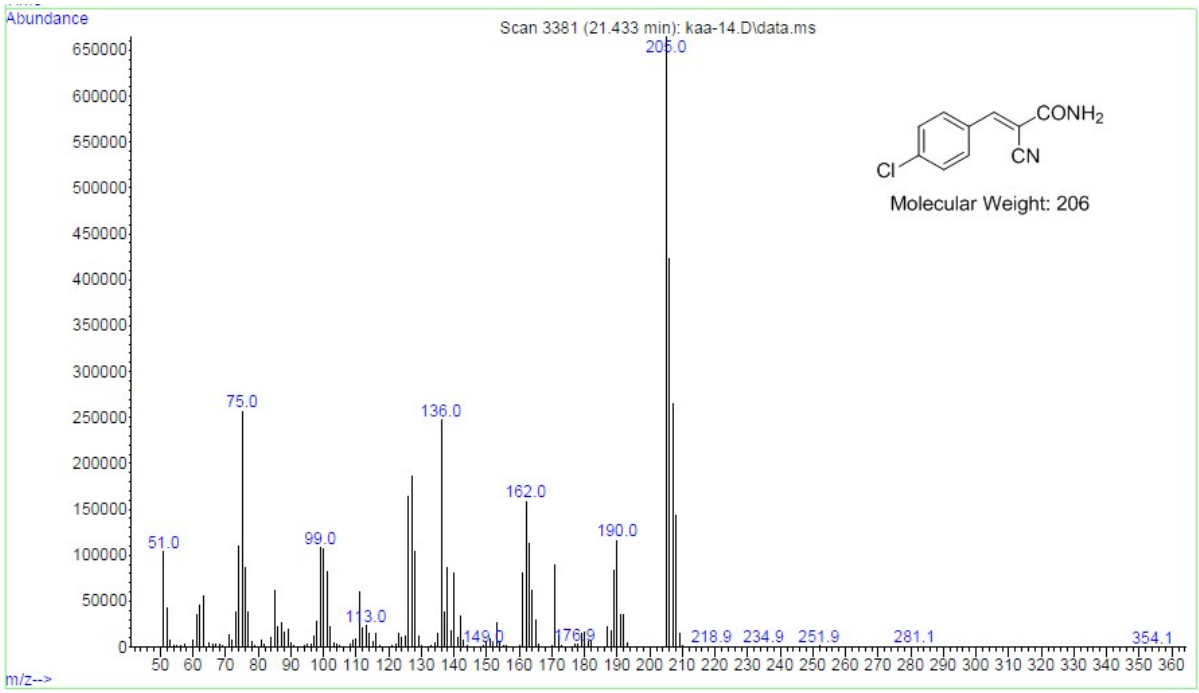

Figure S76. GC-MS trace of 3-(4-chlorophenyl)-2-cyanoacrylamide.

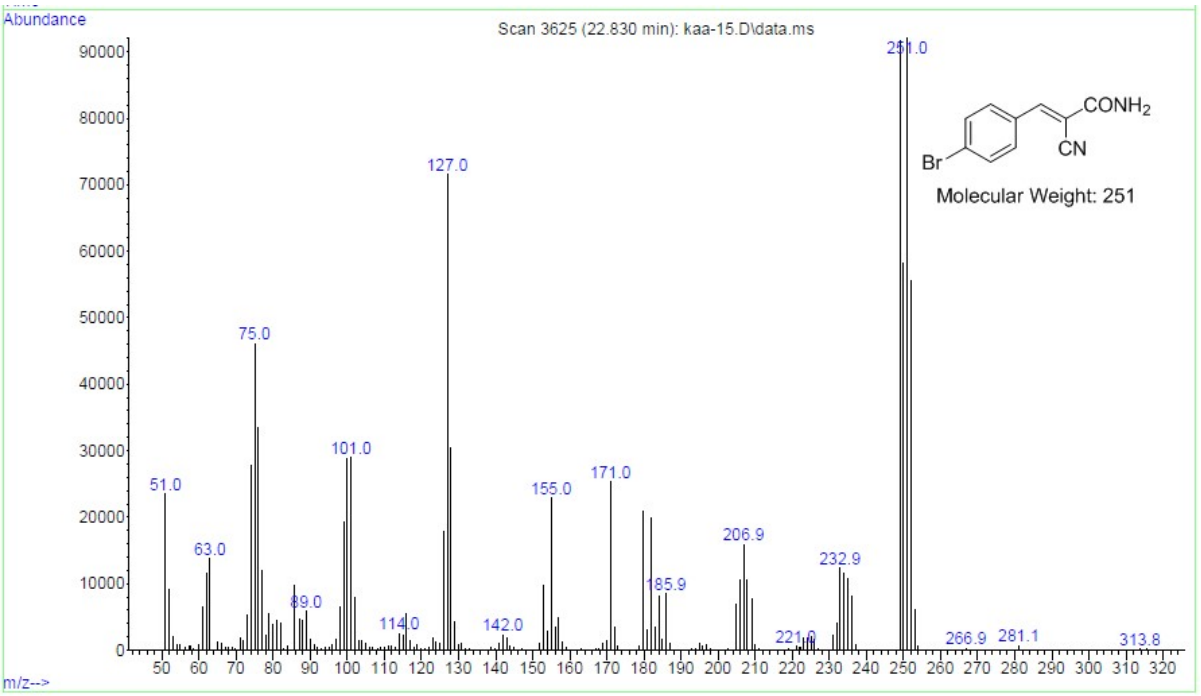

Figure S77. GC-MS trace of 3-(4-bromophenyl)-2-cyanoacrylamide.

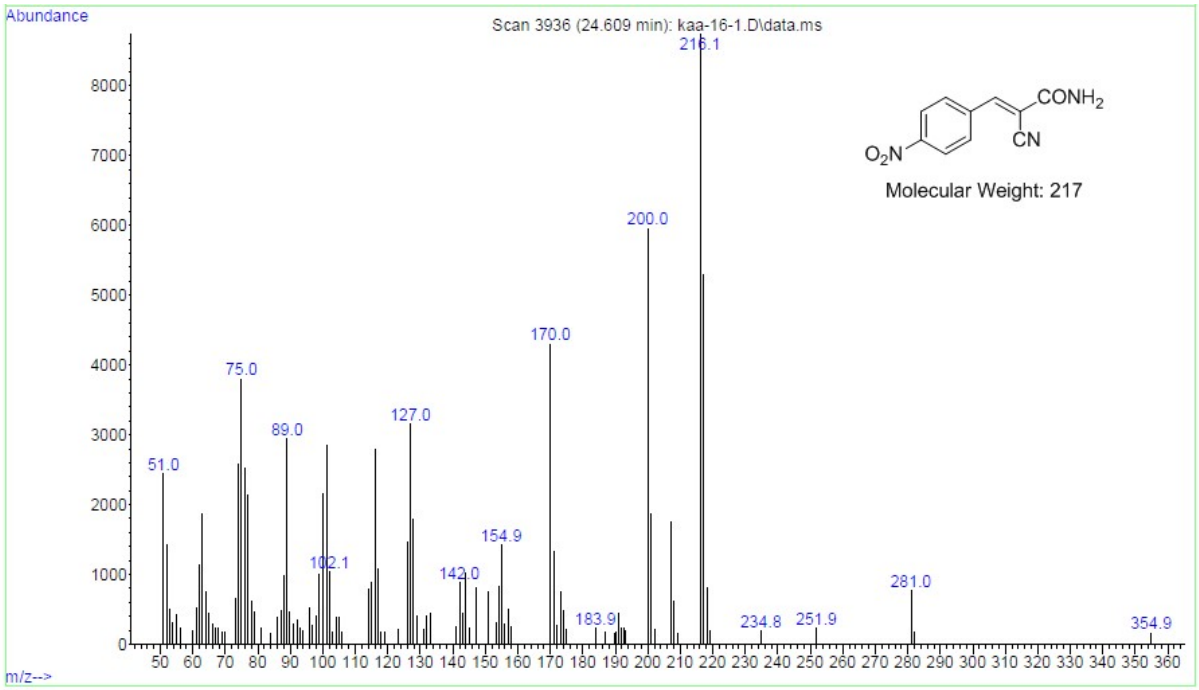

Figure S78. GC-MS trace of 2-cyano-3-(4-nitrophenyl)acrylamide.

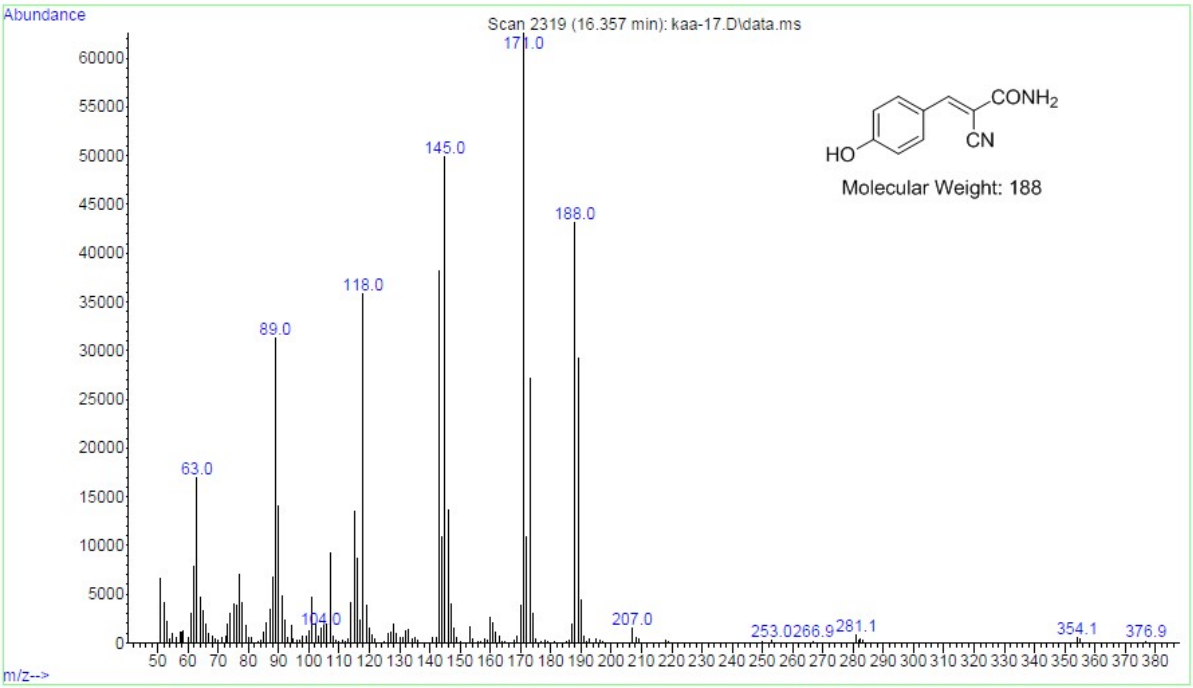

Figure S79. GC-MS trace of 2-cyano-3-(4-hydroxyphenyl)acrylamide.

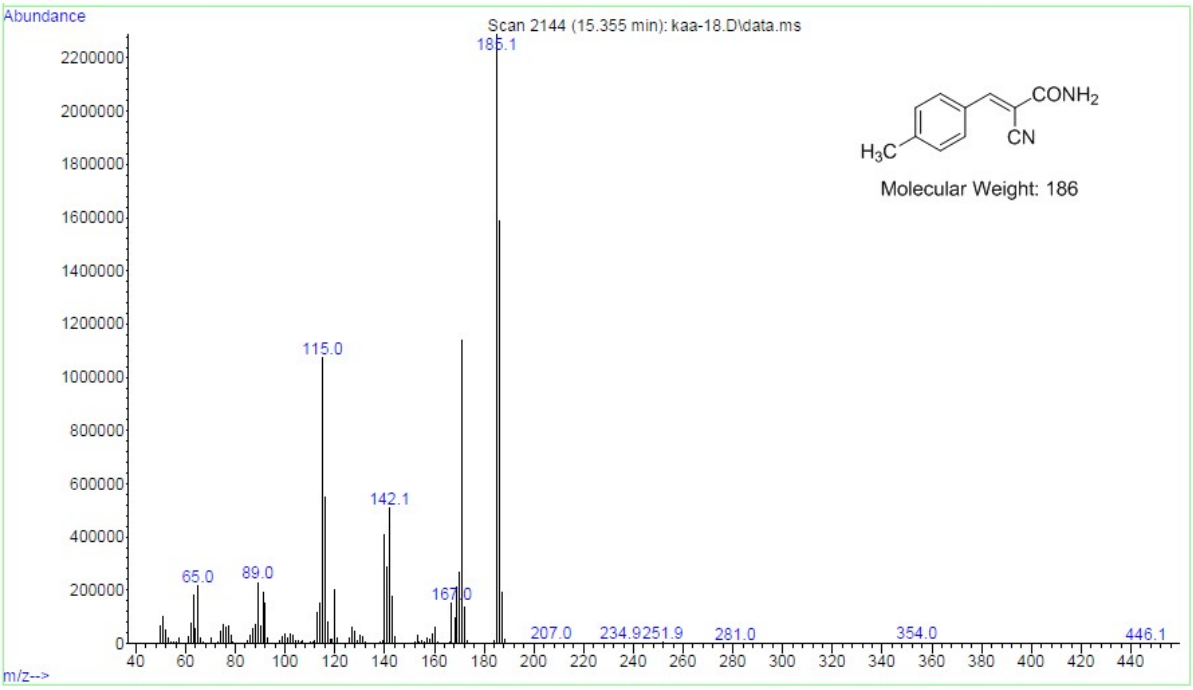

Figure S80. GC-MS trace of 2-cyano-3-(p-tolyl)acrylamide.

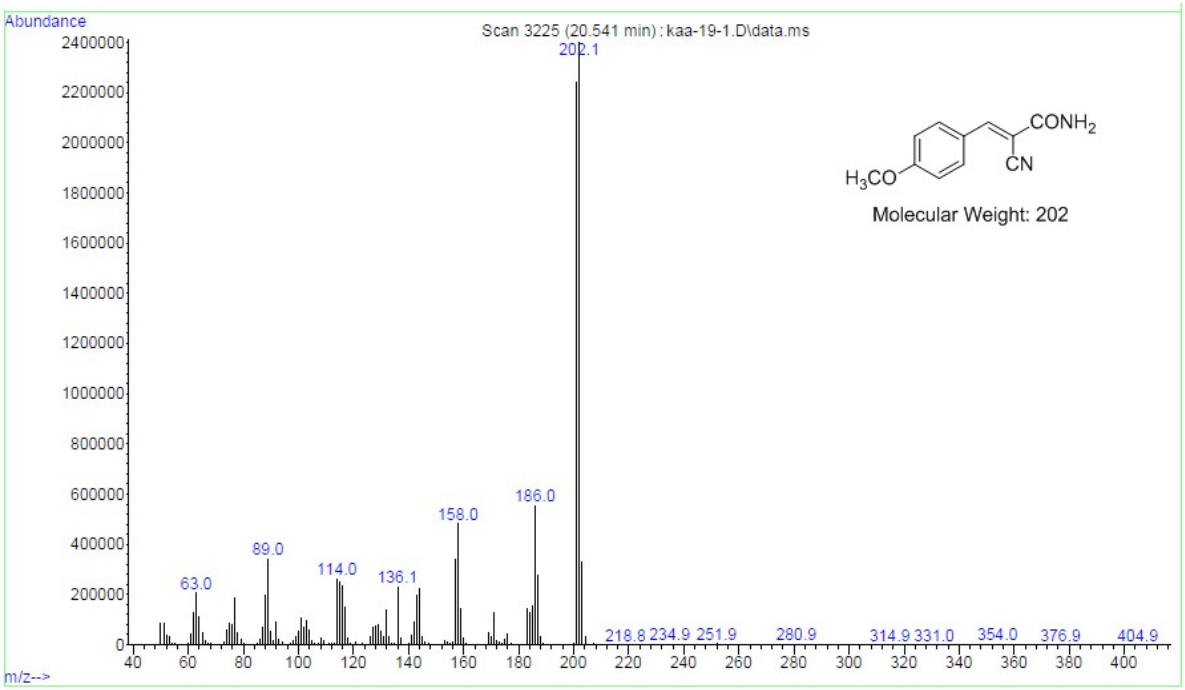

Figure S81. GC-MS trace of 2-cyano-3-(4-methoxyphenyl)acrylamide.

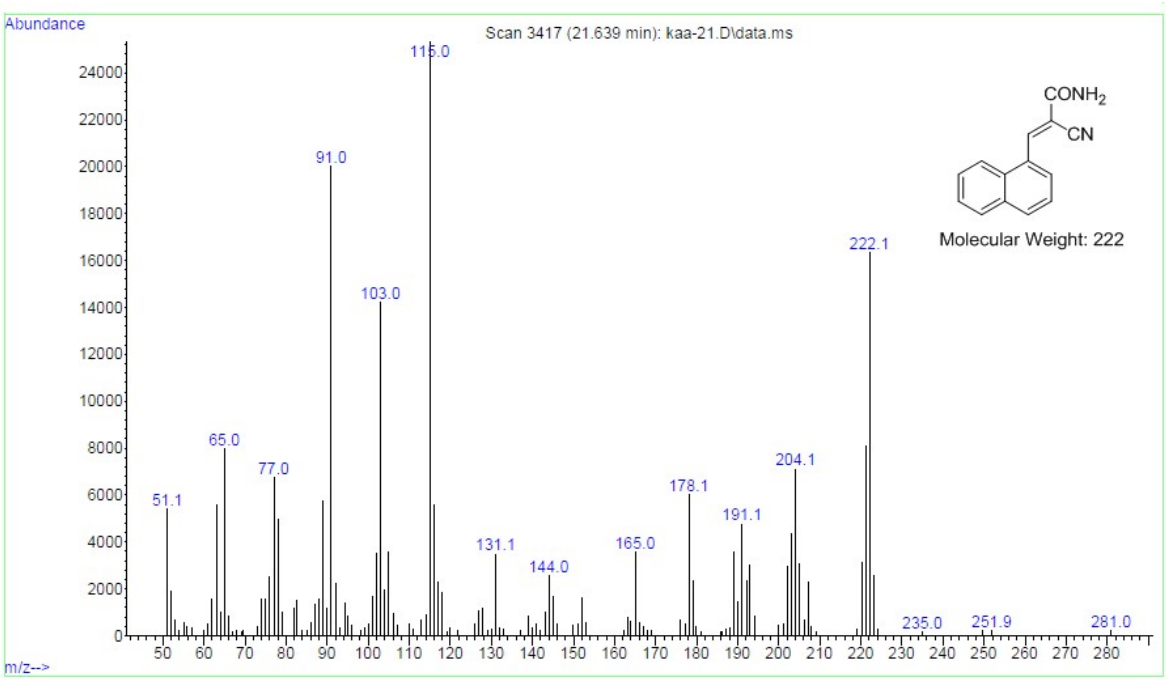

Figure S82. GC-MS trace of 2-cyano-3-(naphthalen-1-yl)acrylamide

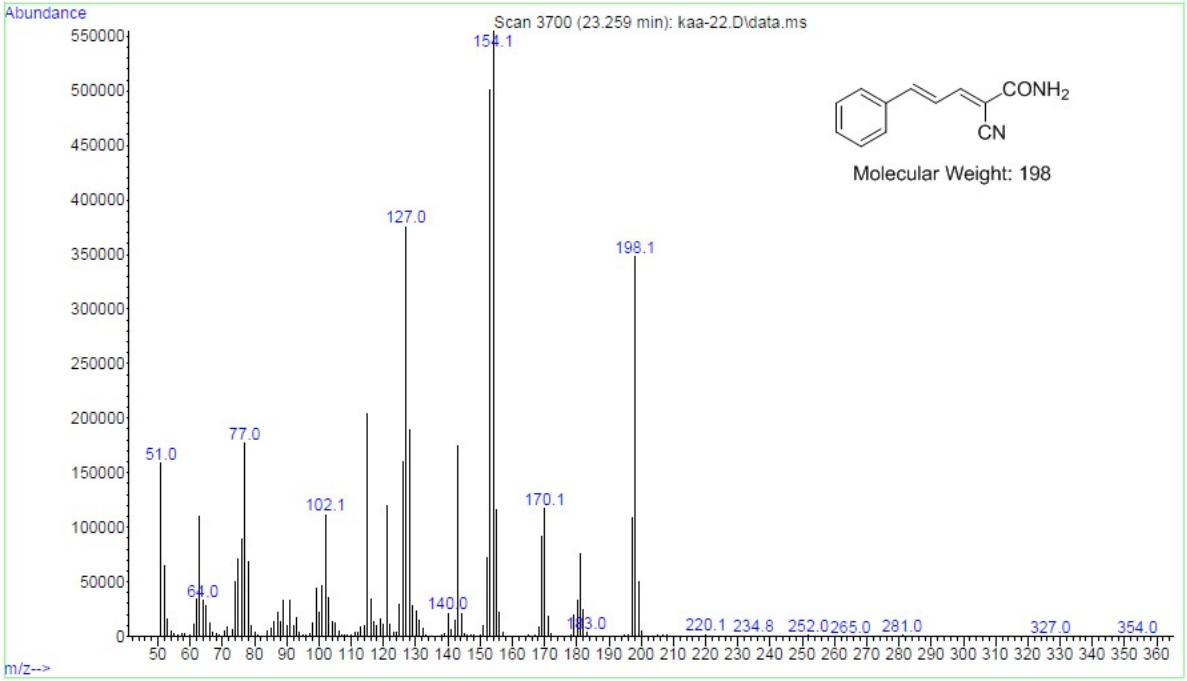

Figure S83. GC-MS trace of 2-cyano-5-phenylpenta-2,4-dienamide.

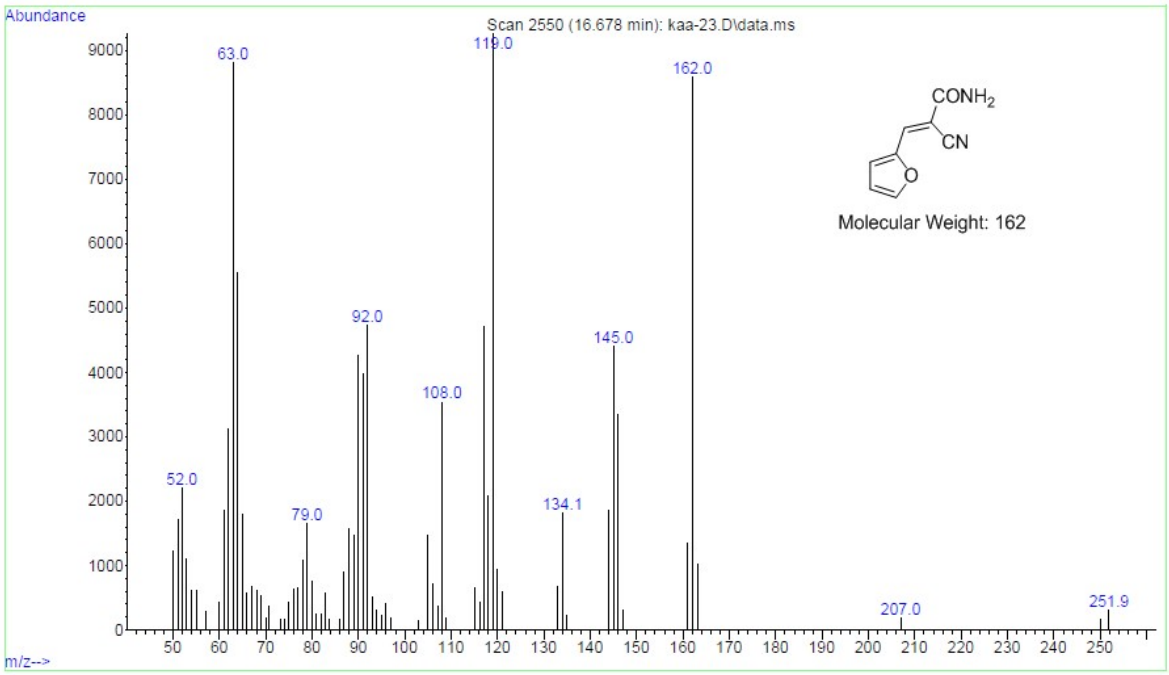

Figure S84. GC-MS trace of 2-cyano-3-(furan-2-yl)acrylamide.

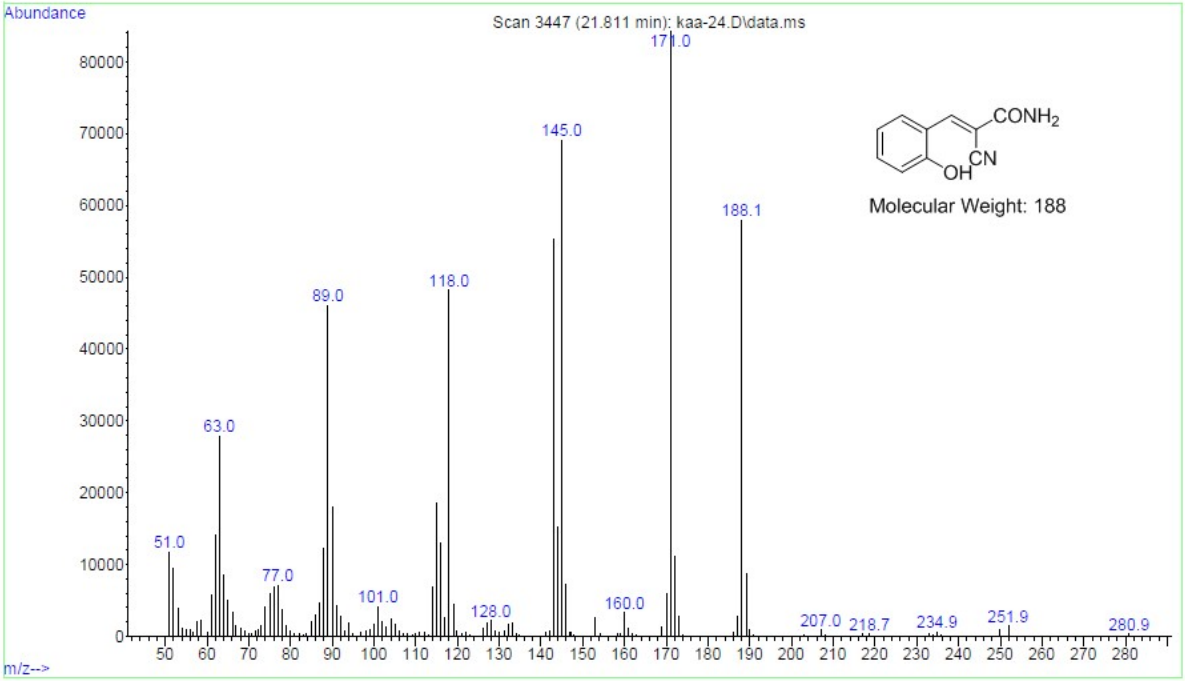

Figure S85. GC-MS trace of 2-cyano-3-(2-hydroxyphenyl)acrylamide

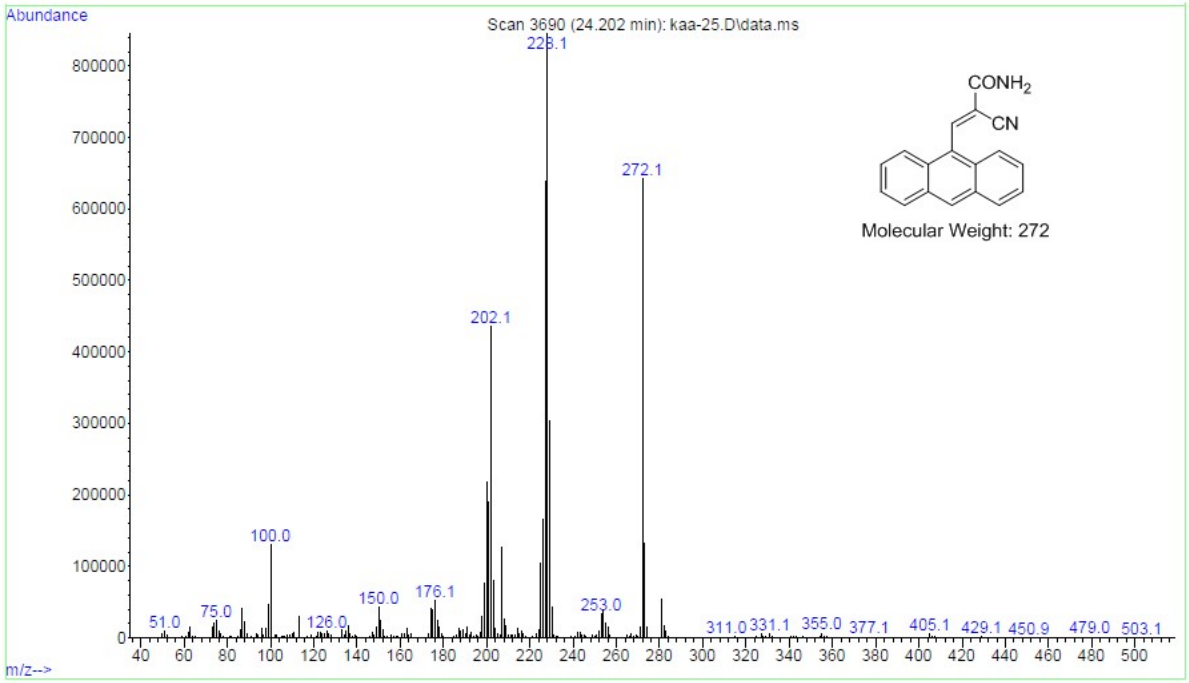

Figure S86. GC-MS trace of 3-(anthracen-9-yl)-2-cyanoacrylamide.

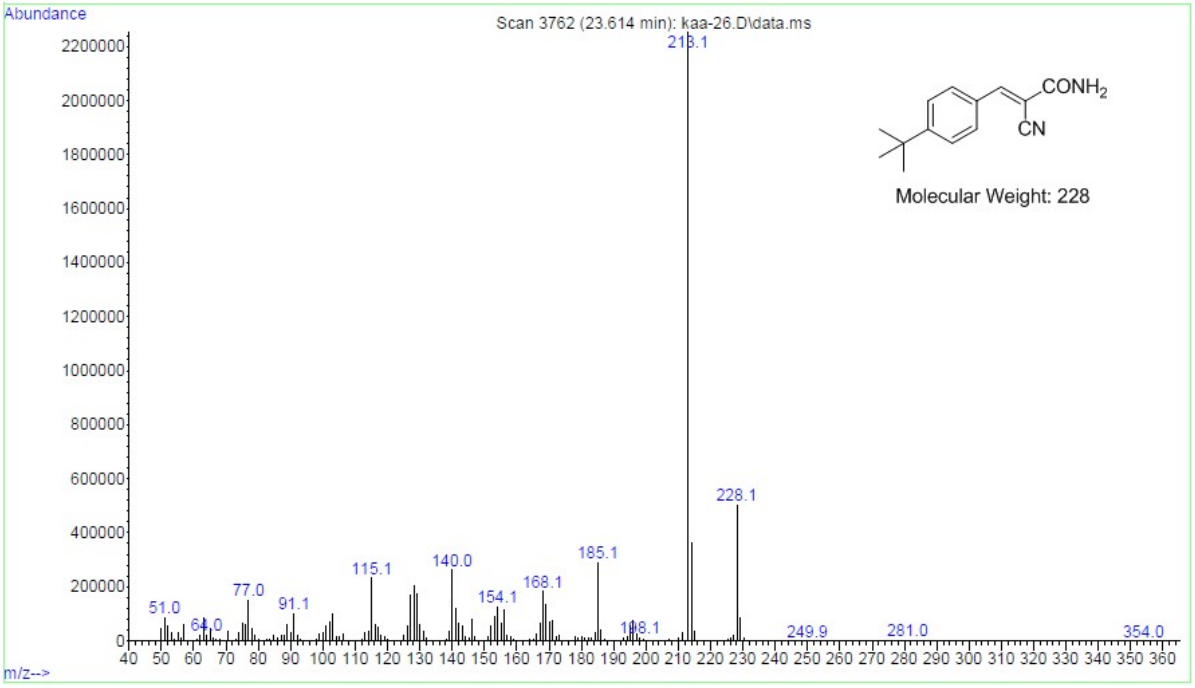

Figure S87. GC-MS trace of 3-(4-(tert-butyl)phenyl)-2-cyanoacrylamide.

Simulated CIF file of compound DUT-52-$(NH_2)_2$-1:

data_Zr-DUT-52-$(NH_2)_2$

_audit_creation_date 2021-04-19

_audit_creation_method 'Materials Studio'

```
_symmetry_space_group_name_H-M    'P23'
_symmetry_Int_Tables_number       195
_symmetry_cell_setting            cubic
loop_
_symmetry_equiv_pos_as_xyz
  x,y,z
  -x,-y,z
  -x,y,-z
  x,-y,-z
  z,x,y
  z,-x,-y
  -z,-x,y
  -z,x,-y
  y,z,x
  -y,z,-x
  y,-z,-x
  -y,-z,x
_cell_length_a                  23.4387
_cell_length_b                  23.4387
_cell_length_c                  23.4387
_cell_angle_alpha                90.0000
_cell_angle_beta                 90.0000
_cell_angle_gamma                90.0000
loop_
_atom_site_label
_atom_site_type_symbol
_atom_site_fract_x
_atom_site_fract_y
_atom_site_fract_z
_atom_site_U_iso_or_equiv
```

_atom_site_adp_type

_atom_site_occupancy

C1	C	0.47818	0.31882	0.28228	0.00000	Uiso	1.00
O2	O	0.50215	0.14521	0.42073	0.00000	Uiso	1.00
C3	C	0.49278	0.26113	0.27721	0.00000	Uiso	1.00
C4	C	0.50330	0.12706	0.36803	0.00000	Uiso	1.00
O5	O	0.00030	0.07398	0.85274	0.00000	Uiso	1.00
C6	C	1.00139	0.23814	0.72211	0.00000	Uiso	1.00
O7	O	0.44795	0.05206	0.55204	0.00000	Uiso	1.00
O8	O	0.44809	0.05204	0.44790	0.00000	Uiso	1.00
O9	O	-0.07433	-0.35269	0.50219	0.00000	Uiso	1.00
C10	C	0.76112	-0.22273	0.50767	0.00000	Uiso	1.00
C11	C	0.18010	0.49404	0.33241	0.00000	Uiso	1.00
C12	C	0.13192	0.49706	0.37299	0.00000	Uiso	1.00
C13	C	0.31925	-0.00171	0.66692	0.00000	Uiso	1.00
C14	C	0.36788	-0.00083	0.62677	0.00000	Uiso	1.00
C15	C	0.26188	-0.22210	-0.00199	0.00000	Uiso	1.00
C16	C	0.12673	-0.13215	0.00044	0.00000	Uiso	1.00
C17	C	0.32603	0.99852	0.27399	0.00000	Uiso	1.00
O18	O	0.42054	1.00122	0.35488	0.00000	Uiso	1.00
C19	C	0.32111	-0.21567	-0.00530	0.00000	Uiso	1.00
O20	O	0.14501	-0.07947	0.00011	0.00000	Uiso	1.00
C21	C	0.35584	-0.26381	-0.00507	0.00000	Uiso	1.00
O22	O	0.42599	-0.35283	0.00021	0.00000	Uiso	1.00
O23	O	-0.07924	0.49893	-0.35489	0.00000	Uiso	1.00
C24	C	0.82540	0.50811	-0.27476	0.00000	Uiso	1.00
C25	C	0.23419	0.47919	0.35368	0.00000	Uiso	1.00
O26	O	0.14724	0.49731	0.42573	0.00000	Uiso	1.00
C27	C	0.50763	0.77474	0.32535	0.00000	Uiso	1.00
C28	C	0.49356	0.83239	0.31985	0.00000	Uiso	1.00

C29 C 1.00114 0.16693 0.81924 0.00000 Uiso 1.00

C30 C 0.99793 0.22602 0.82603 0.00000 Uiso 1.00

C31 C 0.14419 0.76380 1.00454 0.00000 Uiso 1.00

C32 C 0.17891 0.71567 1.00476 0.00000 Uiso 1.00

C33 C 0.85369 0.73424 0.52121 0.00000 Uiso 1.00

C34 C 0.81883 0.78234 0.52221 0.00000 Uiso 1.00

N35 N 0.84278 0.83607 0.53767 0.00000 Uiso 1.00

N36 N 0.15336 0.66058 1.00835 0.00000 Uiso 1.00

N37 N 0.34274 0.66400 0.53740 0.00000 Uiso 1.00

N38 N 0.65332 1.16059 0.99122 0.00000 Uiso 1.00

Zr39 Zr 0.50000 0.09965 0.50000 0.00000 Uiso 1.00

O40 O 0.05199 0.05199 -0.05199 0.00000 Uiso 1.00

Zr41 Zr 0.50000 -0.40056 0.00000 0.00000 Uiso 1.00

Zr42 Zr 0.50000 0.00000 -0.40028 0.00000 Uiso 1.00

Zr43 Zr 0.09954 0.00000 0.00000 0.00000 Uiso 1.00

O44 O 0.05209 -0.05209 -0.05209 0.00000 Uiso 1.00

loop_

_geom_bond_atom_site_label_1

_geom_bond_atom_site_label_2

_geom_bond_distance

_geom_bond_site_symmetry_2

_ccdc_geom_bond_type

C1 C3 1.400 . A

C1 C25 1.392 9 A

C1 N37 1.426 8_656 S

O2 C4 1.307 . A

O2 Zr39 2.144 . S

C3 C10 1.423 6_565 A

C3 C27 1.407 2_665 A

C4 O9 1.288 6 A

C4 C28 1.478 2_665 S

O5 C16 1.286 5_556 A

O5 Zr43 2.063 10_556 S

C6 C15 1.423 5_656 A

C6 C17 1.407 10_756 A

C6 C32 1.399 5 A

O7 Zr39 2.054 . S

O7 Zr42 2.056 1_556 S

O7 Zr41 2.052 10_556 S

O8 Zr39 2.054 . S

O8 Zr42 2.053 3_655 S

O8 Zr41 2.054 10_556 S

O9 C4 1.288 12 A

O9 Zr42 2.069 9 S

C10 C3 1.423 12_655 A

C10 C24 1.407 5_645 A

C10 C34 1.400 1_545 A

C11 C25 1.406 . A

C11 C12 1.478 . S

C11 C24 1.397 3_655 A

C12 O26 1.287 . A

C12 O23 1.306 3 A

C13 C14 1.478 . S

C13 C17 1.396 4_566 A

C13 C21 1.407 10_556 A

C14 O18 1.307 4_566 A

C14 O22 1.286 10_556 A

C15 C19 1.399 . A

C15 C6 1.423 9_544 A

C15 C30 1.407 9_544 A

C16 O20 1.307 . A

C16 O5 1.286 9_545 A

C16 C29 1.478 9_544 S

C17 C6 1.407 7_675 A

C17 C13 1.396 4_566 A

O18 C14 1.307 4_566 A

O18 Zr42 2.145 3_665 S

C19 C21 1.391 . A

C19 N38 1.426 2_664 S

O20 Zr43 2.146 . S

C21 C13 1.407 7_655 A

O22 Zr41 2.064 . S

O22 C14 1.286 7_655 A

O23 C12 1.306 3 A

O23 Zr41 2.144 5 S

C24 C10 1.407 9_654 A

C24 C11 1.397 3_655 A

C25 C1 1.392 5 A

O26 Zr39 2.069 9 S

C27 C28 1.397 . A

C27 C3 1.407 2_665 A

C28 C4 1.478 2_665 S

C28 C33 1.406 8_656 A

C29 C30 1.396 . A

C29 C16 1.478 5_656 S

C29 C31 1.407 5 A

C30 C15 1.407 5_656 A

C31 C32 1.391 . A

C31 C29 1.407 9 A

C32 N36 1.426 . S

C32 C6 1.399 9 A

C33 C34 1.392 . A

C33 C28 1.406 11_566 A

C34 N35 1.426 . S

C34 C10 1.400 1_565 A

N37 C1 1.426 11_566 S

N38 C19 1.426 2_666 S

Zr39 O2 2.144 3_656 S

Zr39 O7 2.054 3_656 S

Zr39 O8 2.054 3_656 S

Zr39 O26 2.069 5 S

Zr39 O26 2.069 8_656 S

O40 Zr43 2.052 . S

O40 Zr43 2.052 5 S

O40 Zr43 2.052 10 S

Zr41 O22 2.064 3_655 S

Zr41 O7 2.052 7_655 S

Zr41 O7 2.052 6 S

Zr41 O8 2.054 7_655 S

Zr41 O8 2.054 6 S

Zr41 O23 2.144 9 S

Zr41 O23 2.144 10_655 S

Zr42 O7 2.056 1_554 S

Zr42 O7 2.056 2_654 S

Zr42 O8 2.053 3_655 S

Zr42 O8 2.053 4 S

Zr42 O9 2.069 5 S

Zr42 O9 2.069 7_655 S

Zr42 O18 2.145 3_645 S

Zr42 O18 2.145 4_565 S

Zr43	O20	2.146	4	S
Zr43	O40	2.052	4	S
Zr43	O44	2.054	.	S
Zr43	O44	2.054	4	S
Zr43	O5	2.063	7_655	S
Zr43	O5	2.063	8_655	S
O44	Zr43	2.054	6	S
O44	Zr43	2.054	10	S

References:

1. Boultif, A.; Louer, D. J., Indexing of powder diffraction patterns for low-symmetry lattices by the successive dichotomy method. *J. Appl. Crystallogr.* **1991,** *24*, 987-993.
2. STOE WinXPOW version 2.11; Stoe & Cie GmbH: Darmstadt, Germany. **2005**.
3. Nielsen, A. T.; DeFusco, A. A.; Browne, T. E., Nitration of bis(amido)naphthalenes. *J. Org. Chem* **1985,** *50*, 4211-4218.
4. Lu, T.; Zhang, L.; Sun, M.; Deng, D.; Su, Y.; Lv, Y., Amino-functionalized metal-organic frameworks nanoplates-based energy transfer probe for highly selective fluorescence detection of free chlorine. *Anal. Chem.* **2016,** *88*, 3413-3420.
5. Li, Q.-Y.; Li, Y.-A.; Guan, Q.; Li, W.-Y.; Dong, X.-J.; Dong, Y.-B., UiO-68-PT MOF-based sensor and its mixed matrix membrane for detection of HClO in water. *Inorg. Chem.* **2019,** *58*, 9890-9896.
6. Nandi, S.; Biswas, S., A diamino functionalized metal-organic framework for fluorometric recognition of free chlorine in environmental water samples. *Microporous Mesoporous Mater.* **2020,** *299*, 110116.
7. Li, H.; He, X.; Zhang, M.; Li, X.; Wang, R.; Xu, Z.; Li, F., Postsynthesis strategy of functional Zn-MOF sensors for the detection of ClO^- and DPA. *Inorg. Chem.* **2021,** *60*, 2590-2597.
8. Sun, Y.-Q.; Cheng, Y.; Yin, X.-B., Dual-ligand lanthanide metal-organic framework for sensitive ratiometric fluorescence detection of hypochlorous acid. *Anal. Chem.* **2021,** *93*, 3559-3566.
9. Zeng, Y.-N.; Zheng, H.-Q.; He, X.-H.; Cao, G.-J.; Wang, B.; Wu, K.; Lin, Z.-J., Dual-emissive metal–organic framework: a novel turn-on and ratiometric fluorescent sensor for highly efficient and specific detection of hypochlorite. *Dalton Trans.* **2020,** *49*, 9680-9687.
10. Ye, Y.; Zhao, L.; Hu, S.; Liang, A.; Li, Y.; Zhuang, Q.; Tao, G.; Gu, J., Specific detection of hypochlorite based on the size-selective effect of luminophore integrated MOF-801 synthesized by a one-pot strategy. *Dalton Trans.* **2019,** *48*, 2617-2625.
11. Li, Y.-A.; Yang, S.; Li, Q.-Y.; Ma, J.-P.; Zhang, S.; Dong, Y.-B., UiO-68-ol NMOF-based fluorescent sensor for selective detection of HClO and its application in bioimaging. *Inorg. Chem.* **2017,** *56*, 13241-13248.
12. Zhou, Z.; Li, X.; Tang, Y.; Zhang, C. C.; Fu, H.; Wu, N.; Ma, L.; Gao, J.; Wang, Q., Oxidative deoximation reaction induced recognition of hypochlorite based on a new fluorescent lanthanide-organic framework. *Chem. Eng. J.* **2018,** *351*, 364-370.

13. Tan, H.; Wu, X.; Weng, Y.; Lu, Y.; Huang, Z.-Z., Self-assembled FRET nanoprobe with metal-organic framework as a scaffold for ratiometric detection of hypochlorous acid. *Anal. Chem.* **2020,** *92*, 3447-3454.
14. Huo, P.; Li, Z.; Fan, C.; Pu, S., Amino-functionalized copper-based metal–organic frameworks for highly selective and sensitive detection of hypochlorite. *New J. Chem.* **2020,** *44*, 19753-19758.
15. Guo, L.; Liu, Y.; Qu, F.; Liu, Z.; Kong, R.; Chen, G.; Fan, W.; Xia, L., Luminescent metal organic frameworks with recognition sites for detection of hypochlorite through energy transfer. *Microchim. Acta* **2019,** (186), 740.